ISSN 8755-6839

SCIENCE OF **TSUNAMI HAZARDS**

Journal of Tsunami Society International

Volume 40 **Number 4** **2021**

IONOSPHERIC TSUNAMI POWER INDEX (ITPI)
TESTING FOR TSUNAMI DETECTION **345**

Nurrohmat Widjajanti[1)], Buldan Muslim[2)], Charisma Juni Kumalasari[3)], and Toifatul Ulma[4)]

[1]Department of Geodetic Engineering, Universitas Gajah Mada, Yogyakarta, 55281, ***INDONESIA***
[2]Space Research Center, National Research and Innovation Agency, Bandung 40173, ***INDONESIA***
[3]Mathematics Department, Master's Programme, Institut Teknologi Sepuluh Nopember, Surabaya 60111, ***INDONESIA***
[4]Department of Geomatics Engineering, Institut Teknologi Sepuluh Nopember, Surabaya 60111, ***INDONESIA***

WWW.TSUNAMISOCIETY.ORG

TSUNAMI SOCIETY INTERNATIONAL, 1741 Ala Moana Blvd. #70, Honolulu, HI 96815, USA.

SCIENCE OF TSUNAMI HAZARDS is a CERTIFIED OPEN ACCESS Journal included in the prestigious international academic journal database DOAJ, maintained by the University of Lund in Sweden with the support of the European Union. SCIENCE OF TSUNAMI HAZARDS is also preserved, archived and disseminated by the National Library, The Hague, NETHERLANDS, the Library of Congress, Washington D.C., USA, the Electronic Library of Los Alamos, National Laboratory, New Mexico, USA, the EBSCO Publishing databases and ELSEVIER Publishing in Amsterdam. The vast dissemination gives the journal additional global exposure and readership in 90% of the academic institutions worldwide, including nation-wide access to databases in more than 70 countries.

OBJECTIVE: Tsunami Society International publishes this interdisciplinary journal to increase and disseminate knowledge about tsunamis and their hazards.

DISCLAIMER: Although the articles in SCIENCE OF TSUNAMI HAZARDS have been technically reviewed by peers, Tsunami Society International is not responsible for the veracity of any statement, opinion or consequences.

Submit manuscripts of research papers, notes or letters to the Editor. If a research paper is accepted for publication the author(s) must submit a scan-ready manuscript, a Doc, TeX or a PDF file in the journal format. Issues of the journal are published electronically in PDF format. There is a minimal publication fee for authors who are members of Tsunami Society International for three years and slightly higher for non-members. Tsunami Society International members are notified by e-mail when a new issue is available. Permission to use figures, tables and brief excerpts from this journal in scientific and educational works is granted provided that the source is acknowledged.

Recent and all past journal issues are available at: http://www.TsunamiSociety.org CD-ROMs of past volumes may be purchased by contacting Tsunami Society International at postmaster@tsunamisociety.org Issues of the journal from 1982 thru 2005 are also available in PDF format at the U.S. Los Alamos National Laboratory Library http://epubs.lanl.gov/tsunami/

ISSN 8755-6839

SCIENCE OF **TSUNAMI HAZARDS**

Journal of Tsunami Society International

Volume 40 **Number 4** **2021**

IMPACT ANALYSIS OF THE 2018 TSUNAMI ON SULAWESI ISLAND USING SATELLITE IMAGERY

Andrey Zaytsev[1], Pavel Pronin[2], Adel Giniyatullin[2], Efim Pelinovsky[1,3] and Marina Zaytseva[2]

[1] *Special Research Bureau for Automation of Marine Researches, Yuzhno-Sakhalinsk, Russia*
[2] *Nizhny Novgorod State Technical University n.a. R.E. Alekseev, Nizhny Novgorod, Russia*
[3] *Institute of Applied Physics, Nizhny Novgorod, Russia*

ABSTRACT

On September 28, 2018, a strong earthquake and tsunami occurred on the island of Sulawesi (Indonesia), which turned out to be the most destructive this year (more than 2,000 people died). The magnitude of the earthquake was 7.5. Its epicenter was located at the base of the Minahasa Peninsula, about 78 km from the city of Palu, the administrative center of the province of Central Sulawesi, at a depth of 10 km. A strong earthquake set in motion several submarine landslides and the departure into the sea of sections of the coast. As a result, the coastal zone and its ecology have been changed that confirmed by analysis of satellite imageries before and after the event.

Key words: *landslide, earthquake, environmental damage, Indonesia*

1. INTRODUCTION

On September 28, 2018, a strong earthquake and tsunami occurred on the island of Sulawesi (Indonesia), which turned out to be the most destructive in the world in 2018 (more than 2,000 people died). The magnitude of the earthquake was 7.5 and tremors were felt almost throughout the island of Sulawesi, as well as in the Indonesian province of East Kalimantan and in the East Malaysian state of Sabah [Heidarzadeh et al, 2019; Goda et al, 2019]. The US Geophysical Agency (https://earthquake.usgs.gov) defined the type of earthquake as "slip-strike" when the fault axis is along the meridians and the fault movement occurs along it. Usually, in such an earthquake, less energy is transferred to the water surface, so the tsunami warning, originally issued by the Indonesian Center, was canceled. Nevertheless, the height of the tsunami waves on the shore in the area of the administrative center of Palu reached 11 m and the tsunami led to significant destruction and casualties along the coast of Palu Bay [Omira et al, 2020].

Several field missions were conducted on the island of Sulawesi, which made it possible to measure wave heights along the coast and assess the nature of destruction and environmental changes [Omira et al, 2020; Zaytsev et al, 2019a ; Zaytsev et al, 2019b]. The authors of this work as part of an international group of scientists took part in these expeditions. The research was carried out on the island of Sulawesi in the Gulf region of Palu from November 7 to 11, 2018 together with scientists from Indonesia, Turkey, Austria, Italy, Morocco, Portugal under the auspices of the Government of Indonesia and UNESCO-IOC.

It should be noted that surveys of tsunami traces are always laborious and costly, so it is important to use modern means of observing our planet from spacecraft. The purpose of this article is to analyse satellite images of the island of Sulawesi and compare them with direct coastal zone survey methods.

2. SATELLITE IMAGES OF SULAWESI ISLAND atellite images of Sulawesi Island

First of all, we note that a satellite image of the earth's surface of the northwestern island of Sulawesi, presented in Figure 1 from the NASA website (https://disasters.nasa.gov/sulawesi-island-indonesia-earthquake-and-tsunami-2018/aria-along-track-deformation-map-m75-september), shows that the eastern part of Palu Bay dropped to a height of 3 m., the western part rose. Such residual displacements over the epicenter of the earthquake, which are difficult to measure by direct methods, are well traced in satellite images and give an idea of the scale of vertical displacements in the tsunami focus. Even if land areas were not covered by water during the tsunami, their displacement changes the landscape of the coastal zone and affects the ecological state of the area. Flooding the coast with tsunami waves only exacerbates the situation.

Tremors during the earthquake caused several large landslides in the bay, which caused a strong tsunami [Zaytsev et al, 2019b; Sassa S. and Takagawa, 2019; Nakata et al, 2020]. The descent of two such landslides in the areas of Benteng (Buenteng) and Tamunggu (Tamungu) was captured (Figure 2) by the pilot Icoze Mafella (https://www.youtube.com/watch?v=WkrBP9bnTcw) of Batik Air, who by a fluke took off a minute before the earthquake. Note that the airport was partially destroyed by an earthquake and this affected the speed of restoration work.

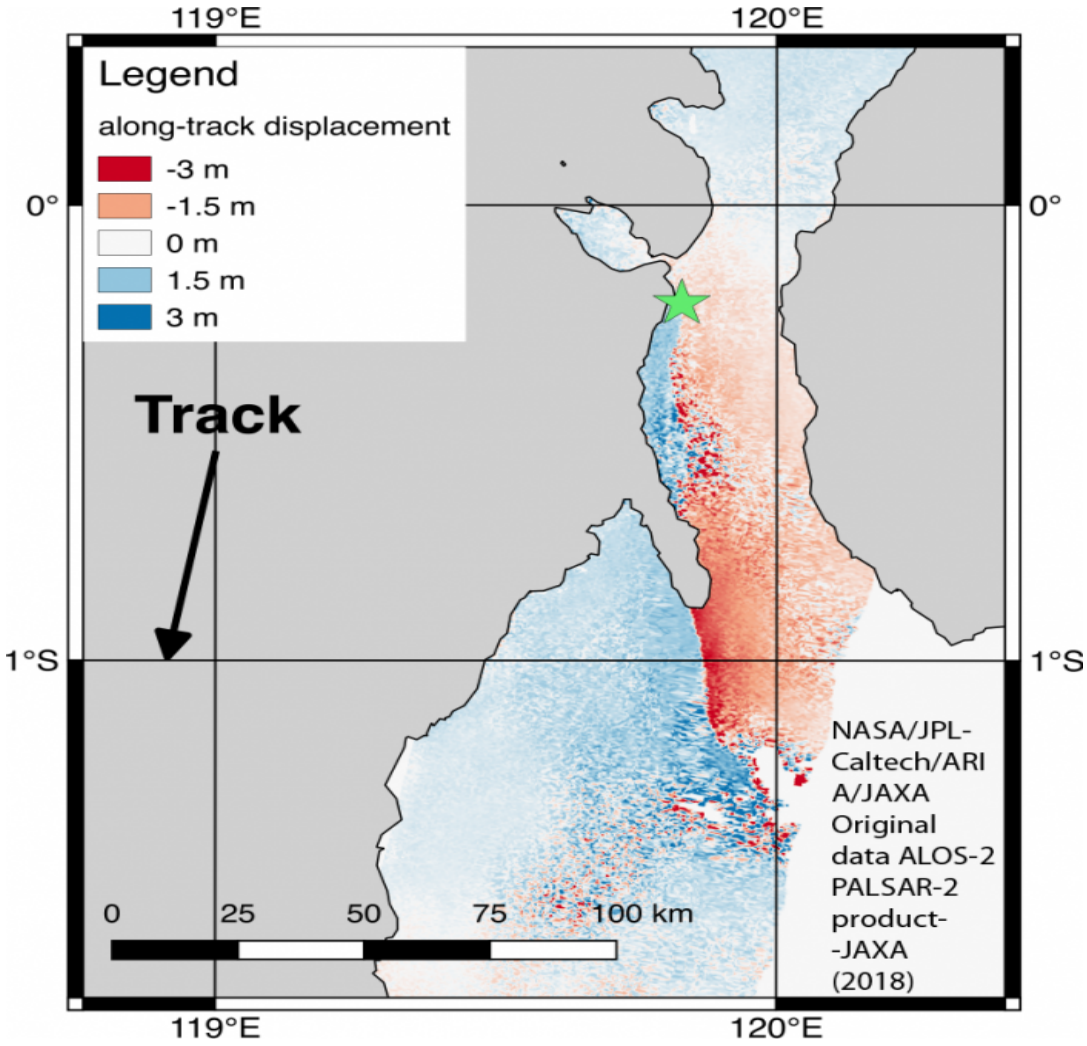

Fig. 1 Displacement of the earth's surface after the earthquake on 28 September, 2018. The position of the epicenter of the earthquake was marked with a star. (https://disasters.nasa.gov/sulawesi-island-indonesia-earthquake-and-tsunami-2018/aria-along-track-deformation-map-m75-september)

Fig. 2 Photo of landslide in Benteng - left and Tamunggu - right

Below, we will discuss in more detail the comparison of satellite imagery with field surveys in some coastal locations following the earthquake and tsunami on Sulawesi Island. Figure 3 shows a map of the island of Sulawesi with marked coastal points, where direct measurements of tsunami wave heights were made [Omira et al, 2020]. Given the possible problems with the correct translation of Indonesian names into Russian, we will mainly use the English coastal names shown in figure 3. Space images made it possible to obtain panoramic images of sections of the coast, which is almost impossible to do during surveys.

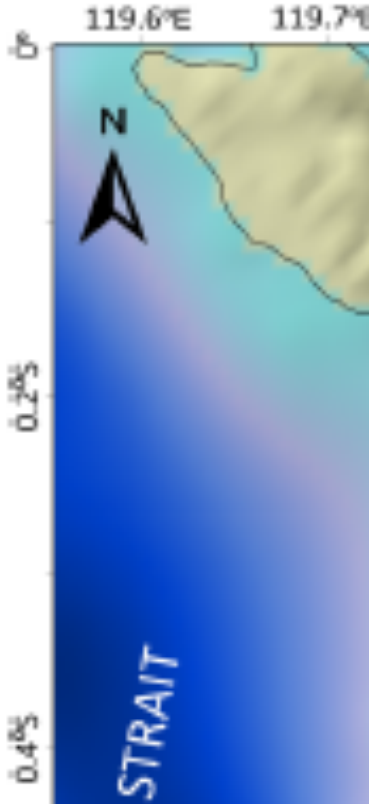

Fig. 3. Map of Palu Bay with marked points of the tsunami wave heights measurements

2.1 BENTENG (0.8464S 119.8226E)

Satellite images and of the tsunami wave heights measurements in the area of the Benteng village showed that a large part of the coast, more than 500 m length and a maximum width of about 120 m, move to sea (Figure 4). Note that a significant part of the landslide was probably under water and therefore the volume of the landslide can be estimated after additional sonar hydroacoustic studies. The height of the tsunami waves at this point reached of 9 m. Tsunamis of landslide origin are usually local in nature and lead to maximum heights in the area of the landslide. Note that this landslide was located in the area of the river bed, like almost all the others that were discovered during the expedition. The layer of bottom precipitation in the river accumulates for a long time and then is driven by external influence.

Fig 4. Benteng region

2.2 LOLI-PESUA (0.70137S 119.84438E)

Satellite images of the Lolli Pesua village area, taken before and after the tsunami, showed that a large part of the coast more than 500 m length and with a maximum width of about 200 move to sea (Figure 5). The height of the tsunami waves at this point reached a height of 4.9 m.

Fig 5. Loli-Pesua area, left satellite picture before earthquake, right after earthquake and tsunami

2.3 TONGGE (0.70137S 119.84438E)

At this point, according to satellite images, a strong displacement of the coastline by 100 meters on land is observed (Figure 6). The black line shows the GPS track along the modified coastline. A photograph of this coast is shown in the same figure, and the measured height of the tsunami wave run up in this area is 4 m.

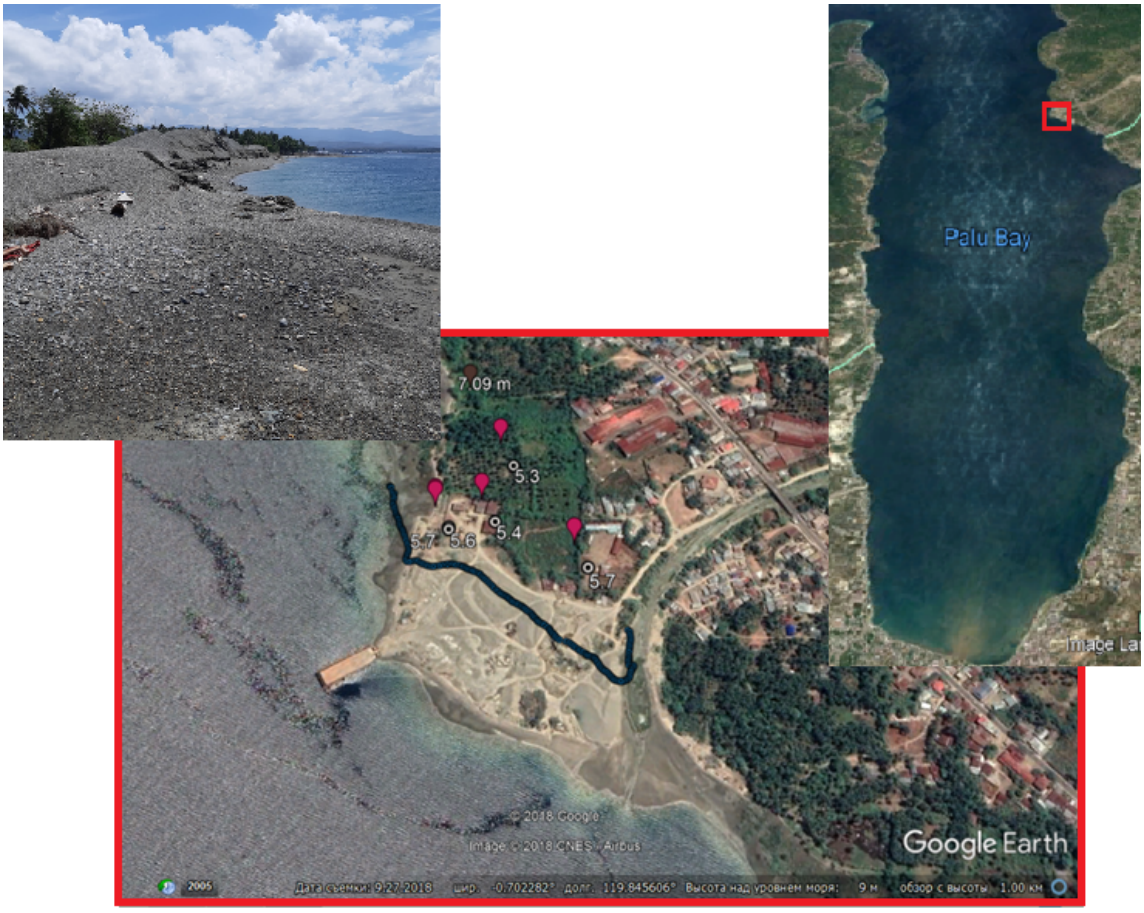

Fig. 5. Tongge area

2.4 BAMBA (0.7408S 119.8548E)

Witnesses reported that the first wave arrived 2-3 minutes after the earthquake. The height of the splashes reached a height of 4.5 m, and the height of the tsunami wave run-up was 2.9 m. The height of the water flow near the structure was 1 m. In this area, part of the coast was submerged by 2 m, which can be seen in the satellite image (Figure 7), and this is practically observed on the entire eastern coast of Palu Bay.

Fig. 7. Bamba region

2.5 PALU (0.8860S 119.8612E)

A survey of tsunami traces was carried out in the affected part of the city of Palu. Located in the center of Palu Bay, with a population of about 350,000, this town has an airport that has been damaged. The city was badly damaged after the earthquake and tsunami (Figure 8). A large bridge was destroyed and a park with buildings along the coastline was destroyed, which is especially clearly visible on satellite images (Figure 9). The height of the tsunami waves here reached a height of 11 m. After the earthquake, part of the coastal zone plunged into the sea to a depth of 2 m. Satellite images of the affected part of the city of Palu before and after this catastrophic event (Figure 9) show that most of the coastal zone is destroyed and soil erosion after the tsunami is observed in a significant area.

Fig. 8. Palu region

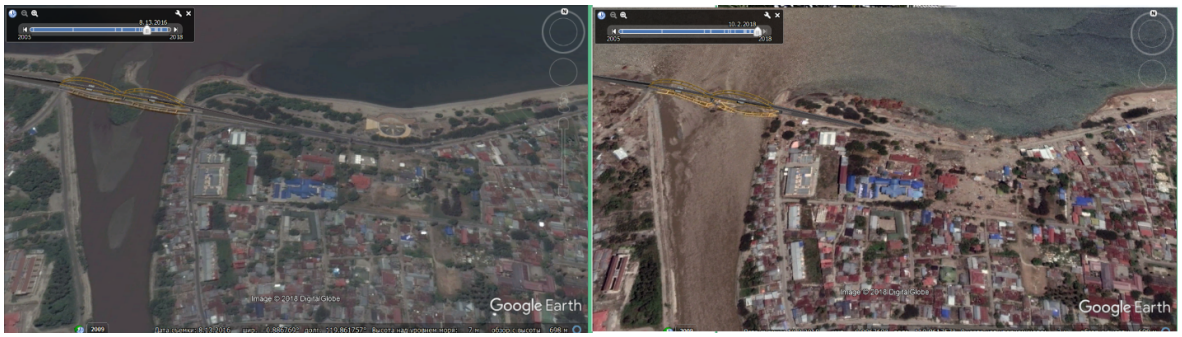

Fig. 9. Satellite image of Palu in the bridge area (left 2017, before the earthquake; October 2018, right, after the earthquake)

3. CONCLUSIONS

The paper presents data from satellite images of Sulawesi before and after the catastrophic earthquake and tsunami in 2018. These images allowed for better planning of the field survey of tsunami trails, in which the authors of the article participated. The importance of satellite images in their panoramic view, allowing you to see the characteristic changes in the landscape and understand their impact on the ecology of the coastal zone. The images show the rise and fall of the level to a height of up to 3 meters, depending on the position of the site from the fault. Detailed characteristics of the tsunami wave heights were obtained in the course of field studies. The earthquake and tsunami have been confirmed to have caused significant environmental changes in the region.

ACKNOWLEDGMENTS

The grants of President of the Russian Federation for the state support of Leading Scientific Schools of the Russian Federation (grant No. NSH- 2485.2020.5) and Young Russian Scientists – Doctors of Sciences (MD-148.2020.5) and RFBR 20-05-00162.
The grants of President of the Russian Federation for the state support of Leading Scientific Schools of the Russian Federation (grant No. NSH- 2485.2020.5) and Young Russian Scientists – Doctors of Sciences (MD-148.2020.5). Grant RFBR 20-05-00162.

REFERENCES

Heidarzadeh M., Muhar A., Wijanarto A.B., 2019. Insights on the Source of the 28 September 2018 Sulawesi Tsunami, Indonesia Based on Spectral Analyses and Numerical Simulations. *Pure Appl. Geophys*. 176 (2019), 25–43

Goda K., Mori N., Yasuda T., Prasetyo A., Muhammad A., Tsujio D., 2019. Cascading Geological Hazards and Risks of the 2018 Sulawesi Indonesia Earthquake and Sensitivity Analysis of Tsunami Inundation Simulations. *Frontiers in Earth Science* 2019, Volume 7, Article 261

Nakata K., Katsumata A., Muhari A. Submarine landslide source models consistent with multiple tsunami records of the 2018 Palu tsunami, Sulawesi, Indonesia Nakata *et al. Earth, Planets and Space (2020) 72:44* https://doi.org/10.1186/s40623-020-01169-3

Omira R., Dogan G.G., Hidayat R., Husrin S., Prasetya G., Annunziato A., Proietti C., Probst P., Paparo M.A., Wronna M., Zaytsev A., Pronin P., Giniyatullin A., Putra P.S., Hartanto D., Ginanjar G., Kongko W., Pelinovsky E., Yalciner A.C., 2020. The September 28th, 2018, tsunami in Palu-Sulawesi, Indonesia: A post-event field survey. *Pure and Applied Geophysics*, 2019, vol. 176, 1379 – 1395.

Sassa S., Takagawa T. 2919a. Liquefied gravity flow-induced tsunami: first evidence and comparison from the 2018 Indonesia Sulawesi earthquake and tsunami disasters. *Landslides* (2019a) 16:195–200. DOI 10.1007/s10346-018-1114-x

Zaytsev A.I., Pronin P.I., Giniyatullin A.R., Kurkin A.A., Pelinovsky E.N., 2019a. 28th September 2018 tsunami influence on an ecological situation at the Sulawesi island (Indonesia) *Ecological systems and devices.* 2019b No. 5, P. 25-29. DOI: 10.25791/esip.05.2019.624

Zaytsev A.I., Pelinovsky E.N., Yalciiner A., Susmoro H., Prasetya G., Hidayat R., Dolgikh G.I., Dolgikh S.G., Kurkin A.A., Dogan G., Zahibo N., Pronin P.I. , 2019b. Generation of the 2018 Tsunami on Sulawesi Island: Possible Sources *Doklady Earth Sciences*. 2019. V. 486. Iss. 1. P. 588-592. DOI: 10.1134/S1028334X19050295.

ISSN 8755-6839

SCIENCE OF **TSUNAMI HAZARDS**

Journal of Tsunami Society International

Volume 40 Number 4 2021

RUPTURE IMAGING FOR THE 30 OCTOBER TSUNAMIGENIC EARTHQUAKE IN THE EASTERN AEGEAN SEA

Madlazim, Muhammad Nurul Fahmi, Arie Realita, Dyah Permata Sari

Universitas Negeri Surabaya, Indonesia

ABSTRACT

On 30 October 2020, an earthquake with a moment magnitude Mw=7.0 occurred in the Aegean Sea close to the coasts of Turkey and of the Greek Island of Samos. The earthquake generated a local tsunami in the area, which had maximum amplitude of 2 meters, and inundation in certain coastal region of up to 155 times the run-up height. The present study provides a measure of the rupture dynamics of this tsunamigenic earthquake and provides the parameters of its rupture velocity, as well as the direction and length of the rupture by using beam forming and Multiple Signal Classification Back Projection (MUSICBP) techniques. In this present study we used 189 AK array stations and 153 European (EU) networks stations. The area of high frequency (HF) radiators extends almost bilaterally for more than 64 km along the rupture dynamics, with almost all ruptures having westward directivity. However, there was also an eastward rupture with high energy and low velocity. The timing of the HF radiators seen by both arrays were plotted against their epicenter distance slope 1 of the blue lines, which indicated rupture speeds of 1.9 km/s (slow), and the slope 2 of the yellow lines indicated very fast rupture speeds of 5 km/s, while the slope 3 of the purple lines indicated average rupture speeds of 3.3 km/s (regular).

Keywords: *Rupture imaging, back projection, rupture velocity, tsunami run-up*

1. INTRODUCTION

Seismologists have identified different types of earthquakes, which are mainly classified according to their duration and frequency during the process of releasing their energy. Several types of large slow earthquakes or non-regular, slow slip events (SSE), episodic and tremor slip earthquakes (ETS), silent earthquakes, and tsunamigeni earthquakes have been detected and observed in certain zones around the world. On October 30th, 2020, there was a magnitude 7.0 earthquake in the Aegean Sea, was followed by a tsunami with a maximum amplitude of 2 meters and 155 times run-up (National Geophysical Data Center / World Data Service: NCEI/WDS Global Historical Tsunami Database. NOAA National Centers for Environmental Information.doi: 10.7289/V5PN93H7).

The tsunami was generated in the Eastern Aegean Sea is interesting to study because such high tsunami wave run-up rarely occurs with earthquakes with a moment magnitude Mw = 7.0, particularly when the earthquake occurs on a normal fault, as this type of of this particular earthquake (Dogan, GG, et al., 2021). Riquelme, S. et al., (2018) have found a relationship between the number of tsunami run-up and the earthquake rupture velocity. They have measured the amplification due to very slow release moment. They found that this rupture velocity parameter plays a key role in run-up amplification. The smaller the earthquake rupture velocity, the greater the number of tsunami run-up. The rupture velocity (Vr) is related to the rupture duration (T) and the rupture length (L) of the earthquake as stated in the equation Vr=(L)/T. This means that the smaller the rupture velocity, the greater the duration of the rupture. Earthquakes that have a rupture duration greater than 50 seconds have the potential to cause a tsunami (Lomax and Micellini, 2011); Madlazim et al., 2021, 2020, 2017, 2013). Ma (2012) explains the possibility of a tsunami from a slow earthquake that changes the pore pressure when an earthquake occurs. In his work, simulations of dynamic pore pressure changes show that as dynamic pore pressures increase, due to upward propagation of rupture causes extensive yielding within the wedge, increase seafloor displacement. Ma and Hirakawa (2013) also suggested that due to dynamic wedge failure, it is possible to generate scenarios with more deformation in the trench, slower rupture rates and less seismic moments in the fault plane. Based on this relationship, it can be assumed that an earthquake that has a small rupture velocity or a slow earthquake has the potential to generate a tsunami. Riquelme1 and Fuentes (2021) have calculated the relationship between tsunami magnitude, rupture velocity and amplitude and the efficiency of very slow tsunamigenic earthquakes. The slow earthquake rupture velocity (< 2 km/s) is most likely to generate a tsunami.

Low velocity of earthquake rupture can be caused by a medium, which includes sediment. The North Aegean Sea and its surroundings are areas that have accumulated Tertiary sediments from the Eocene to the present. During this sedimentation, the general pattern of the basin appears to have been preserved. Overall, the basin has become more abundant in the south through time, and the NW trending basin has become more prominent (Ioannis K. Koukouvelas1 and Atilla Aydin (2002). On the basis of stratigraphy and structural data, it is suggested that the North Aegean Trench began to form during the Miocene. The basin analysis in the NW Turkey shows that the North Anatolian Fault

spreads westward to the Sea. The composition of the terrigenous fraction in the sedimentary sea reflects the geology of the surrounding landmass, as well as the dominant sedimentary processes. The terrigenous fraction in the Aegean Sea has its sources in the Aegean islands and medium-sized river drainage basins flowing into the Aegean Sea (İŞLER, EB, et al., 2016).

This present study focuses on measuring the rupture dynamics of the Mw=7.0 earthquake that generated a tsunami on October 30th, 2020 in the Eastern Aegean Sea, including the parameters of rupture velocity, direction, and length.

2. METHOD

Back projection of high frequency seismic waves (HF) recorded by dense arrays (Fletcher et al., 2006; Ishii et al., 2005) provides unique insights into earthquake rupture processes that complement the limited sources of traditional inversion. The back projection of the array aims to trace the area of the source that produces the highest frequency of the strongest radiation, only based on the phase and coherence of the seismic array signal. This provides a strong constraint on the spatiotemporal evolution of earthquake ruptures, without relying on the assumed Green function or on the restrictive kinematic parameterization of the rupture. We used the back projection method of P-wave seismic waveforms recorded by two arrays at teleseismic distances, AK array and the EU network (Fig. 1). We causally filtered the waveform from 0.5 to 1 Hz, the highest band where the coherent arrival initials are to be strongly aligned. We then applied two different array processing techniques: beam forming technique and Multiple Signal Classification Back Projection (MUSICBP) (Meng, L. et al., 2011; Bao, H., et al., 2019), a resolution technique designed to complete close-range simultaneous sources; and correlation stacking (Fletcher et al., 2006), a technique known to increase robustness in the presence of scattering. Our results based on these two techniques are mutually consistent. To create earthquake rupture imaging,

A back-projection method that uses teleseismic earthquake seismogram data is adopted, using a series of linear equations that relate the observed data to the model:

$$\mathbf{d = Gm} \tag{1}$$

Where d is teleseismic seismogram data from earthquakes with a moment magnitude > 6.5, “G” is Green's function, which is a synthetic seismogram calculated using a certain earth model, and “m” is the model, which is a slip function for each earthquake rupture. Conventional notation “d” is a data vector, “m” is a model vector, and “G” is a linear operator that predicts data from the model. The goal in geophysical inverse problems is to estimate “m” from observations, “d”. Assuming there are more data points than model points, the standard way to solve this problem is to define the residual vector, **r = d - Gm**, and find m that minimizes **r • r**. This is a least squares solution and it can be shown that:

$$m = (\mathbf{G}^{\mathbf{T}}\mathbf{G})^{-1}\mathbf{G}^{\mathbf{T}}\mathbf{d} \tag{2}$$

However, the $\mathbf{G}^T\mathbf{G}$ often is single or unconditioned, or maybe too big to flip. What can be done in these cases? The simplest and most crude way to proceed is to make the following estimation.

$$(\mathbf{G}^T\mathbf{G})^{-1} \approx \mathbf{I} \quad (3)$$

in this case we can estimate the model as

$$\mathbf{m} \approx \mathbf{G}^T\mathbf{d} \quad (4)$$

The GT transposition matrix is an adjoin or back-projection operator. Each model point is constructed as a weighted sum of the data points it affects. Could such a crude approach do any good? It is easy to think of examples where (3) invalid at all. However, in real geophysical problems, it is surprising how often this method works, especially if the scaling factor is allowed to bring the data and the model predicted data into better agreement, that is, assuming $(GT\ G)-1\approx\ I$, with λ being a constant. Indeed, it is sometimes observed that an adjoint (back-projection) performs better than a formal inverse because it is more tolerant of imperfections in the data.

In seismology, the available seismogram data is usually a set of seismograms. In source inversion, we usually assume that the structure of the Earth's velocity is known and we solve for the location and timing of the seismic wave radiator (e.g. solving the slip model). In reflection seismology, we usually assume that the location and time of the source are known and we solve for the location of the reflector that cause the observed arrival. In each case, model estimation at each model point are obtained by finding the time in the seismogram at which model changes will affect the seismogram. Summing or stacking the seismogram values at these points obtains the model estimation of the back-projection. The main thing to calculate is the travel time between the model point and each recording station. This provides the time shift needed to find the time in each seismogram that is sensitive to model disturbance.

The data used in this study are earthquake seismogram data recorded by AK array, and EU network stations (Fig. 2). The following is a map of the earthquake event on October 30th, 2020 that occurred in the Aegean Sea, Turkey and the stations of the 2 Arrays (Fig. 1).

2A. Back Projection App for the 30 October 2020 Earthquake

We used beam forming and Multiple Signal Classification Back Projection (MUSICBP) techniques from Meng, L. et al (2011) and Bao, H., et al (2019). In this study, the focus is on estimating the imaging rupture of the earthquake that occurred in the Aegean, Turkey on October 30th, 2020 using the Back Projection method. We used 189 AK array stations and 153 EU networks stations (Fig. 1). The data from the two locations are in the form of earthquake seismograms in SAC format recorded by AK array, and EU networks (Fig. 2) and downloaded from IRIS DMC via the following link http://ds.iris.edu/wilber3/find_stations/11331986.

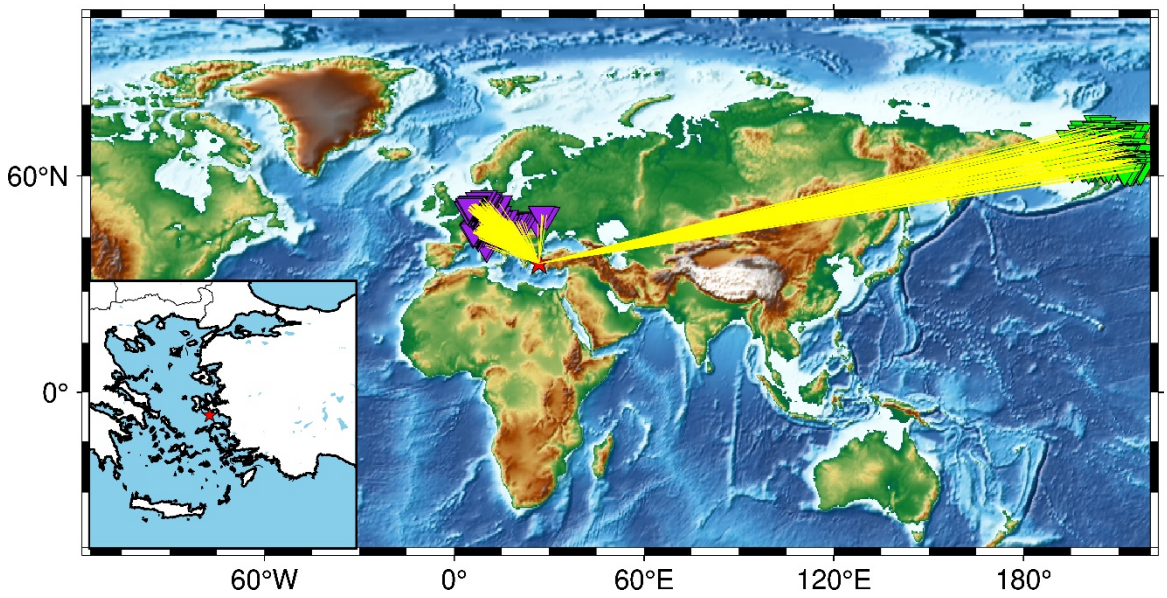

Figure 1. Epicenter of 30-10-2020 Aegean Sea, Turkey Earthquake (red star) and of EU network stations (group of purple triangles) and AK array (group of green triangles) distribution.

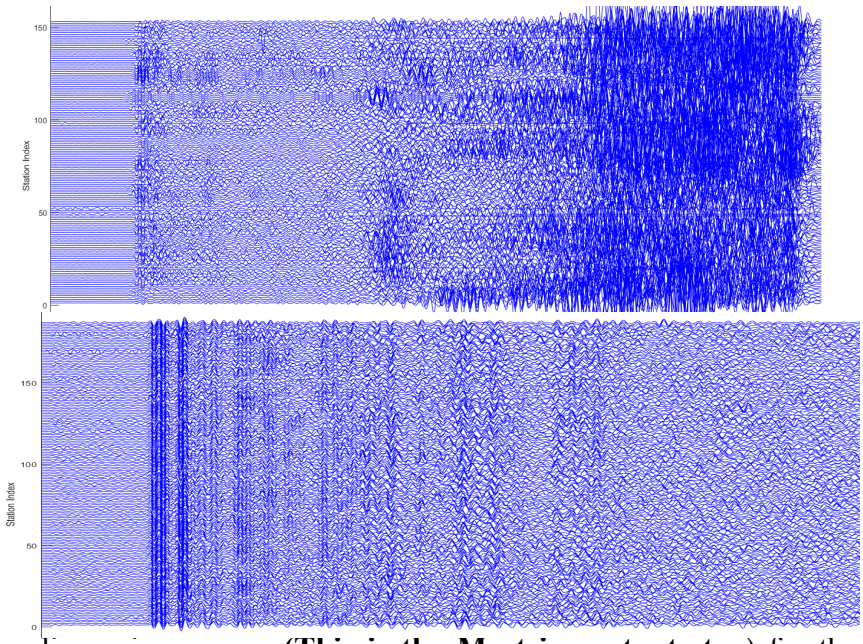

Figure 2. The align seismograms **(This is the Most important step)** for the AK array stations and EU network. The settings are suitable to align any first P arrival recorded at teleseismic distance. The top figure is seismograms from 153 stations of EU_network and bottom figure is seismograms from 189 stations of AK array.

3. RESULTS AND DISCUSSION

3A. High Resolution Array Analysis Using AK Array and European (EU) Network

Figure 3 shows the location of the strongest HF radiation region in a sliding window that is 25 seconds long. Secondary sources are often seen in our back projection images, for example between 26 and 50 seconds. However, our focus here is on first-order features that we can reliably identify by tracking the most coherent phases within each time window. The area of HF radiation extends almost bilaterally for more than 100 km along the rupture dynamics, almost all ruptures are westward, but there is an eastward rupture with high energy and low velocity (Fig. 3). It bridges the rupture area of several historic earthquakes in the Eastern Aegean Sea. The HF rupture is mostly westward from the hypocenter, and partially landward (Dogan, G.G., Yalciner, A.C., Yuksel, Y. et al., 2021). This ground-directed rupture dynamic has the highest energy (Fig. 4 left panel). It is very likely that this caused the enormous energy amplification that triggered the tsunami.

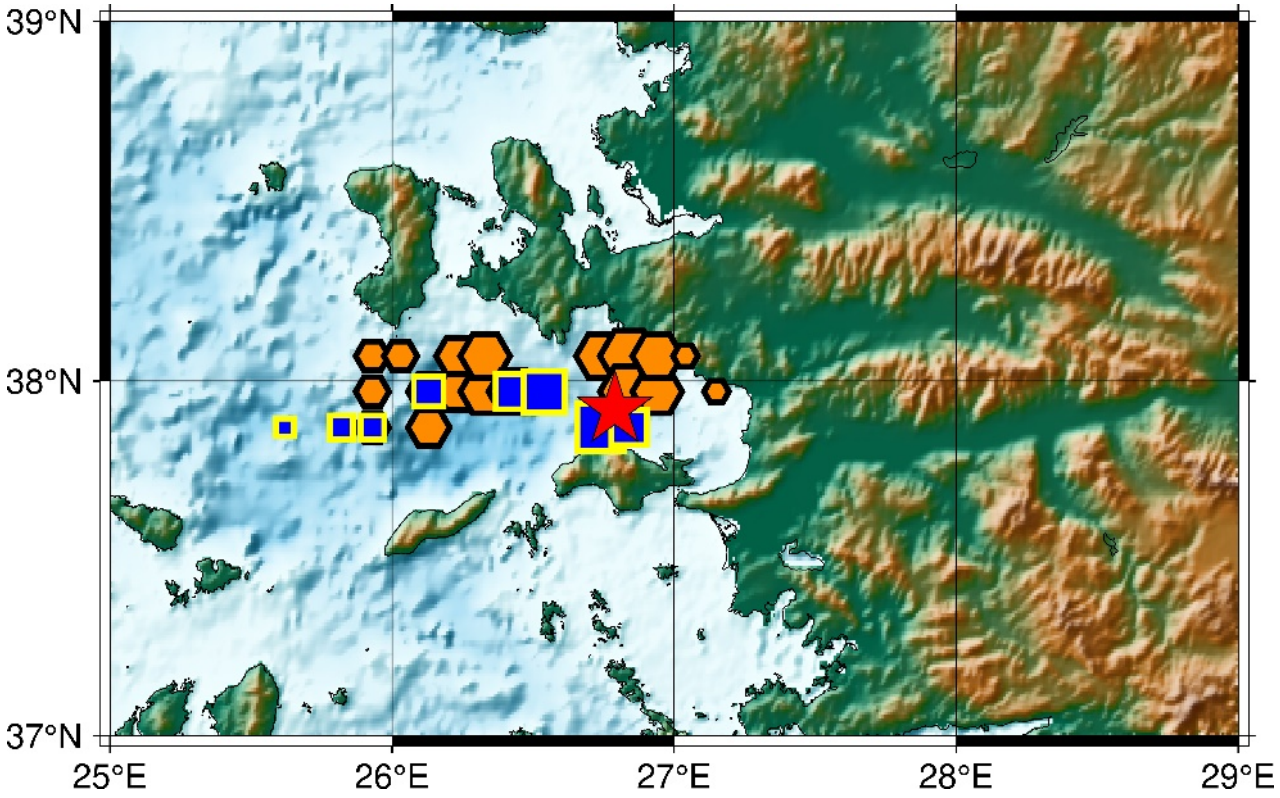

Figure 3. The Aegean Sea, Turkey earthquake imaged by the AK array and EU network. Location of the strongest high frequency radiators of the earthquake, seen by the AK array (blue squares) and by the EU network (brown polygons). The size indicate of relative amplitude of the energy. The red star is the epicenter of the earthquake.

3B. The Spatiotemporal Evolution of the Turkey Earthquake

In this study we used EU network and AK array stations. We have tried using AU array as well, but when we used AU array for the earthquake that occurred in the Aegean Sea on October 30th, 2020 an error occurred, so we decided to only used the AK array and EU networks. The result of this study is the time vs. relative amplitude of earthquake power (Fig. 4-left panel), which shows the temporal evolution of normalized amplitudes estimated at the AK array (blue) and at the European network (red). The numbers in circles mark the two phases with distinct rupture behavior. The timing of the high frequency radiators seen by both arrays are plotted against their epicenter distance, slope1 of the blue lines indicate rupture velocity of 1.9 km/s (slow), the slope2 of the yellow lines indicate very fast rupture velocity of 5 km/s, and the slope3 of the purple lines indicate average rupture velocity of 3.3 km/s (regular). For reference, the local crust S wave velocity is 3.42 to 4.5 km/s (Takahashi et al., 2004).

The length of the earthquake rupture can be estimated from Figure 4, which is about 64 km (Fig. 4-right panel). The spatiotemporal evolution of the strongest high frequency (HF) radiation is shown in Figure 4 right panel. Continuous HF Radiation energy was reliably imaged by our array back projection during the first 25 seconds of rupture (Fig 4 left panel). The overall size of HF rupture during this period of 0 to 10 seconds on average shows a low rupture velocity (1.9 km/s) along the 15 km rupture, which supports the higher tsunami run-up caused by this earthquake. Riquelme, S. et al., (2018) have found a relationship between the number of tsunami run-up and the earthquake rupture velocity. They have measured the amplification due to very slow release moment. They found that this rupture velocity parameter plays a key role in run-up amplification. The smaller the earthquake rupture velocity, the greater the number of tsunami run-up. Madlazim et al (2021a; 2021b, 2020, 2017, 2013) and Lomax and Michelini (2011) have also found that a strong indicator of a tsunami is the duration of an earthquake rupture that is more than 50 seconds. For rupture dynamics 11 seconds to 25 seconds the average shows a very high rupture velocity (5 km/s) along 50 km.

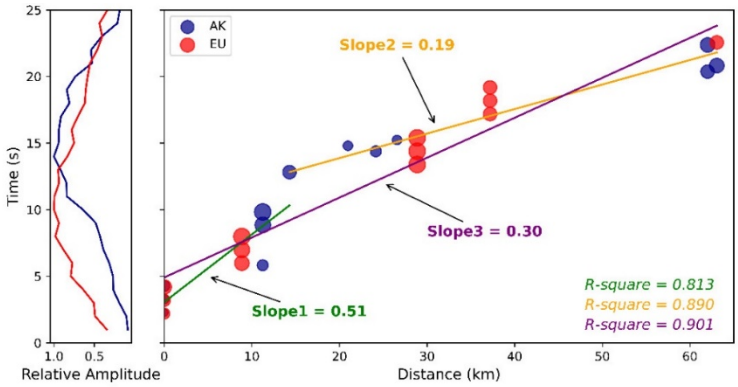

Figure 4. Rupture time versus epicenter distance. The timing of the high frequency radiators seen by both arrays is plotted against their epicenter distance. The color denotes AK array and EU network with respect to the epicenter and their relative amplitude normalized by the maximum amplitude during the event.

4. CONCLUSIONS

We have carried out a rupture imaging study for the earthquake that occurred in the Eastern Aegean Sea on October 30th, 2020. We used beam forming and Multiple Signal Classification Back Projection (MUSICBP) techniques. We found that the area of HF radiation extends almost bilaterally for more than 64 km along the rupture dynamics, and almost all of the ruptures are westward, but there is an eastward rupture with high energy and low velocity. The timing of the high frequency radiators seen by both arrays are plotted against their epicenter distance, slope 1 of the blue lines indicate rupture velocity of 1.9 km/s (slow), the slope 2 of the yellow lines indicate very fast rupture velocity of 5 km/s, and the slope 3 of the purple lines indicate average rupture velocity of 3.3 km/s (regular).

ACKNOWLEDGEMENTS

Our thanks go to Meng, L. and Bao, H. for allowing the use of the MUSICBP software for this research. We also thank IRIS DMC for allowing researchers to download earthquake data via the following link http://ds.iris.edu/wilber3/find_stations/11331986

REFERENCES

Bao, H., Ampuero, J. P., Meng, L., Fielding, E. J., Liang, C., Milliner, C. W., ... & Huang, H. (2019). Early and persistent supershear rupture of the 2018 magnitude 7.5 Palu earthquake. Nature Geoscience, 12(3), 200-205.

Fletcher, J. B., P. Spudich, and L. M. Baker (2006), Rupture propagation of the 2004 Parkfield, California, earthquake from observations at the UPSAR, Bull. Seismol. Soc. Am., 96(4B), S129–S142, doi:10.1785/ 0120050812.

Dogan, G.G., Yalciner, A.C., Yuksel, Y. *et al.* The 30 October 2020 Aegean Sea Tsunami: Post-Event Field Survey Along Turkish Coast. *Pure Appl. Geophys.* **178,** 785–812 (2021). https://doi.org/10.1007/s00024-021-02693-3

Ishii, M., P. M. Shearer, H. Houston, and J. E. Vidale (2005), Extent, duration and speed of the 2004 Sumatra‐Andaman earthquake imaged by the Hi‐Net array, Nature, 435(7044), 933–936

İŞLER, E. B., Ali Engin AKSU*, Richard Nicholas HISCOTT. 2016. Geochemistry of Aegean Sea sediments: implications for surface- and bottom-water conditions during sapropel deposition since MIS 5. *Turkish J Earth Sci* (2016) 25: 103-125©TÜBİTAK. doi:10.3906/yer-1501-35.

Koukouvelas Ioannis K., and Atilla Aydin. 2002. Fault structure and related basins of the North Aegean Sea and its surrounding. *TECTONICS*, VOL. 21, NO. 5, 1046, doi:10.1029/2001TC901037, 2002.

Lomax A, Michelini A (2011). Tsunami early warning using earthquake rupture duration and P-wave dominant period: the importance of length and depth of faulting. Geophysical Journal International 185(1): 283–291. https://doi.org/10.1111/j.1365-246X.2010.04916.x

Madlazim, Eko Hariyono, Muhammad Nurul Fahmi, Dyah Permata Sari. (2021a). Tsunami faulting model analysis for the 30 October 2020 normal earthquake. *Science of Tsunami Hazards*, accepted.

Madlazim, Prastowo T, Fahmi MN, Sari DP, Melianda E, Koesoema S. (2021b). Tsunamis from strike-slip and normal earthquakes and its relation with the product of dominant period and duration more than 50 seconds of earthquake P-wave. *Science of Tsunami Hazards*. 2021, 40(2), pp. 101–113

Madlazim Prastowo T, Fahmi MN (2020). Estimation of rupture directivity, CMT and earthquake tsunami parameters and their correlation with the main source of the first tsunami wave, September 28, 2018. *Science of tsunami hazards* 39(4): 228–242.

Madlazim (2017). Use of The Joko Tingkir Software for Rapid Determination of Tsunami Faulting Parameters Resulting From the Mw-7.8 Earthquake of March 2, 2016, in Southern Sumatra. *Science of Tsunami Hazards* 36(1): 41–48.

Madlazim (2013). Assessment of tsunami generation potential through rapid analysis of seismic parameters: Case study: Comparison of the Sumatra Earthquakes of 6 April and 25 October 2010. *Science of Tsunami Hazards* 32(1): 29-38.

Ma, S., and E. T. Hirakawa (2013), Dynamic wedge failure reveals anomalous energy radiation of shallow subduction earthquakes, *Earth Planet*. Sci. Lett., 375, 113 - 122, doi: 10.1016/j.epsl.2013.05.016.

Meng, L., A. Inbal, and J.-P. Ampuero. 2011. "A window into the complexity of the dynamic rupture of the 2011 Mw 9 Tohoku-Oki earthquake", Geophys. Res. Lett., 38, L00G07, doi:10.1029/2011GL048118.

Riquelme, S. , Fuentes, M. Campos, J., A. Schwarze, H. 2018**.** Implications on Tsunami Run-up due to Slow Ruptures Velocities. *American Geophysical Union*, Fall Meeting.

Sebastián Riquelme, Mauricio Fuentes; Tsunami Efficiency Due to Very Slow Earthquakes. *Seismological Research Letters* 2021;; 92 (5): 2998–3006. doi: https://doi.org/10.1785/0220200198.

Takahashi, N., S. Kodaira, T. Tsuru, J. O. Park, Y. Kaneda, K. Suyehiro, H. Kinoshita, S. Abe, M. Nishino, and R. Hino (2004), Seismic structure and seismogenesis off Sanriku region, northeastern Japan, Geophys. J. Int., 159(1), 129–145, doi:10.1111/j.1365-246X.2004.02350.x.

Kiser, E., & Ishii, M. (2017). Back-projection imaging of earthquakes. Annual Review of Earth and Planetary Sciences, 45, 271-299.

ISSN 8755-6839

SCIENCE OF **TSUNAMI HAZARDS**

Journal of Tsunami Society International

Volume 40 **Number 4** **2021**

SEISMIC WAVE PROPAGATION IN BANDUNG BASIN, WEST JAVA

Anggun Mayang Sari[1]; Afnindar Fakhrurrozi[1]; Arifan Jaya Syahbana[1,2]; Dwi Sarah[1]; Mudrik Rahmawan Daryono[1]; Bambang Setiadi [1]; Rabieahtul Abu Bakar[3]; Jian Cheng Lee[4,5]

[1]Research Centre for Geotechnology – National Research and Innovation Agency (BRIN), Jl. Sangkuriang Gd 70, Bandung 40135, Indonesia
[2]Faculty of Civil and Environmental Engineering, Bandung Institute of Technology, Bandung, Indonesia
[3]Razak Faculty of Technology and Informatics, University Technology Malaysia (UTM), Kuala Lumpur, Malaysia
[4]Institute of Earth Science, Academia Sinica, Taipei, Taiwan
[5]Integrated Research on Disaster Risk-International Centre of Excellence (IRDR-ICoE), Taipei, Taiwan
contact email: anggun.mayang.sari@brin.go.id; anggunnmayangsari@gmail.com

ABSTRACT

Wave propagation is a fundamental issue in all over seismic prone areas, including in the Bandung basin. Bandung basin consists of several geological formations. Based on the tectonic conditions, this area is surrounded by active seismic sources. Several main faults play a role part in dynamic soil conditions. Wave propagation from earthquake shaking has a significant impact on the soil surface. Recent studies in the Bandung basin showed the seismic hazard on the bedrock, but less understanding of hazard on the soil surface. Building construction failures caused by the soil surface's ground-shaking correlate linearly with the Peak Ground Acceleration (PGA) value. This paper discusses the soil surface acceleration on the Bandung basin using the wave propagation method using a non-linear seismic response analysis. The result shows that the highest soil surface acceleration is found in the Tanjung Jaya village, while the lowest is in Ciwastra village. The PGA value varies between 0.42g to 0.70 g. The seismic ground-motion strongly influences these results on bedrock and soil stratigraphy in the survey area.

Keywords: *wave propagation; Bandung basin; soil surface; ground-motion; PGA*

1. INTRODUCTION

The seismic hazard zone is an area that is at risk of experiencing the impact of earthquake events, such as landslides, liquefaction, building failure and human fatality. The seismic zone location is generally close to the seismic hazard zone, the seismic source focus. Nevertheless, many attractive tourism area locations are inside of the earthquake source (Orchiston, 2010). Some of these tourism places, such as Sianok Valley, located at Semangko fault line in West Sumatera and Lembang tourist area, settled down at the top of Lembang fault in West Java (Sieh et al., 2000; Novianti et al., 2021).

These areas then transformed entirely into densely populated area that urgently requires preparedness efforts for disaster risk reduction. The seismic event in Bandung basin occurred more frequently in thelast two decades. The distribution of earthquake sources that affect seismicity in the Bandung Basin area is shown in Figure 1. Some of them have a more significant impact due to their location close to the Bandung Basin, namely Lembang Fault, Cimandiri Fault and Baribis Fault.

The Lembang Fault has a length of 29 km, stretches from Cipogor to Batu Lonceng area (Daryono, 2019). Moreover, the slip rate moves continuously by 1.95–3.45 mm/year. It also has magnitudes around Mw 6.5 – 7.0 with a recurrence time between 170-670 years. As for Cimandiri Fault is materialized in the form of a straight valley and hills that stretches from the west of Pelabuhan Ratu to the east of Mount Tangkuban Parahu (Haryanto et al., 2017). Meanwhile, The Baribis Fault is located in the eastern part of West Java, which stretches from the Subang area to Majalengka and Kuningan (Bemmelen, 1949).

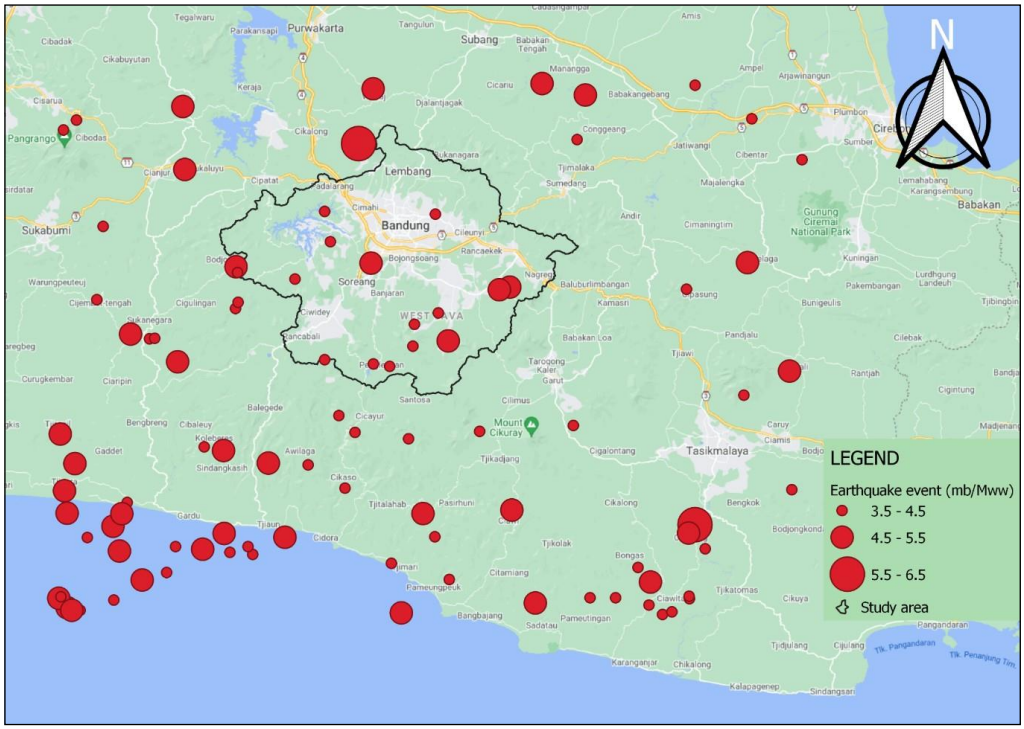

Figure 1. A series of earthquake events in the last 20 years in the surrounding Bandung basin (USGS., 2021).

Several major earthquakes have caused heavy losses of both property and life in the Bandung basin. One of the major earthquakes that involved significant damage was the Tasikmalaya earthquake on September 2, 2009, with an earthquake magnitude of 7.0 Mw in a depth of 46.2 km(Meilano et al., 2010). It caused 771 people to be injured, 23 people have died, and 75805 residents were evacuated (Badan Penanggulangan Bencana Nasional, 2009). Furthermore, it also caused heavy damage to physical infrastructure, around 15,538 residential houses were severely damaged, and 30,591 houses were slightly damaged (Pusat Data Informasi dan Komunikasi Kebencanaan, 2021).

In this study, we hypothesized that the earthquake wave on the soil surface has a significant correlation with the number of building failures and lives losses based on the existing dataset. Hence, we analyzed the seismic wave propagation from bedrock to soil surface using non-linear earthquake response analysis. Several vital factors in the study are ground-motion characterization at bedrock and geological interpretation on specific survey locations. The dynamic soil response on the surface quantity is shown from the PGA value.

2. GEOLOGICAL SETTING

Bandung city and its surroundings consist of a large intermountain basin surrounded by volcanic highlands. The central Bandung plain is situated at 665 m above sea level and is surrounded by up to 2400 m high Late Tertiary and Quaternary volcanic terrain (Dam et al., 1996). The Bandung basin is bounded by the Tangkuban Perahu volcanic complex, Mandalawangi Mount in the North to the East, and Patuha-Patuha-MalabarMalabar volcanic complex in the South. The Bandung basin is considered a graben-like depression controlled by geological structure and lithology, as shown in Table 1 (Delinom, 2009).

Table 1. The lithology of the Bandung basin (Hutasoit, 2009; Silitonga, 1973).

Formation	Remarks
Tertiary sedimentary and volcanic rocks	The Tertiary sedimentary and volcanic rocks are the oldest units of Late Miocene to Early Pliocene, widely exposed in the West Bandung.
Cikapundung Formation	Cikapundung Formation comprises the intercalation of volcanic breccia and conglomerates, lahar, and lava of Pleistocene age. This Formation lies unconformably on top of the Tertiary rocks. The Cikapundung Formation occupies the northern part the of Bandung basin.
Cibereum Formation	Cibereum Formation consists of a sequence of volcanic breccia and tuff deposits with some lava intrusion, is of Late Pleistocene to Holocene age. The Cibereum Formation and other Quartenary volcanic products from volcanic fans spreading from the northern and southern volcanic complexes to the centre of the basin

Kosambi Formation	Kosambi Formation is of the Holocene age, widely distributed in the centre of the Bandung Basin. Kosambi Formation consists of unconsolidated clay, organics, silt, and sandstone, also known as the lake deposit. This Formation is inter-fingering with the Cibereum Formation.

Major geological faults and lineaments in the study area are generally E-W, SW-NE, SE-NW oriented, and a few are oriented almost N-S (Figure 2) (Marjiyono et al., 2008). The E-W faults are the Lembang fault at the North and Gunung Geulis and Citarum faults at the South. SW-NE faults are the Cicalengka and Cileunyi-Tanjungsari faults, and the almost N-S fault is Bandasari fault; all these faults are left strike-slip faults. A conspicuous geomorphic ridge trending east-west of 29 km is observed in the North part of the Bandung basin, the Lembang active fault. Dam (1996) divided the Lembang fault segments into a normal fault in the western part and strike-slip in the East part. According to Daryono et al. (2018), the Lembang fault has predominantly sinistral movement capable of generating 6.5-7.0 Mw earthquake with a recurrence time of 170-670 years.

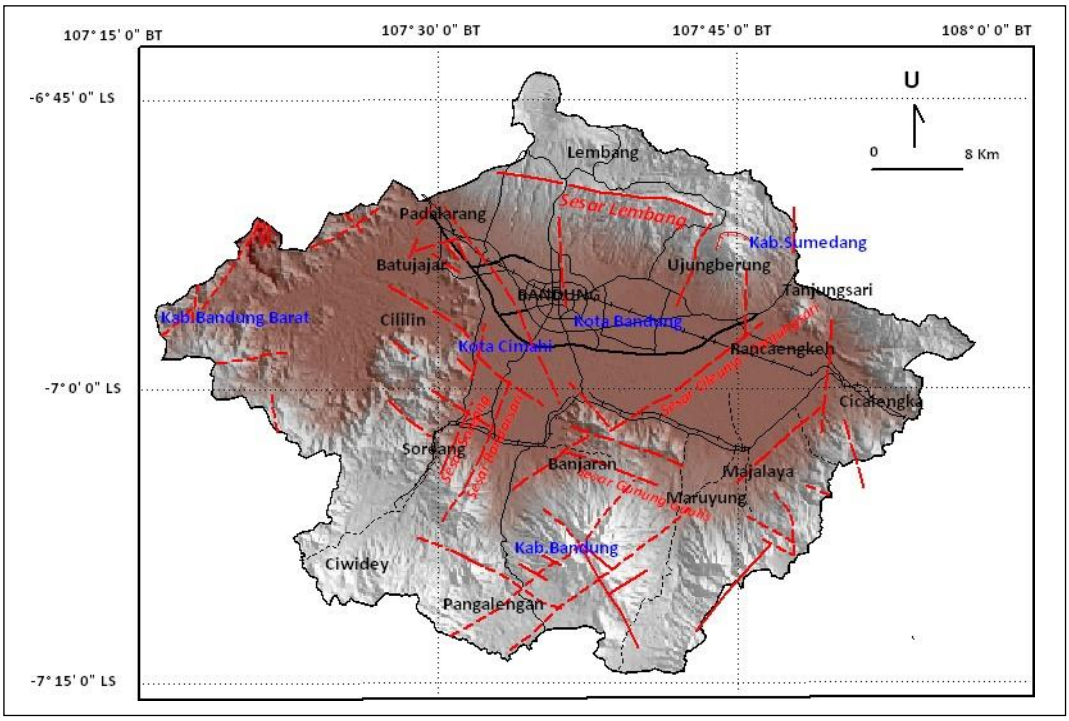

Figure 2. Geological Condition and Tectonic Setting of Bandung basin (compiled and modified from Silitonga (1973), Marjiyono (2008), Hutasoit (2009), Daryono (2018)).

The study locations spread on 35 soil investigation test locations in Bandung basin. The soil investigation test consists of the Cone Penetration Test unit (CPTu) and Bore Hole test (BH). These locations are distributed on several regencies in Bandung basin: Bandung City, Bandung regency, and West Bandung Regency. The distribution of survey point locations can be seen in Figure 3.

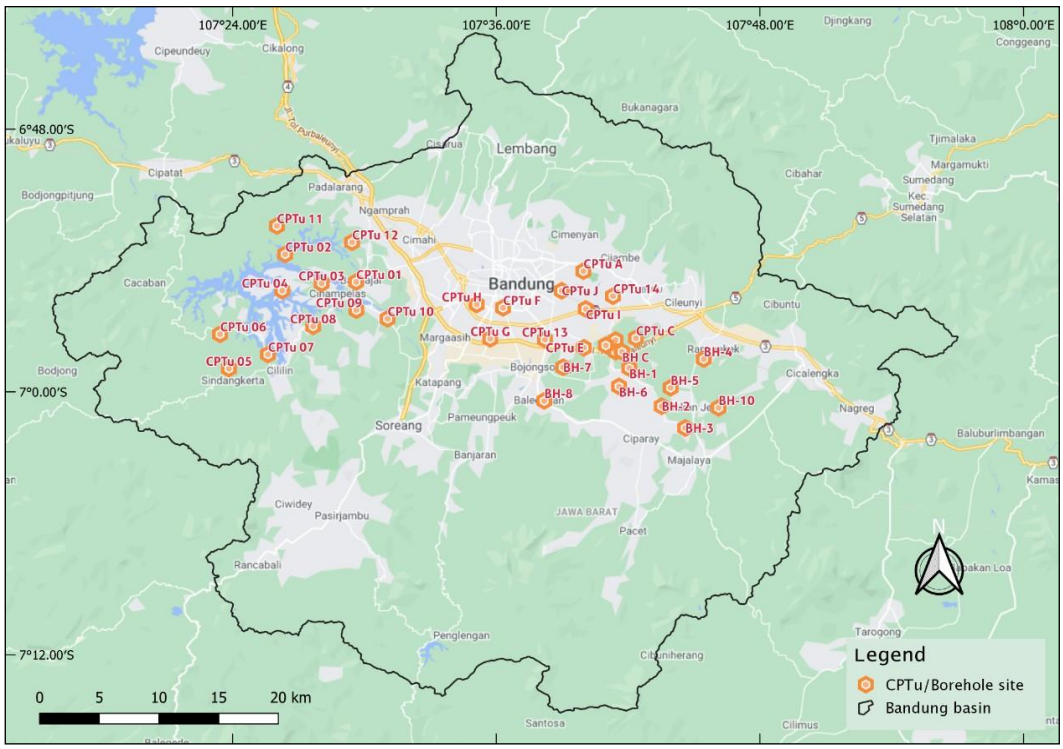

Figure 3. Study locations of wave propagation analysis in Bandung basin

3. METHODS

A. Ground Motion Synthetic (GMS) Modelling

The GMS. Modelling is a technique for generating the series event of acceleration, velocity or displacement concerning the function of time that correspond to ground motion modification in other locations (Gavin & Dickinson, 2011; Vlachos et al., 2018). There are several steps in the input data preparation before the GMS modelling. Firstly, the Probabilistic Seismic Hazard Analysis (PSHA) was used for the ground motion quantification at a particular location in a period of time. The PSHA computation also considers various earthquake mechanisms sources, which are faults, shallow to deep backgrounds, and megathrust. The earthquake source was determined using the logic tree of the Ground Motion Prediction Equation (GMPE). The 2017 Indonesia earthquake source mechanism compilation can be seen in Table 2 (Azwar et al., 2021; Irsyam et al., 2020; Sari et al., 2019; AJ Syahbana et al., 2021; Yuliastuti et al., 2021).

Table 2. The logic tree of GMPE.

No	Seismic Source	GMPE and Weighting
1	Active shallow crust (Fault and Shallow Background)	Boore Atkinson 2008 0.2 Campbell Bozorgnia 2008 0.2 Chiou Youngs 2008 0.2 Boore et al. 2014 0.133 Campbell Bozorgnia 2014 0.133 Chiou Youngs 2014 0.134

2	Subduction/Megathrust	Youngs et al. 1997 Sinter 0.15 Atkinson Boore 1995 GSC Best 0.15 Zhao et al. 2006 Sinter 0.30 Abrahamson et al 2015 Sinter 0.40
3	In slab Subduction (Deep Background)	Youngs et al 1997 SSlab 0.333 Atkinson Boore 2003 SSlab NSHMP 2008 0.333 Atkinson Boore 2003 SSlab Cascadia NSHMP 2008 0.334

Secondly, the de-aggregation or disaggregation technique was used to obtain the most dominant earthquake source in sequential time. Thirdly, earthquake records selection has parameters that are close to the result of the deaggregation. The equations are given by

$$M_{dominant} = \frac{\Sigma\, M_i\, x\, (\text{contribution of events/year})}{\Sigma\, (\text{contribution of events/year})} \quad (1)$$

$$R_{dominant} = \frac{\Sigma\, R_i\, x\, (\text{contribution of events/year})}{\Sigma\, (\text{contribution of events/year})} \quad (2)$$

With M is magnitude (Mw) and R is the distance (km). In this study, a synthetic ground motion was made using the EzFrisk software since no actual earthquake data recordings were available (Risk Engineering, 2011; A. Syahbana et al., 2019). The output of GMS will later be used in conducting further analysis, for example, wave propagation on the surface or as input for dynamic modelling of building structures.

B. Wave Propagation methods

Previous studies related to wave propagation of seismic motion on the surface have been accomplished using a similar algorithm (Scanlan, R. H. , 1976; Semblat et al., 2005; Semblat, J.F., 2011; Cheng et al., 2020). In contrast, Bardet and Tobita (2001) successfully developed a new algorithm for seismic wave propagation on the surface. It consists of non-linear elements to model soil behavior as the repercussions of earthquake waves. This algorithm is manifested into an application known as Nonlinear Earthquake Response Analysis (NERA). The main parameters of NERA are stress-strain, velocity, amplification by considering material models such as linear equivalent models, viscoelastic models and material models.

The first stage in the NERA modelling is an initialization, followed by the strain increment, strain andstress computation that is given by:

$$\gamma_{i,n} = \frac{d_{i+1,n} - d_{i,n}}{\Delta\, z_i} \quad (3)$$

$$\tau_{i,n} = IM(\tau_{i,n-1}, \Delta\, \gamma_{i,n} \quad (4)$$

Where $\gamma_{i,n}$, $\tau_{i,n}$, $d_{i,n}$, and z_i are the strain, the stress, displacement and thickness at node i (1, ..., n) respectively. NERA modelling use IM model to simulate non-linear stress-strain curves. The second stage of NERA modelling is to compute the velocity that is given by:

$$V_{i,n} = V_{i,n-1} + \frac{1}{2}(a_{i,n} + a_{i,n-1})\,\Delta t \tag{5}$$

Where $V_{i,n}$, $a_{i,n}$ are the velocity and the acceleration at node i (1, ..., n) and time respectively. The predicted velocity at time t_n and t_{n+1} can be obtained using $V_{i,n}$ and the Newmark algorithm is given by:

$$\tilde{v}_{N,n+1} = \frac{\tilde{v}_{N,n}(\Delta z_{N-1} - v_s \Delta t) + 4 v_s V_{i,n} \Delta t - 2\tau_{N-1,n}\frac{\Delta t}{\rho_N}}{\Delta z_{N-1} + v_s \Delta t} \tag{6}$$

Where $\tilde{v}_{N,n+1}$ is predicted velocity at N grid and n (n, …., n+1) sequence, is depth, and is unit mass. The final step in NERA modelling is to compute displacement (d), velocity ( ) and acceleration ( ) using equations on each parameter, given by:

$$d_{i,n+1} = d_{i,n} + \tilde{v}_{i,n+1}\,\Delta t \tag{7}$$

$$v_{i,n} = \frac{1}{2}(\tilde{v}_{i,n+1} + \tilde{v}_{i,n}) \tag{8}$$

$$a_{i,n} = \frac{1}{2}(\tilde{v}_{i,n+1} + \tilde{v}_{i,n}) \tag{9}$$

The result of wave propagation from bedrock to the ground surface computation can be acquired from the highest acceleration value, as shown in Figure 4. The main parameters as input data in the NERA modelling that need attention are ground motion data in the bedrock and soil layer data. The ground motion data is the earthquake input motion data that was acquired from the ground-motion synthetic modelling. While the soil layer data were obtained from the soil field investigation test data, namely the cone penetration test and the borehole test.

C. Amplification factors

The amplification factor is a ratio of peak ground acceleration on bedrock to peak ground accelerationon the soil surface (Horri et al., 2019). The equation for calculation amplification factor is given by:

$$F_{PGA} = \frac{PGA_{surface}}{PGA_{bedrock}} \tag{10}$$

Where $PGA_{surface}$ is peak ground acceleration based on wave propagation calculation (g), and $PGA_{bedrock}$ is peak ground acceleration based on ground motion at bedrock (g).

The amplification factor was applied to validate the amplification factor from the previous calculation using site class coefficients. The amplification factor was determined using site coefficient FPGA from ASCE 7-10, as shown in Table 3.

Table 3. F_{PGA} Site Class Coefficient.

Site Class	Peak ground acceleration adjusted from site class				
	PGA≤0.1	PGA=0.2	PGA=0.3	PGA=0.4	PGA≥0.5
A	0.8	0.8	0.8	0.8	0.8
B	1.0	1.0	1.0	1.0	1.0
C	1.2	1.2	1.1	1.0	1.0
D	1.6	1.4	1.2	1.1	1.0
E	2.5	1.7	1.2	0.9	0.9
F	See section 11.4.7				

The site class of study locations were determined using ASCE 7-05 Site Class Definitions. The CPTu and borehole data are collected to analyze the average standard penetration resistance ($\bar{N}$). After calculating $\bar{N}$ value, the site class of certain point locations can be defined using Table 4.

Table 4. Site Class Definitions from ASCE 7-05.

Site Class	Site Profile Name	Soil Shear Wave Velocity, $\bar{V}_s$ (ft/sec)	Standard Penetration Resistance, $\bar{N}$	Undrained Shear Strength, $\bar{S}_u$ (psf)
A	Hard rock	$\bar{V}_s$ > 5,000	NA	NA
B	Rock	2,500 < $\bar{V}_s$ ≤ 5,000	NA	NA
C	Very dense soil and soft rock	1,200 < $\bar{V}_s$ ≤ 2,500	> 50	> 2,000 psf
D	Stiff soil	600 < $\bar{V}_s$ ≤ 1,200	15 to 20	1,000 to 2,000 psf
E	Soft clay soil	$\bar{V}_s$ ≤ 600	< 15	< 1,000 psf
		Any profile with more than 10 ft of soil having the following characteristics: • Plasticity index PI> 20 • Moisture content ω ≥ 40%, and • Undrained shear strength S_u < 500 psf		
F	Soil requires site response analysis	Liquefiable soils, peat, high plasticity clay		

4. RESULTS AND DISCUSSION

A. GMS on Bedrock

The dominant seismic sources resulting from the GMS modelling on bedrock are earthquakes originating from Lembang Fault and West Central Java Megathrust. The maximum acceleration values were obtained by performing spectral matching on dominant M and R. The results of GMS modelling as shown in Table 5.

Table 5. Ground motion acceleration on bedrock ($PGA_{bedrock}$)

Point Location	a_{max} (g)	Point Location	a_{max} (g)	Point Location	a_{max} (g)	Point Location	a_{max} (g)	Point Location	a_{max} (g)
BH-01	0.50	BH-08	0.52	CPTu-06	0.53	CPTu-13	0.46	CPTu-D	0.48
BH-02	0.51	BH-10	0.50	CPTu-07	0.51	CPTu-14	0.50	CPTu-E	0.48
BH-03	0.49	CPTu-01	0.58	CPTu-08	0.53	BH-A	0.49	CPTu-F	0.49
BH-04	0.55	CPTu-02	0.60	CPTu-09	0.51	BH-B	0.49	CPTu-G	0.50
BH-05	0.49	CPTu-03	0.52	CPTu-10	0.54	BH-C	0.49	CPTu-H	0.53
BH-06	0.51	CPTu-04	0.69	CPTu-11	0.69	CPTu-A	0.62	CPTu-I	0.50
BH-07	0.54	CPTu-05	0.52	CPTu-12	0.67	CPTu-C	0.51	CPTu-J	0.51

The peak ground acceleration on bedrock (PGAbedrock) value varies from 0.46g to 0.69g. The maximum acceleration found on CPTu-04, which is located at Tanjung Jaya village, West Bandung Regency. The PGAbedrock value is around 0.69g, heavily influenced by Lembang fault mechanism, based on deaggregation analysis. The point location is closed to Lembang fault. Meanwhile, the minimum acceleration value on bedrock found on CPTu-13, around 0.46g. This point location is located at Buah Batu district, Bandung City. From the deaggregation analysis result, the ground-motion acceleration is affected by the West-Central Java Megathrust mechanism.

B. Peak Ground Acceleration on Surface

After calculating the GMS on bedrock, the next step to estimating PGA on the ground surface. It is to interpret the soil layer profile. The soil layer profile was obtained from the CPTu test and BH test. The cross-section from the Northwest (NW) to the Southeast (SE) of Bandung basin, as shown in Figure 4. Clay deposits dominate the soil properties, while some organic soils are found in the middle of soil depth. The sand soils are distributed at the thin layer over the section and become thicker at the bottom of the soil depth. Difference to NW-SE section, the Northeast (NE) to southwest (SW) cross-section has the heterogeneity of soil deposit, as shown in Figure 5. The organic soil and clay to silty clay soil are found at 35 meters of soil thickness. The volcanic breccia was also found at CPTu-G to CPTu-H cross-section. The hard soil settles down from 601 to 641 meters above sea level, consisting of silt soil and granular sand soil. The altered volcanic breccia lay down at 601 meters above sea level, located under the granular soil layer.

The soil profile and GMS data were used as input in surface soil acceleration modelling. The soil profile uses geological interpretation data from soil investigation tests. The results of the PGA on the surface analysis in Bandung basin area can be seen in Figure 6.

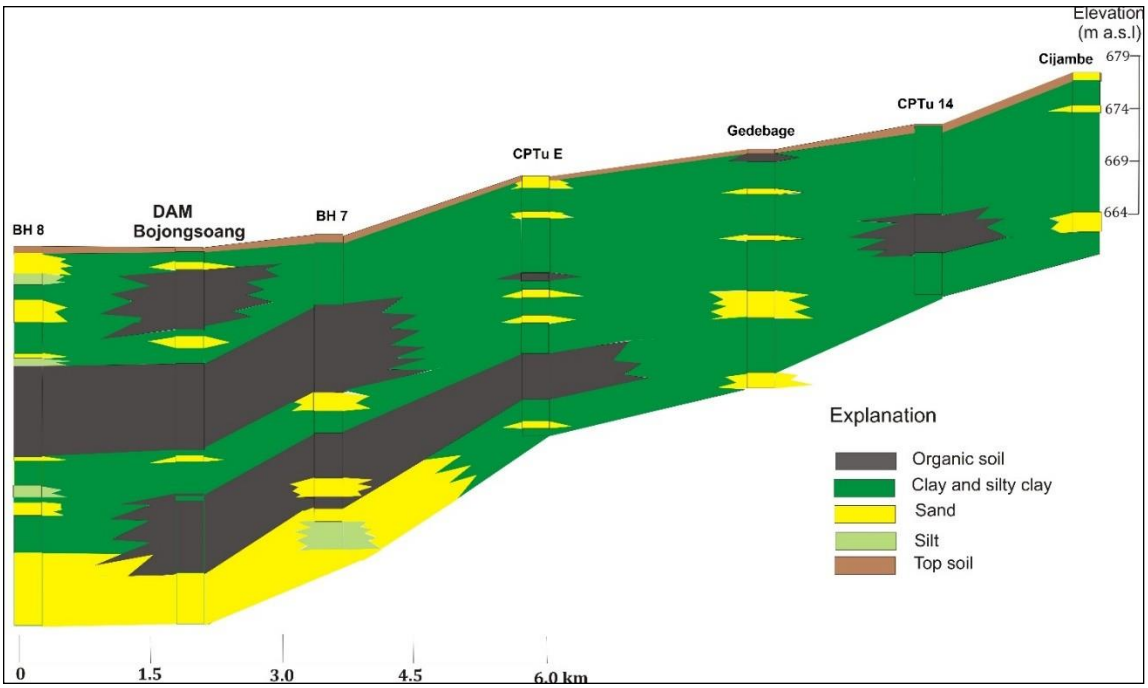

Figure 4. Cross section of Bandung basin from NE – SW

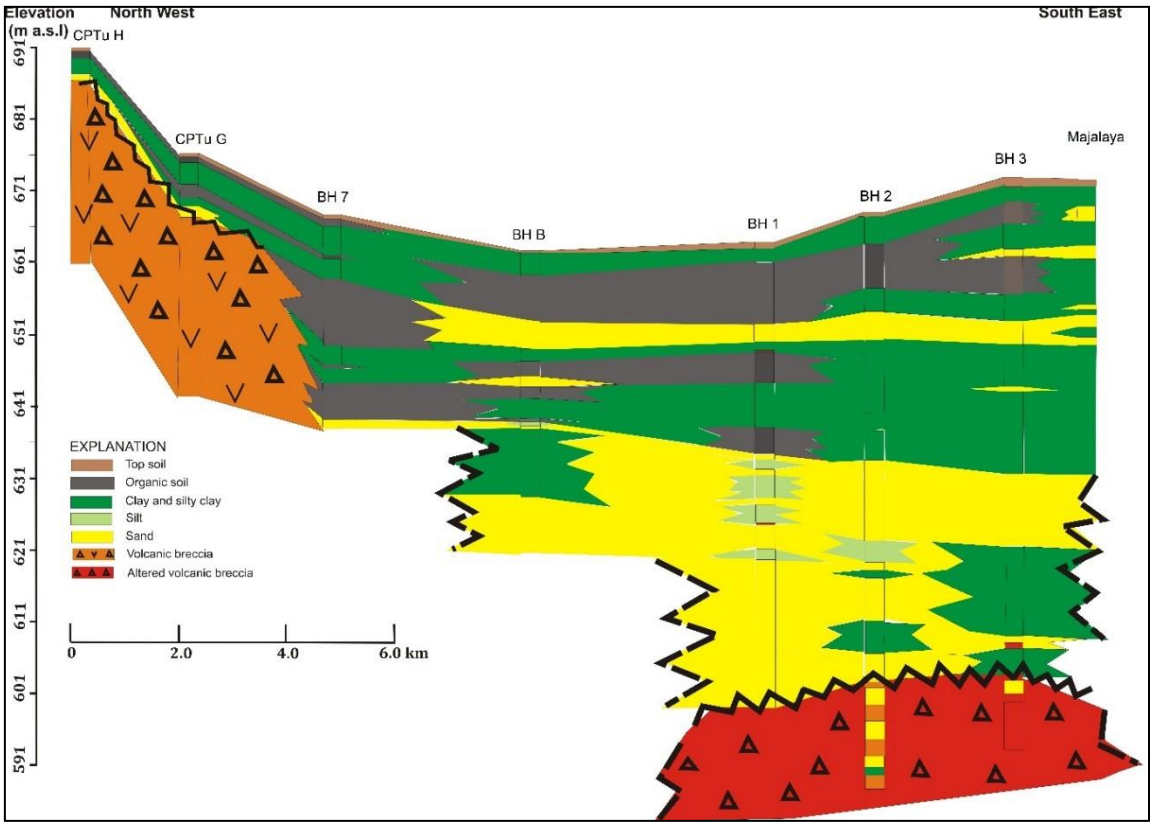

Figure 5. Cross section of Bandung basin from NW – SE

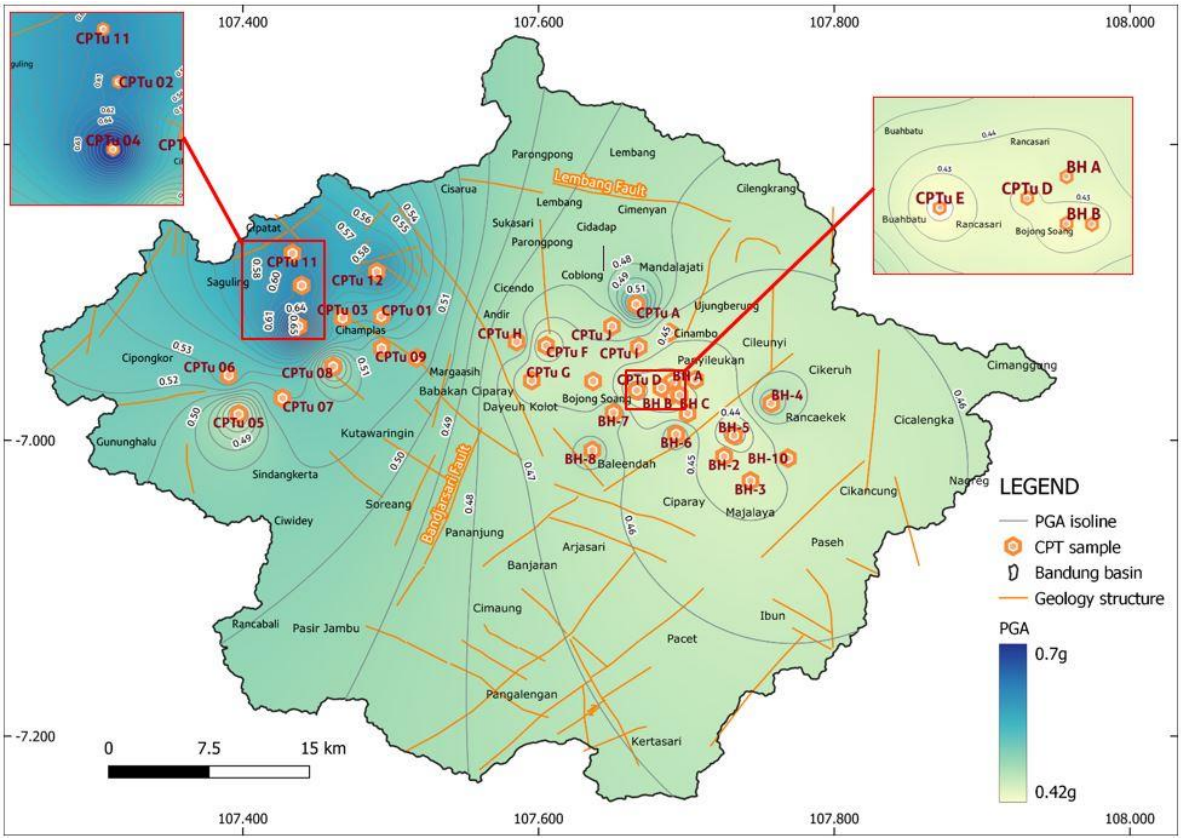

Fig. 6. Seismic Wave Propagation Map using $PGA_{surface}$ value on Bandung basin

Based on wave propagation analysis from bedrock ground-motion to the soil surface, the maximum PGA on the ground surface (a_{max},surface) is found at CPTu-04, which is located at Tanjung Jaya village, West Bandung regency. The result shows a value of 0.70g. The surface acceleration value is strongly influenced by stiff soil deposits that consist of silt soil and sand soil in 20 meters depth based on Cone Penetration Test data. This result is also affected by the ground- motion analysis at bedrock, where the bedrock acceleration value is relatively high, which is about 0.69g. The geological lithology on this location consists of tertiary sedimentary rocks. Besides, the tectonic condition plays a vital role in the bedrock acceleration since Lembang Fault is closed to this location.

Unlike Tanjung Jaya village, the minimum PGA value on the soil surface is found at Ciwastra village, Bandung City. The CPTu-E is located in this area. The surface acceleration value is around 0.42g. This value is affected by the soft soil deposit obtained 25 meters deep using the Cone Penetration Test. The soft soil deposit is dominated by clay soil and silt soil.

In contrast to the CPTu-04 case, the bedrock acceleration on CPTu-E is higher than the soil surface acceleration. The bedrock acceleration showed a value of 0.48g, while the soil surface acceleration presented a 0.42g value. The de-amplification phenomenon is happened in this location due to the thick, soft soil conditions (Villalobos et al., 2019; Midorikawa et al., 2014).

C. Amplification Factors

The ratio of amplification factor using PGA bedrock to PGA surface values can be seen in Table 6. The table presents the amplification factors (FPGA) value that varies from 0.9 to 1.0. Most of the area on Bandung regency and a few parts of Bandung City has an FPGA value is 0.9. From the cross-section of NW-SE and NE-SW, these locations are formed by soft soil deposits. These areas also lay down on the top of Kosambi formation, which is consists of clay, organics, silt, and sandstone.

In contrast to these locations, the West Bandung regency is dominated by stiff soil consisting of sand, silt, and rock formation. The FPGA value is 1.0. These locations settle down at the Cibereum Formation, tertiary sedimentary and volcanic rocks formation consisting of volcanic breccia and tuff deposits.

Validation of the amplification factor using dataset resulting from calculation to the amplification factor using site class coefficient, as shown in Table 7. The site class of 35 study locations in Bandung basin is also presented in this table. From this table, the site class E provides in Bandung regency and a few areas of Bandung City. Meanwhile, site class D shows some parts of West Bandung regency, which is CPTu-02, 03, 04, 07, 09 and CPTu-13 at Bandung City. Site class C remarkably is found at CPTu-06, which is located at West Bandung regency. The soil profile data shows that this point location consists of silt, sand and gravelly sand. Moreover, the data shows hard soil from 8 meters below.

After determining the site classification, the FPGA was estimated using the site class coefficient as depicted in Table 3. The PGA value is obtained from PGAbedrock value as depicted in Table 5 and interpolated to the FPGA value based on each site class determination. The FPGA from the site class coefficient can be seen in Table 6. It also presents the amplification and de-amplification phenomenon of each point location.

Table 6. F_{PGA} versus F_{PGA} using Site Class Coeff.

Point Location	$PGA_{bedrock}$ $a_{max,}$ (g)	$PGA_{surface}$ $a_{max,}$ (g)	F_{PGA}	Site Class	F_{PGA} (Site Class)	Amplification
BH-01	0.502	0.446	0.9	E	0.9	deamplification
BH-02	0.505	0.448	0.9	E	0.9	deamplification
BH-03	0.489	0.445	0.9	E	0.9	deamplification
BH-04	0.545	0.479	0.9	E	0.9	deamplification
BH-05	0.490	0.418	0.9	E	0.9	deamplification
BH-06	0.510	0.475	0.9	E	0.9	deamplification
BH-07	0.538	0.469	0.9	E	0.9	deamplification
BH-08	0.520	0.478	0.9	E	0.9	deamplification
BH-10	0.500	0.451	0.9	E	0.9	deamplification
CPTU01	0.578	0.544	0.9	E	0.9	deamplification
CPTU02	0.596	0.616	1.0	D	1.0	amplification
CPTU03	0.518	0.538	1.0	D	1.0	amplification
CPTU04	0.695	0.698	1.0	D	1.0	amplification
CPTU05	0.517	0.448	0.9	E	0.9	deamplification
CPTU06	0.526	0.537	1.0	C	1.0	amplification
CPTU07	0.509	0.520	1.0	D	1.0	amplification
CPTU08	0.525	0.467	0.9	E	0.9	deamplification
CPTU09	0.509	0.509	1.0	D	1.0	amplification
CPTU10	0.543	0.511	0.9	E	0.9	deamplification
CPTU11	0.677	0.607	0.9	E	0.9	deamplification
CPTU12	0.668	0.603	0.9	E	0.9	deamplification
CPTU13	0.457	0.456	1.0	D	1.0	amplification
CPTU14	0.499	0.449	0.9	E	0.9	deamplification
CPTU A	0.621	0.535	0.9	E	0.9	deamplification
CPTU C	0.506	0.447	0.9	E	0.9	deamplification
CPTU D	0.481	0.428	0.9	E	0.9	deamplification
CPTU E	0.483	0.417	0.9	E	0.9	deamplification

CPTU F	0.486	0.435	0.9	E	0.9	deamplification
CPTU G	0.500	0.451	0.9	E	0.9	deamplification
CPTU H	0.532	0.480	0.9	E	0.9	deamplification
CPTU I	0.497	0.458	0.9	E	0.9	deamplification
CPTU J	0.512	0.459	0.9	E	0.9	deamplification
BH A	0.488	0.440	0.9	E	0.9	deamplification
BH B	0.492	0.420	0.9	E	0.9	deamplification
BH C	0.488	0.426	0.9	E	0.9	deamplification

As seen in Table 5, the FPGA values are almost similar to the FPGA value using the site class coefficient. These values have a strong correlation to the properties of the soil layer. The stiff soil tends to have a high amplification factor, while the soft soil has a lower value. Moreover, the amplification and deamplification characteristics are influenced by the soil deposit. The amplification occurs in the hard soil layer in Site Class C and D, while deamplification occurs in the soft soil layer in Site Class E.

5. CONCLUSIONS

The wave propagation method is one of the procedures to estimate the seismic hazard on the ground surface. The PGA on the soil surface was obtained through several steps, including modelling ground-motion at the bedrock and characterizing the soil layer properties. The results show that the low potential seismic hazard occurs predominantly in Bandung regency and the eastern part of Bandung City. The site class calculation shows that these locations are strongly influenced by soft soil deposit, which is dominated by Site Class E. Meanwhile, the West Bandung regency has a high potential of ground shaking hazard, shown by the high PGA on the surface values. These conditions are affected by stiff soil deposits, presented from Site Class C and D determination.

The distance and magnitude of seismic sources to the point locations also significantly contribute to the acceleration calculation. From the deaggregation analysis, the western part and northern part of Bandung basin is influenced by Lembang fault. In contrast, the southern part and eastern part is affected by West-Central Java Megathrust mechanism. These whole analyses, from modelling the synthetic ground motion, interpreting the soil layer profile, and calculating the site classification, provide a systematic analysis of seismic hazard prediction. Future research direction needs to develop a complete stages computation and also consider the other parameters such as the effect of basin form on the surface acceleration and determining many soil properties uncertainties. Nonetheless, this research can provide basic earthquake mitigation information to deliver preliminary studies to estimate earthquake-resistant buildings through numerical and computational procedures.

AUTHOR CONTRIBUTIONS

Anggun Mayang Sari was in charge of conceptualization, design of methodology, data processing and manuscript writing – original draft and finishing. **Afnindar Fakhrurrozi** was in charge in both spatial and non-spatial data collection and curation, geospatial modelling and analysis, validation, data visualization and manuscript writing – original draft, review and editing. **Arifan Jaya Syahbana** was in charge of investigation, validation and manuscript writing - editing. **Dwi Sarah** was in charge of investigation, geological data analysis and manuscript writing - editing. **Mudrik Rahmawan Daryono** was in charge of investigation, seismic data resources. **Bambang Setiadi** was in charge of investigation. **Rabieahtul Abu Bakar** was in charge of manuscript writing – review. **Jian Cheng Lee** was in charge of supervision the project and provided financial support for the project leading to this publication.

ACKNOWLEDGMENT

This work was supported by the Research Incentive of National Innovation System (INSINAS)[grant number:10/INS/PPK/E4/2021] and the International Science Council Regional Office implements for Asia and the Pacific (ISC ROAP) and Integrated Research on Disaster Risk and the International Centre of Excellence Taipei (IRDR ICoE-Taipei) [the Advanced Institute Seed Grant Program, grant number:2G6G7Y4A].

REFERENCES

American Society of Civil Engineers (ASCE) 7-05. (2005). Minimum Design Loads for Buildings and Other Structures. Published by American Society of Civil Engineers, USA.

American Society of Civil Engineers (ASCE) 7-10. (2010). Minimum Design Loads for Buildings and Other Structures. Published by American Society of Civil Engineers, USA.

Azwar, C., Syahbana, A., Sari, A., Irsyam, M., Pamumpuni, A., and Sadisun, I. (2021). The Sensitivity of Maximum Magnitude Range Parameter in Bedrock Acceleration Calculation for 2500 Years of Return Period, Case Study: Bengkulu Province, Indonesia. 832(1), 012006.

Badan Nasional Penanggulangan Bencana (BNPB) (2009) Laporan Harian dari Pusdalops BNPB. 15 September 2009. Website www.bnpb.go.id.

Bardet, J.P and Tobita, T. (2001). A Computer Program for Nonlinear Earthquake site Response Analyses of Layered Soil Deposits. Manual Program. University of Southern California. Department of Civil Engineering.

Cheng, H., Luding, S., Saitoh, K., and Magnanimo, V. (2020). Elastic wave propagation in dry granular media: Effects of probing characteristics and stress history. International Journal of Solids and Structures 187 (2020) 85–99.

Dam, M.A.C., Suparan, P., Nossin, J.J., Voskuil, RPGA, Group, GTL (1996): A chronology for geomorphological developments in the greater Bandung area , West-Java, Indonesia. J. Southeast Asian Earth Sci. 14, 101–115.

Daryono, M. R., Natawidjaja, D.H., Sapiie, B. and Cummins, P. (2019): Earthquake Geology of the Lembang Fault, West Java, Indonesia. Tectonophysics,751, 180–191.

Delinom, R.M. (2009) : Structural geology controls on groundwater flow: Lembang Fault case study, West Java, Indonesia. Hydrogeol. J. 17, 1011–1023. https://doi.org/10.1007/s10040-009-0453-z

Gavin, H. P., & Dickinson, B. W. (2011). Generation of uniform-hazard earthquake ground motions. Journal of Structural Engineering, 137(3), 423–432.

Haryanto, I., Hutabarat, J., Sudradjat, A., Ilmi, N.N.,and Sunardi, E. (2017): Tektonik Sesar Cimandiri, Provinsi Jawa Barat. Bulletin of Scientific Contribution, 15, 3, 255 – 274.

https://dibi.bnpb.go.id/xdibi/read/7666/32/04/108/2009//2//1

https://www.usgs.gov/natural-hazards/earthquake-hazards/lists-maps-and-statistics

Horri, K., Mousavi, M., Motahari, M., and Farhadi, A. (2019). Modelling and studying the impact of soil plasticity on the site amplification factor in ground motion prediction equations. Journal of Seismology, 23, 1179–1200.

Hutasoit, L.M. (2009) : Kondisi Permukaan Air Tanah dengan dan tanpa peresapan buatan di daerah Bandung : Hasil Simulasi Numerik. J. Geol. Indones. 4, 177–188.

Irsyam, M., Cummins, P. R., Asrurifak, M., Faizal, L., Natawidjaja, D. H., Widiyantoro, S., Meilano, I., Triyoso, W., Rudiyanto, A., Hidayati, S., Ridwan, M., Hanifa, N. R., and Syahbana, A. J. (2020). Development of the 2017 national seismic hazard maps of Indonesia. Earthquake Spectra, I(25), 25. https://doi.org/10.1177/8755293020951206

Marjiyono, Soehaimi, A., Karnawan. (2008): Identifikasi Sesar Aktif Daerah Cekungan Bandung Dengan Citra Landsat dan Kegempaan. J. Sum XVIII, 81–88.

Meilano, I., Abidin, H. Z, Andreas, H., Anggreni, D., Gumilar, I., Kato, T., Harjono, H., Zulfakriza, Dewi, O., Agustan, and Arif Rahman. (2010). Pergeseran koseismik dari Gempa Bumi Jawa Barat 2009. Jurnal Lingkungan dan Bencana Geologi, Vol. 1 No. 1 April 2010: 35 – 42.

Midorikawa, S. Miura, E H., Atsumi, T. (2014). Characteristics of strong ground motion from the 2011 gigantic Tohoku, Japan earthquake, International Symposium for CISMID. 25th Aniversary.

Novianti, E., Endayana, C., Lusiana, E., Wulung, S.R. and Desiana, R. (2021): Persuasive Communication: Disaster Literacy in Tourism Areas. Review of International Geographical Education (RIGEO),11(4), 1203-1210.

Orchiston, C.H.R. (2010): Perceptions, preparedness and resiliencein the zone of the Alpine Fault,Southern Alps,New Zealand. University of Otago, Dunedin, New Zealand. 342 p.

Pusat Data Informasi dan Komunikasi Kebencanaan (Pusdatinkom) Badan Nasional Penanggulangan Bencana (BNPB). (2021).

Risk Engineering, I. (2011). EZ-FRISK (7.52).

Sari, A. M., Fakhrurrozi, A., and Syahbana, A. J. (2019). Peak Ground Acceleration on Bedrock using Probability Seismic Hazard Analysis Methods in Bandung City. Proceedings of the Proceedings of the 7th Mathematics, Science, and Computer Science Education International Seminar, MSCEIS.

Scanlan, R.H. (1976). Seismic Wave Effects on Soil-Structure Interaction. Earthquake Engineering And Structural Dynamics, Vol. 4, 379-388.

Semblat, J.F., Kham, M., Parara, E., Bard, P.Y., Pitilakis, K., Makra, K., Raptakis, D. (2005). Seismic wave amplification: Basin geometry vs soil layering. Volume 25, 7–10, 529-538.

Semblat, J.F. (2011). Modeling Seismic Wave Propagation and Amplification in 1D/2D/3D Linear and Nonlinear Unbounded Media. International Journal of Geomechanics. Volume 11, 6, December 2011.

Sieh, K. and Natawidjaja, D.H. (2000): Neotectonicosf the Sumatran fault, Indonesia. Journal Of Geophysical Research, 105, 295-28.

Silitonga, P.H. (1973): Peta Geologi Bandung.

Syahbana, A. J., Iqbal, P., Irsyam, M., Asrurifak, M., and Hendriyawan, H. (2021). Smoothed Gridded Seismicity Effect for Land-Use Development, Case Study: Kalimantan Island, Indonesia. Rudarsko-Geološko-Naftni Zbornik, 36(3), 115–126.

Syahbana, A., Sari, A. M., Soebowo, E., Irsyam, M., Hendriyawan, H., & Asrurifak, M. (2019). The sensitivity of earthquake input motion correlation with arias intensity and amplification, case study: Yogyakarta Special Region. 1280(2), 022069.

Van Bemmelen, R. W. (1949): The Geology of Indonesia. Vol. IA, Government Printing Office, Martinus Nijhof, The Hague. Netherlands.

Villalobos, M.A and Romanel, C. (2019). Seismic Response of a Soft Soil Deposit Using Non-Linear and Simplified Models. Proceedings of the VII ICEGE 7th International Conference on Earthquake Geotechnical Engineering. Rome, Italy, 17-20 June 2019.

Vlachos, C., Papakonstantinou, K. G., & Deodatis, G. (2018). Predictive model for site specific simulation of ground motions based on earthquake scenarios. Earthquake Engineering & Structural Dynamics, 47(1), 195–218.

Yuliastuti, Y., Syaeful, H., Syahbana, A. J., Alhakim, E. E., & Sembiring, T. M. (2021). One dimensional seismic response analysis at the non-commercial nuclear reactor site, Serpong—Indonesia. Rudarsko-Geološko-Naftni Zbornik (The Mining-Geological-Petroleum Bulletin), 36(2), 1–10. https://doi.org/10.17794/rgn.2021.2.1

ISSN 8755-6839

SCIENCE OF **TSUNAMI HAZARDS**

Journal of Tsunami Society International

Volume 40 Number 4 2021

SEDIMENTOLOGICAL, GEOARCHAEOLOGICAL AND HISTORICAL EVIDENCES OF THE 881 AD EARTHQUAKE AND TSUNAMI IN THE WESTERN MEDITERRANEAN SEA (ESTEPONA, MÁLAGA)

José María Tomassetti Guerra[1], Carlos Arteaga Cardineau[2], Ildefonso Navarro Luengo[3], Leonor Parra Aguilar[4], Sayantani Neogi[5], Sean Taylor[6], Carlos Narváez Flores[7], Francisco Torres Abril[8] and Javier Alcántara-Carrió[9]

*[1] Archaeologist at Arqueotectura. Estudios de Patrimonio Arqueológico S.L. Post office box 307, 29692-Manilva (Málaga).**Spain.** info@arqueotectura.com*

*[2] Departament Geography, Universidad Autónoma de Madrid, **Spain**. Calle Francisco Tomás y Valiente, 1, 28049, Madrid. **Spain.** carlos.arteaga@uam.es*

*3 Archaeologist of the Estepona City Council.**Spain.** patrimonio@estepona.es*

*[4] FPI-UAM: Departament Geography, Universidad Autónoma de Madrid, Spain. Calle Francisco Tomás y Valiente, 1, 28049, Madrid, **Spain.** leonor.parra@uam.es*

*5 Department of Archaeology, Durham University, **United Kingdom.***

neogi.sayantani09@google.mail.com

*6 McDonald Institute for Archaeological Research, University of Cambridge, **United Kingdom**. st435@cam.ac.uk*

*[7] Departament Geography, Universidad Autónoma de Madrid, **Spain**. Calle Francisco Tomás y Valiente, 1, 28049, Madrid. atnarvaez@hotmail.com*

*8 Geologist. Universidad de Cádiz. **Spain.** patrimonio.campodegibraltar@uca.es*

*9 Departament of Geology and Geochemistry, Universidad Autónoma de Madrid, **Spain**. Calle Francisco Tomás y Valiente, 7, 28049, Madrid. javier.alcantara@uam.es*

***Corresponding author:** Carlos Arteaga Cardineau, Carlos.arteaga@uam.es*

ABSTRACT

A spectacular earthquake struck the southern margin of the Iberian Peninsula and part of the western fringe of North Africa in 881 AD. Historical sources suggest it was followed by a tsunami. However, the origin and characteristics of this event are yet to be determined. We present evidence, both historical and geo-archaeological, of a tsunami and outline the characteristics for the catastrophe. The presence of a sedimentary layer rich in marine and continental materials, appears to be of a tsunami *backwash artifact*, and in addition to archaeological remains, provides compelling data supporting our present study.

Keywords *Iberian Peninsula • Tsunami • AD 881 • Geo-archaeology • Backwash*

1. INTRODUCTION

Studies related to tsunamis in the Mediterranean Sea and of their historic impact are very extensive (Papadopoulos et al., 2005; Pararas-Carayannis & Mader, 2010; Pararas-Carayannis, 2011; Papadopoulos et al., 2014; Pararas-Carayannis, 2021). Without a doubt, one of the most prominent and oldest is the catastrophic event caused by the Santorini volcano around the 16th -17th century BC. (Pararas-Carayannis, 1992; Goodman-Tchernov et al., 2009), with important implications for the Minoan culture and civilization. Obviously, most of these Mediterranean catastrophes have a greater incidence due to their location between tectonic plates, particularly those located in the easternmost sector of the Mediterranean, which account being more than 75% of 400 catalogued tsunamis (Maramai et al., 2014). However, the westernmost sector of the Mediterranean coast that surrounds a good part of the Iberian Peninsula, is not exempt from specific tsunamis, as is the case presented in this present study. Indeed, a spectacular earthquake struck the southern margin of the Iberian Peninsula and part of the western fringe of North Africa in 881 AD. Historical sources suggest that it generated a significant tsunami; however, the characteristics of this event are yet to be better determined. The objective of the present study is to present an analysis of the evidence of this particular tsunami event, as it was registered in a sedimentary deposit of Estepona City (Málaga, Western Mediterranean), as well as an analysis and an outline of the origin and characteristics for this catastrophic event.

2. METHODOLOGY

2.1 Study Area

2.1A Geological Context

Estepona City is located on the southern coast of Andalusia (Spain, Western Mediterranean), halfway between the Strait of Gibraltar and Malaga City (Fig. 1). The historic centre of the city is located about 40 m. above the Mediterranean Sea, on a Pleistocene glacis deposit consisting of marls, sands and clays. At the base of this deposit are friable materials such as calcarenites, with varied sandy-clay materials from the Pliocene and Miocene and with traces of Quaternary alluvial sediments (IGME, 1978).

The most outstanding nearby relief close Estepona City is Sierra Bermeja (1,443 m. in height), which is part of the Baetic Mountain Ranges. It consists of an amalgamation of materials of Palaeozoic origin that had elevated in the last Alpine Orogeny. The rocks that make up this sector are predominantly metamorphic peridotites (IGME, 1978) (Fig. 1).

The thickest materials of Estepona City of Sierra Bermeja are a set of peridotites but also Precambrian-Palaeozoic rocks belonging to the "Alpujarride Unit", such as gneiss, marbles and micaschists. However, the extreme complexity of the unit between the "Alpujarride Unit" and the "Malaguide Unit" located in turn in the Betic Cordilleras and in transition to the Tertiary deposits, define the "Campo de Gibraltar" (IGME, 1978; Guerra-Merchán et al., 1996).

2.1B Background

Archaeological prospecting was carried out by the Arqueotectura S.L. Company between April and May 2017 in 98 Real Street, which is located at the southern base of a hill, dominating a stretch of the Rada anchorage between the Calancha stream to the east, and the Monterroso River to the west. Two other streams drain further north, supplying sediments to the beaches of Estepona: the creek of La Cala and the Padrón river (Fig. 1).

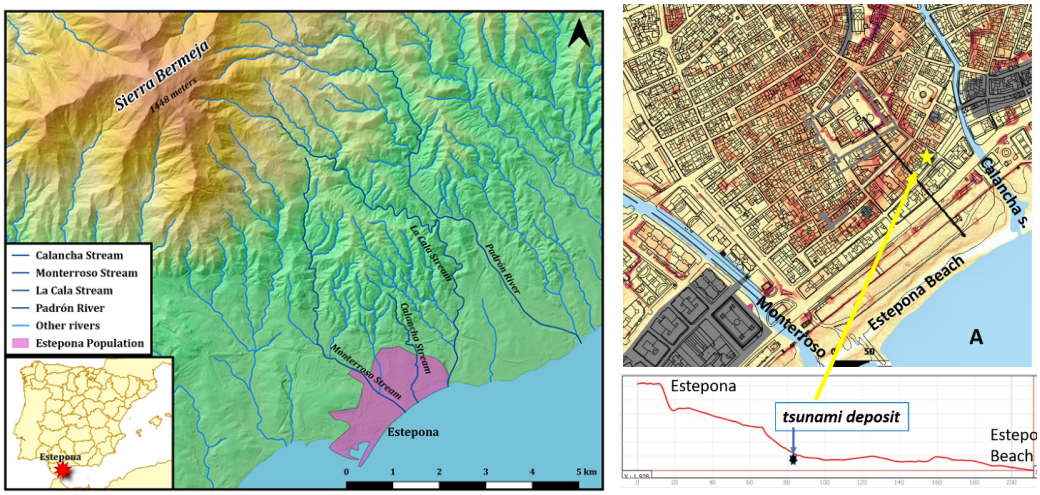

Fig. 1. Location of Estepona City (A) and the prospecting site in the historic centre of the city (B), in the base of a small hill (C).

Archaeological interventions carried out in the environment indicate that in late Roman times it was a dune area but without any instance of its anthropic use until our evidence from the 9th century. Between the 10th and 15th centuries the area was part of the periphery of the Andalusian population, occupied by commercial and artisan facilities. After the Castilian conquest, and until the end of the 18th century, it was prohibited to populate the area for military reasons, in order to create a clear space in front of the artillery fortification of the Castillo de San Luis. Finally, from the middle of the 18th century, the area between the castle and the beach has been urbanized through the layout of a series of streets (Real, Santa Ana, Castillo and Viento) that constitute the basis of current urban planning (Suárez et al., 2017).

2.1C Sedimentological Analyses

The upper strata of the trench were discarded as they contained deep anthropic alterations. In this context, samples of the trench from levels A36, A37, A39 and A42 were taken. Level A-36 occurs in the middle of the profile, more than 1.5 m below the current surface and over 2.5 meters above mean sea level.

Sands from the different beaches that border the municipality of Estepona were also sampled: Estepona Beach, Padrón Beach, Casasola Beach and Saladillo Beach. At the same time, sediments samples were taken from the Monterroso stream, La Cala stream and El Padrón and Guadalmina rivers, to rule out not only storm surge deposits, but also fluvial flood levels. Lastly, sediment samples from relict dunes close to Saladillo and Mateas Verdes beaches were analyzed. In total, 22 samples were taken to compare the site's current and past dynamics.

The 22 samples were subjected to textural and morphoscopic analysis. Once the samples were sifted and treated, statistical grain size parameters were obtained in order to determine the nature and classification of the sediments. These analyses were carried out following classic sedimentology criteria set out by Trask and Wu (1932), Cailleux and Tricart (1963), Folk and Ward (1957) and Soil Survey Division Staff (1993). When the presence of silt and clay was noted, Bouyoucos' criteria were applied (Bouyoucos, 1936; Day, 1965). The studies were carried out in the Physical Geography Laboratory of the Autonomous University of Madrid.

The Trask index (S0) is a statistical variable obtained from the particle accumulation curves designed by Tricart and Cailleux (Trask and Wu, 1932) using the 25% (Q25) and 75% (Q75) quartiles: $S_0 = \sqrt{(Q75/Q25)}$. This statistical index (**S0**), despite its antiquity and simplicity, was the choice due to its effectiveness in recognizing the sediments worked by the different geodynamic agents. In most cases, it is important to consider that this variable usually ranges between S0=1, and 3 when natural modelling agents (rivers, dunes, beaches, etc.) are present. On the other hand, slopes and colluvium material often produce higher Trask values (> 4) (Trask and Wu, 1932). Therefore, it is very useful showing in palaeo-tsunami deposits that the sediment is selected, but within the stratigraphy it is usually the least selective of the different overlapping strata, as we have seen in other deposits on the coast of Andalusia (Arteaga, 2004; Arteaga et al., 2015).

In addition, thin-section micro morphology analyses were applied to obtain a more detailed understanding of the characteristics for the soil block of level A-36. The sample was prepared for thin section analysis at the McBurney Laboratory of the Department of Archaeology, University of Cambridge (UK), according to Murphy (1986) and Courty et al. (1989). Soil micro-morphology is a well-established geoarchaeological method and a very powerful tool for understanding landscape changes and other geo-morphological phenomena (French, 2015), particularly because of its ability to investigate and interpret environmental and cultural signatures that are typically concealed within the landscape itself (French, 2003). Geoarchaeological field research, therefore, is aimed primarily at understanding human-landscape relations (Goldberg and Macphail, 2006).

Finally, a large number of spines, ichthyofauna tissues, and plant remain and bio-clasts with clear marine morphometry were identified and separated for the subsequent identification in the Physical Geography Laboratory of the Autonomous University of Madrid. Mollusc fragments were classified according to Lindner (2008).

2.1D Archaeological Analyses

The archaeological excavation was developed according to a stratigraphic process (Harris, 1991; Roskam, 2002; Carandini, 2007; Ruiz, 2013), manually excavating to clear the stratigraphic units that, once identified and described, were raised in the opposite direction to that of their deposition. The information obtained goes with graphic documentation, such as profile drawings, photographic and topographic documentation. For the dating of the sequence, a techno-typological classification of the artifacts, mostly composed of ceramic fragments within their contextual levels, were taken into consideration.

2.1E Analysis of Historical Documents

For a critical review of historical documents citing the AD 881 earthquake, two Islamic historical texts were considered: i) *Kitāb al-bayān al-muġrib fī ājbār mulūk al-āndalus wa-l-maġrib* – better known as *Al-bayān al-muġrib*, attributed to Ibn Idari – and ii) *Kitāb al-ānīs al-muṭrib bi-rawḍ al-qirṭās fī ājbār mulūk al-maġrab wa tārīj madīnah Fās* – better known as *Rawd al-Qirtās*, attributed to Ibn Abi Zar. Among all the transcripts of these documents that have been consulted for this study, we have chosen several to be reproduced in Spanish, due to some ones being longer, and therefore, greatly enriching the case study.

3. RESULTS

3.1 Sedimentological Features

3.1A Stratigraphic Units and Textural Description

The investigated trench presents an alternation of strata of different thickness and origin, alternating mostly anthropic levels with others that still have natural connotations. The trench was divided in a total of 44 stratigraphic units (Fig. 2).

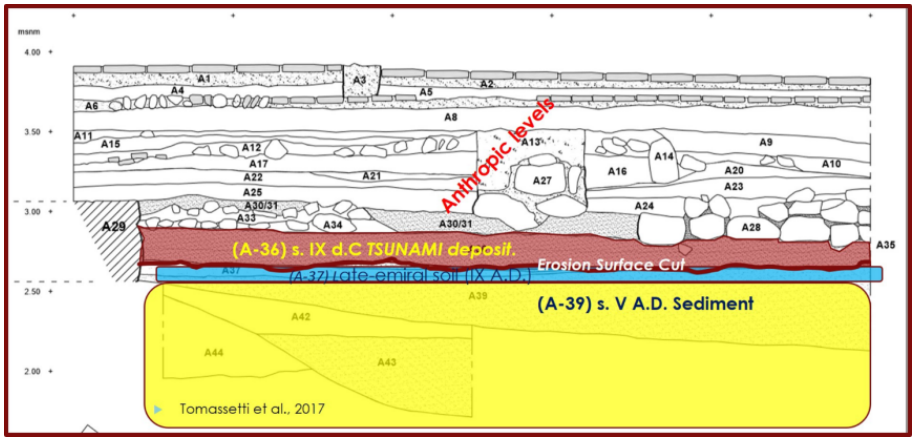

Fig. 2 North section of the trench. Numbers indicate stratigraphic units.

Phase II of the trench presents a clear stratigraphic unconformity with Phase I, i.e., an erosive contact. It includes levels A37, which corresponds to a narrow sandy deposit, and A-36, which is composed by a mixture of sands, gravels, marine fauna and archaeological settlement debris.

Just over a meter from the current surface, the A-36 level is located with a thickness of 25-30 cm. This horizon is greyish-brown (10YR5/2) and is composed of edges and tapes of centimetric to decimetric size (45% to 68%), broken by a high percentage and separated by a matrix of sand and silt that increases towards the lower zone (32% to 55%). The sedimentary deposition (A-36) has a *clast-supported* structure at the top and *matrix supported* at the bottom (Miall, 2016) (Fig. 2). Strata are arranged with some overlap towards the sea and in turn rest on a sandy layer with morphologies of ripples of centimetric thickness that culminate in erosive contact with the underlying level. The level has lateral continuity until it is interrupted by ashlars of later chronology. Throughout the stratum, broken molluscs are visible. The coarse sediments of the deposit (A-36) (Fig. 3) are mainly composed of peridotite gravels and, secondarily, gneiss and phyllites. These rocks are imbricated towards the sea, flattened (71 %) and broken in a relatively high percentage (34,6 %), example, of high-energy transport and deposition. The matrix of A-36 also contained fragments of mudstones, whose origin can be diverse: vestiges of a riverbed or marsh plucked by high energy (Table 1).

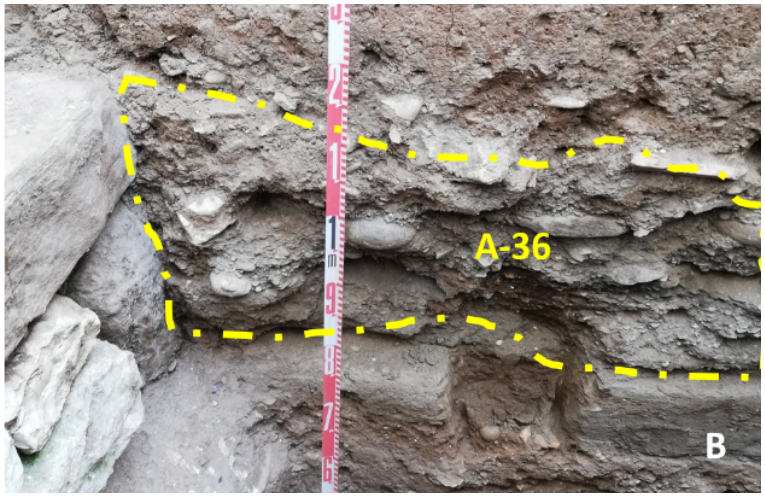

Fig. 3. Photograph of level A-36.

On other hand, the sand is moderately well sorted and is upwardly fining. The average grain size of the A-36 sediment is 330 microns (0,33 mm). Then, it is finer sand than the other of samples taken from the nearby beach and the nearest streams. The coarser sediments are from the river systems; on the beaches of Estepona, medium to coarse sands make up the majority, but grain size increases towards the mouth of the main rivers, where the materials are mixed (i.e., 0.6 mm in Guadalmansa River and 0.71 mm in Guadalmina River). The dune sediments are the finest and the best classified (Table 1).

Table 1 Granulometric and morphoscopic indexes obtained according to their nature of samples from the trench (levels A-36, A-39) and the present surrounding environments.

Samples	**Mean size (mm)**	**Trask Sorting Index (S0)**	**Textural classification**	**Morphoscopy - rounded quartz-**	Morphoscopy **matte rounded**
Streams-Rivers	0,59-1,7	1,42-1,84	Sand-Sandy loam /grabel	15-20%	< 3%
Beaches	0,27-0,7	1,20-1,33	Sand (coarse – fine sands)	24-32%	11-16%
Dunes	0,24-0,32	1,18-1,20	medium to fine sands	>50%	> 30%
A-39 (ancient dune)	0,35	1,26	Medium sand	36%	8%
A-36 (high energy event-possible "tsunami "deposit?)	**0,33**	**1,64**	**Medium sand**	**16%**	**8,6%**

The Trask sorting index (S0) ranges between 1.4 and 1.85 for rivers and streams, and from 1.18 to 1.33 for beaches and dunes, in the study area. However, in the trench, level A-36 has a S0 value of 1.64, and mean grain size corresponds to medium sand (0.3 mm); it is also standing out as being the sample with the highest percentage of silt-clay (> 11%).

The lower levels present an alternation of different sedimentary environments. A-37 is a level of medium-fine sands around 0.25 mm, and A-39 represents a build-up of deposits of marine origin, with the presence of bioclasts and a Trask index of 1.26 (possible beach) and more than 54% of sub-rounded-rounded grains. The base of the profile culminates with stratum A-42, with an average grain size of coarse sand (0.5 mm) and S0 close to 1.4, also typical of a marine nature. Morphoscopic analysis shows that fluvial systems of the Estepona environment rarely reach the roundness of the quartz in their flow beyond 15%. It must be taken into account that they are rivers and streams with a very short route. Once on the beaches, the action of the waves works and well-rounded grains up to 32% and, as a result of the dune dismantling due to coastal erosion, you can see rounded quartz matt up to 16%. In contrast, A-36 has 16% rounded quartz, very similar to that of river systems, but contains rounded quartz by wind action (above 8%).

3.1B Micro-morphological Description of the A-36 Thin Section

Thin section of level A-36 is porous (30-40%) and *apedal*, but it has a complex microstructure, a dominant single grain and vughy microstructure superimposed onto a bridged grain microstructure. Voids are dominantly compound packing voids, vughs and a

few chambers. The groundmass shows a dominant concave *gefuric* and a coarse *monic* related distribution pattern. It has a *c/f* 50μm ratio of 2/1. The coarse fraction has a strongly expressed banded basic distribution pattern. The coarse material is dominantly (>90%) moderately sorted, rounded and sub-rounded fine and medium sand (150-275μm). There are also larger rounded limestone (<5%) gravels (5-50mm). The remainder consists of fine and medium sand sized (500-2500μm).

There are places where the groundmass becomes predominantly extremely thin, with dominant large gravels (<10cm) forming 5% of the horizon and these are sub-rounded and sub angular. The organic components are marine shell (500-1250μm) and other marine fauna (10-30μm) and tissue and cell fragments within the groundmass located in compound packing voids. There are a relatively large amount of tile, brick, plaster and charcoal fragments derived from an archaeological context. The micro mass is humic brown speckled clay exhibiting a weakly calcitic crystallitic b-fabric. The dominant pedofeatures are typical clay and silt coatings on sand grains. Pedofeatures are characterised by those that show the movement and accumulation of calcium carbonate. Many rock fragments have compound juxtaposed calcite and clay pendants (<750μm). Most of the sands and coarser clasts have been bridged and coated by calcite. In addition, there are coatings of needle-fibre calcite on the walls of voids (25-100μm). Throughout the groundmass moderately impregnated Fe-hydroxide typical orthic nodules are observed (25-75μm).

This thin section clearly shows the sedimentation of well sorted medium and fine sand, horizontally bedded between finer clays, silts, comminute organic matter and marine diatoms, some of them broken, and the sand generally tend to fine upwards. The sand has been deposited unconformably in thin, horizontally orientated lenses as a result of tsunami processes. Thicker bands containing larger limestone gravels, stones and bioclasts among other materials; brick and plaster fragments have been deposited generally separating the larger clasts first. The coarser material and archaeological is clearly evident from the close vicinity of the deposit. Within the matrix is well-sorted sand, almost certainly from a coastal context (Govorushko, 2012).

Within this aggrading sedimentary system, vegetation evidence of organic material comes from charcoal fragments within the groundmass. These fragments clearly have a cultural origin and are almost certainly derived from one of the many medieval buildings that are thought to occupy the surrounding landscape. Humified and Fe-replaced root tissue can be observed in various states of preservation. Abundant comminuted plant tissue and cell fragments are evidence for the breakdown and cycling of organic matter. The humic brown speckled clay is primarily the end member of these processes.

3.1C Results from Faunal Remains

Throughout the stratum A-36, contained within the sandy matrix is a mixed assemblage of fragments of seashells, coal, vertebrate and fish bones that will be the subject of subsequent analysis.

In the 600 grams of sample A-36, around 2.5% suppose remains of molluscs, ichthyofauna and remains of plant tissues. Centimeter-sized mollusc fragments correspond to *Acanthocardia tuberculata* (32%) and *Venus verrucosa* (68%).

The habitat of both species is below 5 m deep, although it should not be ruled out that it was a material taken from the beach. More specifically, the first usually lives between 5 and 100 m deep, while the second barely reaches 20 m (ICTIO.TERM, 2018).

One of the main factors that reveal the violence of the event, is the presence of the ichthyofauna trapped in the sediment included crushed fish scales, spines and vertebrae, among the matrix of gravel and sand (Fig. 4). It has been possible to identify the tuna (*Thunnus thynnus*) as the majority species by the spines, which correspond to young specimens.

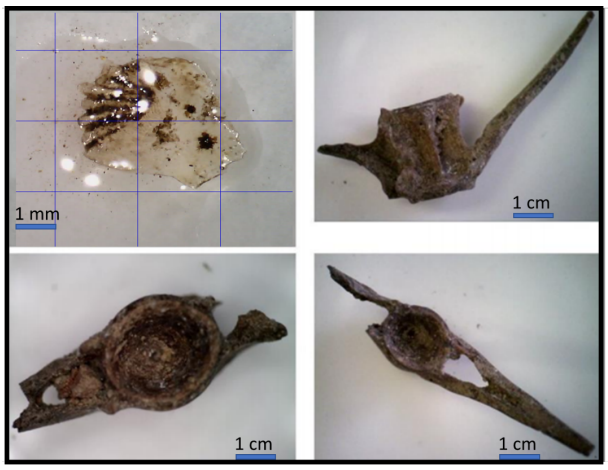

Fig. 4 Fish scale (upper left image) and tuna spines found in the sedimentary deposit. The wave had to have high energy to be able to catch and crush several fish between the gravel and sand.

It is truly anomalous to find ichthyofauna remains in storm surge or river flood deposits, and less in the volume of the sediment analyzed. Although the spines do not correspond with adult specimens, more heavier, it is difficult for a wave to carry them in its bosom if it does not carry with it a great transport capacity. The presence of this species also perfectly corroborates the proposed date of the tsunami, since in historical times the passage of tuna between spring and June is recognized (Florido y Menanteau, 2006).

Together with molluscs and ichthyofauna of a clearly marine character, continental plant remains typical of wetlands, marsh environments or riverbanks were also found. This is the case of the presence of *Carex sp.* pertaining to the family of the sedges. In fact, in Estepona there are up to three taxa of this genus: *Carex halleriana, Carex hispidia y Carex pendula*. Although several fragments were found, their state of preservation prevents further identification.

3.1D Ceramic Debris

The ceramic acquires a great value, since it helps the dating of the strata. For the Phase II it can be classified as a horizon corresponding to a room with the following elements: in level A37 the space is conditioned for use in the open air by inserting several post holes (A40 and A41) and the installation of a fireplace (A38).

The ceramic materials found in levels A36, A37 and A38 form a set of 224 fragments and an almost complete piece. For their analysis we divided them into two large series: glazed ceramics and unglazed ceramics. Only six fragments represent the glazes: three of ataifores (deep plate representative of Andalusian tableware), one of cup and two closed forms. The glazes are represented by only six fragments (three of ataifores, one of cup and two closed forms). As will be seen later, this type of glazed pottery is representative of the 9th Century Acién et al., 2003; Acién et al., 2009; Martínez Enamorado, 2003; Melero et al., 2015).

The set of unglazed ceramics constitutes the largest (Fig. 5), with an almost complete piece and 217 fragments. The most represented type is the little jug, with highly flown handles on the edge. Some specimens are slipped in black, sometimes with strokes of white paint. In a more minority, there are black or red brush decorations. Another type that is highly represented in the sample is the slow lathe *alcadafe,* with three different models: the small one, with vertical walls and projecting edge, the one with sloping walls and, finally, the large one with vertical walls and fingered cords in the body.

Fig. 5 Selection of unglazed ceramics from phase II. 1. Slow lathe edge of alcadafe (UE-36). 2. Rim of the jar on a slow lathe with finger cord (UE-36). 3. Jar handle with white paint stroke (UE-36). 4. Edge of *alcadafe* with slow lathe (UE-36). 5. Slow lathe chuck edge (UE-36). 6. Arranged fragments of glass cup (UE-38). 7. Background fragment of glazed ataifor (UE-36). Photo by J. .M Tomassetti (Arqueotectura S. L.).

Other minority slow-lathe types have also been studied, such as jugs, jars, pots and pans. The only almost complete piece is a kettle made on a lathe, with a slightly convex bottom, a spherical body and a recessed frustoconical neck, with vertical mamelons on the shoulder. It appeared overturned on the ground near the hearth and contained an ocher-colored matter. Although the dating of unglazed ceramics is, as a general rule, more imprecise than that of

glazed ceramics given the durability of some types, the set fits perfectly with those dated to the second half of the 9th century (Acien et al. 2003).

The ceramics of phase III (units A32 / 33, A34 and A35) are, on the whole, similar to those of the previous phase, also with the presence of glazed and unglazed fragments. Among the former, a roasted *ataifor* on both sides and interior decoration with manganese lines, as well as some roosters and a flask handle with "green and manganese" decoration, can be dated as corresponding to the second quarter of the 10th century (Acién et al., 2003; Acién et al., 2009; Martínez Enamorado, 2003; Melero et al., 2015). Unglazed productions confirm the survival of those made on a slow lathe (jars with finger cord, pots, casseroles) and some simple-rimmed jugs. Therefore, it is a material set similar to that of the previous phase, but it includes clear guide examples, such as green and manganese ceramics, which determine its chronologies as directly related to the Caliphate of Córdoba. If the beginning of the production of these glazed ceramics must be dated towards the middle of the 9th century, level A37 corresponds to the 9th century too, dated from the ceramic evidences and coinciding with the high-energy episode documented by Galbis (1932). The stratigraphic sequence of the trench continues until the 20th century, with alternating periods of occupation and abandonment that do not affect the subject of this study.

3.1C Identification of the AD 881 Earthquake and Tsunami in Historical Documents.

The first text that we are going to take into consideration is the most well known. It appears in the quoted work of Ibn Abi Zar, which was translated by Ambrosio Huici Miranda (1964) and José Antonio Conde (1820). While Conde has transmitted this text to us through his studies, it must be said that, in his work, he mixes and transcribes various Islamic sources to create a complete history of Muslims in the Iberian Peninsula, often making it difficult to recognize his original sources.

When comparing Conde's translation with other translations of the same text, it can be seen that Conde's is broader. This leads us to think that he is translating texts that we don't know or that have been lost over time. Conde's work was highly reviled in the mid-nineteenth century, but for a few years it has been recovering and re-giving the importance it deserves, proving its historical and linguistic value in various studies (among them Calvo Capilla, 2016, Calvo Pérez, 2003, Domínguez Prats, 2006, Haro Cortés, 2012, Hitchcock, 1986, Manzanares de Cirre, 1968 can be cited).

Both texts describe the same seismic phenomenon according to Souto (1995, p. 230 and citation 131), who has demonstrated this by comparing the two texts. Having established this, the facts can be laid out, providing us a wealth of information regarding the seismic episode that occurred in Al-Ándalus and other neighbouring areas in 881. From the texts we can ascertain the following (view appendices):

The Date: The various catalogues ascribe a differing date to the AD 881 earthquake. The *Catálogo de Tsunamis en las Costas Españolas* compiled by the Instituto Geográfico National, records that the tsunami of the 881 earthquake occurred on the 10th of June.

The IGN extracts this information from one of Galbis's catalogues, which derives its information from Juan García Lomas, without giving further references (1940, p. 12). In that same work, Galbis quotes Roux (1934) and reproduces a fragment of one of the texts discussed here, but he transcribes it incorrectly and with erratum, changing the date. Another possible option is May 26th, 881, according to the catalogue of Martínez Solares and Mezcua Rodríguez (2002). No one has questioned why several dates are not given, nor has any effort been made to correct it – researchers adopt one or the other depending on their choice.

After verifying the documentary sources and resorting to the most reliable translations of the *Rawd al-Qirtās*, the earthquake can be date to the 22nd day of the moon of Xarwâl (Shawwal) in the year 267 of the Hegira, according to the established formulas for converting AH to AD, a date of May 26th, AD 881 is derived.

The Hour: The text by Ibn Idari provides the most relevant information as to the approximate time of the earthquake. According to the two translations that have been provided from *Al-bayān al-muġrib*, the earthquake occurred *at the hour of the azallah of sunset* or, *when the prayer of al-Magrib*. In both translations they refer to the same moment: the Magrib prayer. *Azallah* or *salat* is the sunset prayer, the fourth daily *salat* of Islam. It takes place just a few minutes after sunset. For May 26th this would correspond to a time close to 21:30.

3.1D Historical and Geographical Context.

At this time this part of the Iberian Peninsula was part of the Emirate of Córdoba, under Emir Muhammad I (852-886). The Christians had not yet crossed the Duero River in their conquest; their king was Alfonso III of Asturias.

Geographically two different realities are embodied in the texts, two testimonies from two different places where the earthquake was felt. The first place is Córdoba, the then capital of the emirate, where the court resides. In a place of such political importance like Córdoba, they collected all the relevant events that occurred, and for this reason the text of Ibn Idari has been preserved. The second place comes from the text of Ibn Abi Zar. In the year 267 of the Hegira a population uprising took place from the towers (*husûn*) of the territorial divisions (*kūrah* or *coras*) of *Rayya*, *Tākurunnā* and in the Algeciras area, which had to go to solve Muhammad I or his son Al-Mùndir. This event was the one that made the earthquake witness from another geographical perspective that is the one that *Rawd al-Qirtās* provides us and that we present in the following map.

Places Affected by the Earthquake*:* According to the different copies of Ibn Abi Zar and Ibn Idari that have been consulted (Huici Miranda, 1964; Fernández González, 1860; Roux, 1934, Souto, 1995), the earthquake was felt particularly strongly in *El Adoua* or *Al-Magrib* (possibly in the vicinity of Fez, Morocco), Tlemcen (Algeria), Tangier (Morocco) and throughout Al-Andalus. Likewise, they say that the earthquake had its affected from the Mediterranean Sea or *Al-Sham* Sea – the Syrian Sea, one of the names that Muslims used for

the Mediterranean in the Middle Ages – to the northernmost part or *al-Magrib al -Aqsa* – a term for the westernmost region of Morocco. They also report that the earthquake was felt even "in the last part of the land of Christendom" or, as Muslims sometimes prefer to call Christians, "even the most remote polytheistic land" (Lapida Gutiérrez, 1997). The earthquake was felt in Christian lands and could be recorded, because the Muslims were fighting against them at this time, as reflected in Conde's text (1860). In other words, it was felt across the entire Iberian Peninsula (Fig. 6). For his part, Ibn Idari mentions that the earthquake was felt with great force in Córdoba and, for his own, Ibn Abi Zar affirms that there was a tsunami, confirmed in this study for Estepona.

Fig. 6 Map showing the places where there was an earthquake in 881 and the places where it was felt.

Singular Phenomena: Earthquake Lights: Among the information that can be extracted from these texts, a singular fact stands out. They refer a singular phenomenon reported in the city of Córdoba, related to so-called "earthquake lights" (Derr et al., 2011). The text narrates how several people were in the mosque preparing for the *Magrib* prayer and how electricity produced by the earthquake affected them. The first thing they relate is the appearance of a lightning-bearing cloud, which killed two people by electrocution. Although death associated with these phenomena is not common, the description is very similar to so-called "earthquake lights". Several studies report the appearance of this type of cloud in the moments leading up to an earthquake or at the exact moment of its occurrence (Derr et al., 2011; Thériault et al., 2014).

Could this not just have been a thunderbolt? This is unlikely because firstly the phenomenon occurred alongside the earthquake, and second because the text reports that no damage was done to the fabric of the building. Considering that the text says that these six people were knocked down on their backs, it is very likely that there was an explosion resulting from the thunder (St-Laurent, 2000). Two people died and showed burns on their faces. Four others felt "a fire like a heavy wave". It has been mentioned that after this incidence the environment had a burning smell resulting from the burnt human flesh.

According to the studies already mentioned, these luminaires can occur up to 150 kilometres from the epicenter, with even greater distances being reported in some cases. This phenomenon provides us with a better idea of the magnitude of the earthquake since, among the earthquakes studied by Derr (2011) or Thériault (2014), all exceeded M5 on the Richter scale. The number of earthquake lights and their power increase proportionally with the strength of the earthquake. This released energy can take various forms: tongues of light, bright flashes from the ground, spheres and lightning. This electricity moves through an environment and is only a problem if it meets someone, just as reported in Córdoba.

4. DISCUSION

4.1 Sedimentary identification of a Tsunami deposits

Identification of "tsunamites" from sedimentology should be as accurate as possible. For this reason, it is sometimes convenient not only to take samples from the deposit creditor of said event, but also to compare all the sedimentary material deposited by the different natural agents of the geographical framework in which it is circumscribed, including beaches, dunes, rivers and streams. Especially if there is a risk of incorrect identification with storm deposits, it will have different implications altogether. Extreme tsunami events imply the presence of continental and marine material (especially of different depths), erosive scars, gravels imbricated towards the sea, anthropic and natural materials mixed in a chaotic and fragmented manner, and decimetric thickness of the stratum (Nott, 2004; Morton et al., 2007; Kench et al., 2008; Komatsubara et al., 2008; Goto et al., 2010; Lario et al., 2010a; Papadopoulos et al., 2014; Shinozaki et al., 2015; Mottershead et al., 2015; Usani et al., 2017).

The excavation of Trench A offered a complex sequence. It begins in late Roman times (phase I, centuries IV and V), with alternation of continental and marine events in a dune environment. In the nearby-inhabited area there are levels of abandonment during the 5th century, both in residential areas and in artisanal facilities (sinks for fish processing, amphora furnaces for marketing, etc). This confirmed abandonment was perhaps due to the passing of the vandals in 429, which left its reflection in the stratigraphy (Bernal, 2018, p. 107). In line with this, the intervention of C / Real, 98 shows a first occupational hiatus between phases I (5th century) and II (9th century), which must be interpreted as an absence of population for more than 450 years in the excavated area.

The analysed trench has made it possible to establish a historical sequence between the 4th and 20th centuries.

Within the stratigraphic unit A36, anomalous sediments appeared along with archaeological remains dated to the 9th century. The presence of some elements of apparent marine origin at about 2.6 m above sea level and 150 m from the seashore, suggested the possibility of a past high-energy event. S0 values (Trask index) close to 1 are generally related to sediment well selected by a dynamic agent (i.e. dunes and beaches; Trask an Wu, 1932), coinciding with a grain size of medium to fine sand. However, level A-36 has a S0 value of 1.64, relatively high if we consider its mean sizes corresponds to medium sand (0.3 mm), and it also standing out as being the sample with the highest percentage of silt-clay (> 11%).

The presence of eolian rounded quartz in level A-36, together with the high Trask index, its composition of medium sands, the presence of silts and clays, peridotites with fluvial morphologies, tuna bones, numerous fragments of fish scales, various mollusk bioclast and the existence of mudstones positioned chaotically in the level, leads us to think that the sandy matrix presents both continental and marine sediments.

In fact, in micro morphological analysis we can observe containment of abundant small red tile or ceramic, which appear to be of the medieval period date. These are generally sub-rounded due to various weathering processes, not least those associated with the mass movement of sediment within a high energy wave environment associated with a possible tsunami.

The diatoms observed, have been embedded within the sandy matrix containing geological and anthropogenic material because the tsunami has inundated the coastal margin and inland areas, eroding, mixing, transporting, and redepositing a variety of components. Some of the diatoms have been observed broken due to their relatively fragile valve constructions; perhaps suggesting that the preservation is related to the speed and violence of transportation and burial (Smol 2010). Consequently, from the micro morphological analysis it can be deduced that the horizon became emplaced very quickly because of a catastrophic sequence of high-energy related waves. Therefore, A-37, with medium-fine sands, representing the soil of the 9th century (dated after the chronological identification of the ceramic remains) that would have been eroded by the tsunami. On the other hand, A-39 represents a build-up of deposits of marine origin, with the presence of bioclasts and a Trask index of 1.26 (possible beach) and whose morphoscopy also indicates this origin with more than 54% of the sub-rounded-rounded grains. The base of the profile culminates with stratum A-42, with an average grain size of coarse sand (0.5 mm) and with an S0 close to 1.4, also typical of a marine nature.

During the archaeological excavation, it was possible to verify how the stratigraphic elements of phase II were destroyed by a high-energy event that the joint relative chronology of the sequencing and the ceramic typology places in the second half of the 9th century. The contrast of this data with the records of historical earthquakes yielded from the beginning a single coincidence (Suárez et al., 2017): that of the earthquake of the year 881 that the late medieval Islamic sources have transmitted to us. This catastrophe caused the abandonment of, at least, this sector of the settlement, giving rise to a phase III that dates back to the first third

of the 10th century, some 50 years later. This discontinuity can be explained by referring to the repercussion in the entire Malaga region of the rebellion of Ibn Hafsun, which began a little before the tsunami of 881 (Manzano, 2006, p. 276-287; Martínez, 2003, p. 534).

In principle, the sedimentological characteristics of A36 fit with a sedimentary deposit of extreme wave events (EWE) (Lario et al., 2010a). If we add to this the absence of multiple interior lamination, its clear contact with the underlying layers and its thickness of no more than 25 cm, it seems to fit a tsunami deposit, according to Lario et al. (2010b). In short, the alternation of both marine and inland materials seems to correspond at first with a backwash phenomenon.

4.2 Archaeological dating of the Phase II

In relation to the fragments of glazed pottery, similar assemblages have been published in Malaga sites, both coastal (Cortijo Félix, Cerro Luis, Marbella, Málaga or Bezmiliana), and inland (Vélez-Málaga, Valsequillo, Belda), as well as in numerous other Andalusian locations in the provinces of Granada (El Castillón), Almería (Pechina), Córdoba (the same capital, Priego), Jaén, Murcia, etc. In general terms, in most of these sites the dating of these first glazed ceramics is very extensive and they are classified as "emiral pottery", "emiral-caliphal pottery", "andalusian pottery", etc., proposing *as terminus ante quem* for its dating the appearance of green and manganese ceramics in the 10th century, and on the other hand, the beginning of the production of these glazed ceramics must be dated towards the middle of the 9th century. (Acién et al., 2003; Acién et al., 2009; Martínez Enamorado, 2003; Melero et al., 2015).

In summary, the set of glazed materials from the levels of our phase II is consistent with those that, roughly, are considered to belong to the second half of the 9th century. These glasses most likely come from pottery located in the city of Malaga, if we stick, for example, to the similarity of the cup specimen (honey on all its surfaces, decorated with manganese lines) with the Malacite parallels (Acien et al. 2003, p. 420). In general, dating of unglazed ceramics is more imprecise than that of glazed ceramics. Nevertheless, given the durability of some types, the set fits perfectly with those dated to the second half of the 9th century (Acien et al., 2003).

Therefore, the historical context to which we can refer to phase II as a whole places us around the reign of Emir Muhammad I (852-886). In the middle of the 9th century, we found a varied population, where it is not possible to know the percentage of Mozarabs, Muladis and Berbers that were in the area. This led to the existence of different types of settlements, such as inland villages and/or in height, as well as towns along the coastline, as is the case of Estepona, which made it a well-connected anchorage and in which commercial and artisan activities would be promoted. An indication in favor of this interpretation would be the appearance in the intervention of C / Real, 98, of glazed ceramics produced in Malaga, a city that currently knows an authentic re-foundation based on trade and pottery production (Gutiérrez, 2011; Melero, 2015, p. 272).

Other examples of this type of population are the settlements on the Malaga coast, Marbella and Bezmiliana, for which it has been proposed that at the time of their foundation, the second half of the 9th century, they would not have an urban character, being classified as farmhouses (Martínez, 2009, p. 100; Acién y Salado, 2009, p. 145).

In summary, the set of glazed materials from the levels of our phase II is consistent with those that, roughly, are considered to belong to the second half of the 9th century (Fig. 7). On the other hand, these glasses most likely come from pottery located in the city of Malaga, if we stick, for example, to the similarity of the cup specimen (honey on all its surfaces, decorated with manganese lines) with the Malacite parallels (Acien et al., 2003, p. 420).

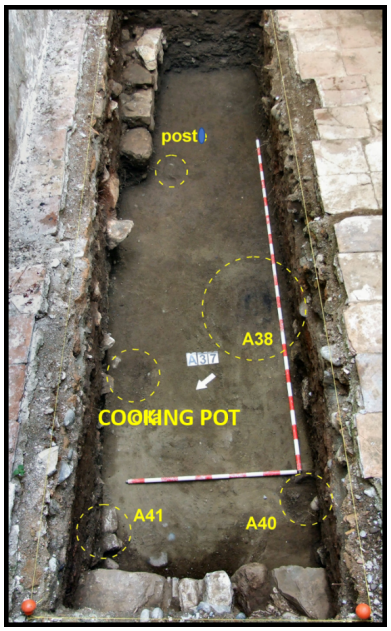

Fig. 7 Plan of the habitation horizon of Phase II of ditch A from the West. Numbers indicate stratigraphic units. The A36 tsunami tank mounts on the units shown. A38 is home. A40 and A41 are post holes

In the top, Phase III has been dated as corresponding to the Caliphate of Córdoba by the ceramic analyses. In our opinion, the revolt caused by Ibn Hafsun and the destructive effects of the tsunami reflected in the A36 level, led to the abandonment of the place for several decades. It was not until the rule of Abderramán III (924 A D), in which the Cordovan troops conquered the nearby castle of Nicio (Navarro et al., 1998; Salado and Navarro, 2001). This historical event again implied Cordovan dominion over the Strait region. On a local scale, it presents a very different aspect to the previous scenario, since the first constructions with stone walls (A28 and A29) are verified, evidence of the reoccupation of a previously abandoned space.

4.2 Analysis of Historical Sources

Analysis of historical sources in both the Eastern Atlantic and the Central and Eastern Mediterranean, indicate that past earthquakes and coastal landslides have generated damaging or destructive tsunamis along the coasts of Southern Spain. For example, the 1755 Lisbon earthquake caused considerable damage not only in Portugal but also in southwestern Spain. The tsunami generated by this event, caused damage to Cadiz and Huelva, and its waves penetrated the Guadalquivir River, reaching Seville (Pararas-Carayannis, 2021).

Also, destructive earthquakes and tsunamis in the Eastern Mediterranean region have had significant impacts on the ancient world and even changed the course of history. One of the most destructive earthquakes which occurred on July 21, 365 AD along the western coast of the Island of Crete generated a mega-tsunami, which mainly devastated the southern and eastern coasts of the Mediterranean Sea, but numerical modeling studies indicate that it must have also impacted to some extent its eastern coastlines as far as Spain (Pararas-Carayannis & Mader, 2010). According to historic records, this 365 AD earthquake was felt throughout the Eastern and Western Mediterranean and as far away as the eastern coast of Spain, particularly in the area where present Malaga is located (Pararas-Carayannis, 2011).

The first stage of the present study includes a historiographical review of events. It is clear from the reviewed documentation that a series of conflicts exist that has the potential to inhibit efforts to gain a clear understanding of the AD 881 earthquake. Realizing a state of the question that covers only the AD 881 earthquake, serious deficiencies have been found in the usual lines of investigation. The main problem is that: in the investigation of historical earthquakes, the catalogues published from the end of the 18th century to the present day are often used, and all of these require substantial revision. In these widely known catalogues, for example the Galbis Catalogue (1932), the information provided is not always evaluated one by one, but we will say that practically all of them have been collected in more recent works such as by Martínez Solares, by Mezcua Rodríguez (2002) and by Udías (2015, 2017).

The historical texts compiled in the catalogues have not always been contrasted with the original documentary sources, and often the authors have been copying the texts among themselves. In this way information can be mixed, losing its origin, meaning and context. For this reason, it is necessary to update and critically review the existing documentation concerning the AD 881 earthquake, so as not to show doubt on a historical event that undoubtedly occurred and shook the Andalusian world.

With regards to the Islamic historical sources, the first thing to keep in mind is that any such texts that address the 881 earthquake and that have survived to this day, have been repeatedly recopied throughout the Middle Ages. Islamic chroniclers, historians, and geographers copied each other's texts to create their own. This is why we have different translations of the same text, and also why we have chosen to resort to the closest translations to the originals.

Both Islamic historic texts considered, *Kitāb al-bayān al-muġrib fī ājbār mulūk al-āndalus wa-l-maġrib* – better known as *Al-bayān al-muġrib*, attributed to Ibn Idari – and ii) *Kitāb al-ānīs al-muṭrib bi-rawḍ al-qirṭās fī ā jbār mulūk al-maġrab wa tārīj madīnah Fās* – better known as *Rawd al-Qirtās*, attributed to Ibn Abi Zar, date from the beginning fourteenth century, although ascertaining the original their composition is problematic. Most probably, both *Al-bayān al-muġrib* and *Rawd al-Qirtās* come from other chronicles of an Islamic leader previous to the 14th century (Fernández Fonfría, 2010; Souto, 1992, 1995). This is very common and has been studied in various works, some as important as the *Kitāb al-muqtabis fī aḫbār al-Andalus*, better known as *Al-Muqtabis*, one of the great works of Ibn Hayyan Al-Qurtubi and which also references and intersects our sources (Molina, 2005; Penelas and Molina, 2011).

4.3 Possible Origin of the Earthquake

The precise origin of the earthquake that caused the tsunami is not yet fully understood, although there are at least two plausible possibilities. The first is that it originated from a tectonic event in the Betic Cordillera, which, directly or indirectly, triggered an underwater landslide leading to a tsunami. The other option is an underwater earthquake caused by one of the nearby Mediterranean faults, halfway between Africa and the Iberian Peninsula.

The Estepona coast is part of the imposing and long geological framework of the Alpine-origin Cordilleras de las Béticas that run through southern Spain. It is located in a convergence zone, from 4 to 6 mm/year (Argus et al., 1986; DeMets et al., 2010), between Africa and Eurasia, two much larger plates (Argus et al., 1986). The Azores-Gibraltar fracture zone represents the western boundary between these two plates approximately from the Lower Miocene, at which point the Iberian Plate became part of Eurasia (Srivastava et al., 1990). Finally, during the Cenozoic, its paleogeographic and tectonic evolution is linked to the closure of the Tethys ocean and the Alpine Orogeny (Jabaloy et al., 2002). All this makes this sector of the Iberian Peninsula the most active in terms of seismicity.

Although earthquakes and tsunamis in the Iberian Peninsula do not match the frequency and intensity of other coasts, they have occurred approximately every 99 years in the last 2000 years (IGN catalog, 2020). The most intense, depending on the definition, occur between 450 years (Carreño, 2005) and 1.200-1.500 years over the course of the Holocene (Lario et al., 2011).

The most devastating tsunamis originate on the Atlantic coast from the Bank of Goringe, the Gloria Fault and the Arc of Gibraltar (Carreño, 2005; Lario et al., 2011; Alonso et al., 2011; Pararas-Carayannis George, 2021.), west of the Gulf of Cádiz, but the Mediterranean world is also no stranger to this natural phenomenon. Numerous catalogues, updated by researchers, have reported such catastrophes for centuries, although their effects appear to be of a lesser degree. The last tsunami that hit the Spanish coast in 2003 affected the Balearic Islands. In the analysis of the historical texts identified in this work, two important facts have been confirmed. The first is that the earthquake was sizeable in magnitude and intensity, close to 8 (Mw). Its incidence radius is significant, since the seismic shock reached a large part of

North Africa and the Iberian Peninsula. Locating the epicentre is difficult, but it is likely to have been located between the Betic Cordilleras and the Mediterranean Sea. When its destructiveness and reach are described in the texts, it is said that it "feels" in North Africa and even "in the last part of the Land of Christianity" and damage to the same mosque in Córdoba. But the destruction, and the greater ruin in buildings with the fall of "magnificent buildings and fortresses" that were "very broken" with the disappearance of towns, is mentioned as a geographical framework on the coast to the Baeticas. An earthquake in this zone is not bound to produce a tsunami, but a few cases are documented such as the earthquakes that occurred between the 15th and 19th centuries on the Andalusian Mediterranean coast. The most powerful occurred in 1884, with a magnitude of 6.7Mw (Sánchez, 2011), and had disastrous consequences for local populations, but did not cause tsunamis. Only those that occurred in 1522, associated with the aforementioned Carboneras Fault (Reicherter and Becker-Heidmann, 2009), and 1680, with a possible epicenter in the vicinity of the city of Malaga, were associated with tsunamis. According to chronicles, the sea rose to about 5 m in the port and claimed several dozen victims (El Mrabet, 1991; Macías et al., 2013).

Both Ibn Abi Zar and Ibn Idari explain the effects of the earthquake, which allows us to get an idea of its destructive level. The first thing they mention is the loud sound they heard when they said the earth shook with a dreadful noise and shudder. It had to be a significant earthquake as Ibn Abi Zar reports that men had never seen or heard such an even, and were forced to seek truces in their various battlefields – the most educated Muslims understood that earthquakes were part of nature, but a large part of the population saw it as divine punishment for their actions.

In Córdoba great destruction is not reported. Fortresses and mountains shuddered or moved, but the fall of buildings was not described. However, the text of Ibn Abi Zar, closer to the Malaga coast, reports that many fortress and magnificent buildings fell, others were ruined, mountains sank, crags opened, and the earth sank and swallowed towns and heights, just as many towns on the southern and western coast of Spain were ruined. Clearly the intensity of the earthquake was higher closer to the coast, further exacerbated by a tsunami. The text says that the sea retreated and separated from the coasts, and islands and reefs in the sea disappeared. Thanks to the location in which it is known that they were fighting with other Muslims, and to the archaeological remains found in Estepona, we believe it possible that a tsunami affected, at least, a sector of the eastern coast of Andalusia.

Returning to the sedimentary record of Estepona from the year 881 AD, few works make any kind of allusion about its existence beyond documentary sources (Gracia et al., 2010; Reicherter et al., 2010; Ruiz et al., 2013), and none provides clear evidence in this regard. It is currently assumed that the epicenter of the earthquake/tsunami was located in the Gulf of Cádiz (IGN, 2020), but this possibility can be ruled out. Firstly, this location is surprising because this was never mentioned in documentary sources. Secondly, taking the Lisbon Earthquake of 1755, the largest comparable European catastrophe (Baptista et al., 1998), as an example, the tsunami waves resulting from this event were barely able to flank the Strait of Gibraltar, and caused only very slight disturbances on the Malaga coast (Martínez Solares, 2017; Macias et al., 2013). The same is true of other Atlantic tsunamis.

Another option is that the epicenter was situated the coasts of North Africa. The waves generated from this sector after an earthquake, especially from the Algerian margin and according to recent simulations (Lorito et al., 2008; Álvarez-Gómez et al., 2011), have the capacity to reach the Spanish coast, but on its easternmost side: the coasts of Almería, Alicante, and especially the Balearic Islands, but without incident on the coast of Malaga or Estepona. In any case, slight alterations are recorded from centimetric to decimetric (Macías et al., 2013). Historical data confirms this. If we turn to the memory of earthquakes of some importance that have affected the northwest of the African continent (Hamdache et al., 2010; Soloviev et al., 2013; Maramai et al., 2014), no tsunamis reached the Estepona coast.

For this reason, we point to a third option, to an origin in the faults closest to the Malaga coast and in the spine of the Alboran Sea. In this sector, there are several possible failures that may be related to the paleo-tsunami found in Estepona (González et al., 2010; Álvarez Gómez et al., 2011). One of these is the so-called Al-Idrisi Fault, located just over 100 km from Estepona (Álvarez Gomez et al., 2016). However, other may be a possibility: the Alboran Ridge Southern Fault East, Alboran Ridge Southern Fault West, and the Tofiño Bank Fault (Álvarez Gomez et al., 2011). On the other hand a tsunami caused by an underwater landslide triggered by the earthquake cannot be ruled out, feasible in the deep incision that occurs in the Alborán Ridge, also called Al-Borani Canyon (Macías et al., 2013).

The height of the wave from AD 881, according to the geomorphologic position (>2 m) and its proximity to less than 100 m from the sea implies it must have reached the Estepona coast with a height between 1-2 m. Although simulations do not usually show waves exceeding 1.7 m, the 1680 episode seems to suggest this (El-Mrabet, 1991; Santonja, 1998). Once it reached the continent, and taking into account its geographical and topographic location, and the nature of the sediments found, the wave must have penetrated the "Arroyo de la Calancha" and with the retreat to the sea, the hill being an obstacle, eroded its surface and subsequently deposited the marine-fluvial-continental sediment load.

5. CONCLUSIONS

It has been determined that the deposit named A-36 more than 2 m above sea level found in a small deposit in the city of Estepona (Málaga), corresponds very likely to the tsunami documented in historical sources in the year 881 AD. The lack of recognition is presumably due to its superficial nature and the poor understanding of this type of sediment in coastal of Spain.

The archaeological foundations that support the identification of our archaeological level A36 with a tsunami are developed in different aspects. On the one hand, A36 overlaps in a clear stratification sequence; its analysis reveals that stratigraphic actions occurred as an effect, first, of its deposition, which implied the devastation of an immediately previous housing horizon (phase II) and, second (after a hiatus with exclusively interfacial physical representation), as an effect of the reduction of its volume by the foundation of two buildings and the formation on its roof of a new level of use (phase III).

On the other hand, it has been determined that the ceramic materials present in the units that make up phase II (in their horizons of use and destruction) are techno-typologically located in the second half of the 9th century, while those corresponding to phase III belong and to the repertoires of the first half of the 10th century.

The adjustment of the archaeological chronologies relative to the dating of related historical events (tsunami in 881, caliphal subjugation in 924) suggests that the abandonment subsequent to the tsunami may be estimated at several decades in duration. It should be taken into account that our analysis deals with a specific sampling (6 m^2) and that until now it cannot be contrasted with other local or regional stratigraphies, being the excavation in c/Real 98 in Estepona the first and, until now, the only one in providing contextualized archaeological information on these historical events on the western Costa del Sol and its hinterland. Finally, it has been determined that the archaeological deposit A36, corresponds to the tsunami of the year 881 documented in the historical sources. Thus, it becomes the first witness of its existence.

Several strands of evidence confirm the deposits as the result of a tsunami and not of a storm surge. Two stand out: the presence of sedimentary material with marine elements (bioclasts, ichthyofauna and other organisms) and continental (soft ridges, fluvial ridges and sands, riverside vegetation) intermingled, and the presence of tuna remains indicating high-energy events.

Analysis of the historical texts confirms not only the approximate date of the catastrophe (May 26), but also its possible location in one of the faults or canyons in the Alboran Sea.

The micro morphological study confirms that A-36 samples share characteristics consistent with emplacement through the action of an historic tsunami during the medieval period. The section exhibited distinct facies, mainly distinguished by the degree of sorting and the range in particle size. Medium and coarse sands dominated the sediments; however, there were facies with a greater abundance of heterogeneity in the form of gravels and boulders. This can be interpreted as a consequence of each wave associated with the tsunami event forming a distinct sedimentary unit. Distinct upper and lower sub-units representing run-up and backwash are probably represented although there is considerable uncertainty about when most deposition occurred. There appeared to be cross bedding within the sedimentary units and perhaps these correspond with landward and backwash seaward currents associated with the individual tsunami waves. Certainly the imbrications of shells and the rounding and sorting of archaeological material can be included in these processes. The association of building debris, archaeological residues and beach sediments and marine fauna are perhaps compelling evidence of a geoarchaeological tsunami signature.

However, considering the height of the wave, the subsequent continuity of the human presence in the vicinity of the site and the exceptional nature of these events in this part of the Mediterranean, it seems that the tsunami had a limited capacity for destruction and did not result in the discontinuity of Estepona as a local focus of the population.

ACKNOWLEGEMENTS

The authors are indebted to Arqueotectura company for transferring the materials for this study. We also thank Prof. Charles French and Dr. Tonko Rajkovaca, from University of Cambridge, for manufacturing thin sections. We also thank to Dr William Deadman from Durham University for reading the draft of the paper and to Dikran Jarekian for his support in the Arabic translations. Finally, many tanks to the Estepona City Council for their support and efforts.

APPENDICES

The text that we reproduce below is the translation made by Conde (1820, p. 310-311):

> *In the year two hundred and sixty-seven, Thursday, twenty-two of the moon of Xawâl, the earth shook with such terrible noise and trembling, that many fortresses and magnificent buildings fell, and others were very broken, mountains sank, rocks were opened, and the earth sank and swallowed up towns and heights, the sea retreated and moved away from the coasts, and islands and reefs disappeared in the sea. The people left the towns and fled to the fields, the birds left their nests and the frightened beasts left their caves and burrows in general embarrassment and upset: men never saw or heard such a thing: many towns on the southern and western coast of Spain were ruined. All these things so influenced the moods of men, and especially the ignorant multitude, that Almondhir couldn't persuade them that these were natural things, although infrequent, that these hadn't influence or relation with the behaves of men or with their endeavour, but because of their ignorance and vain fears, that the earth shook the same for Muslims as for Christians, for beasts and for innocent creatures. In agreement with King Muhammad, Almondhir arranged truces with the King of the Christians, who sent his messengers to Córdoba, accompanied by Muslim knights.*

The second text comes from Ibn Idari's quill. There are two similar translations that provide information to help us understand the event (Fernández González, 1860, p. 205-206; Souto, 1995, p. 230).

> *And of the admirable things that happened that year (Hegira 267), which shook the earth with a horrible shudder at the hour of the azala of sunset, and it raised a cloud full of darkness, and it thundered and flashed and six men were struck by the thunderbolt and fell on their backs, dying two and the people prostrated themselves in adoration, minus the imam that remained standing, although it was the two who died, those of the people who were closest to the imam and the hair of one of them was*

> *Among the wonders of this year (Hegira 267) is what Ar-Rāzī and others tell. They say: The earth shook in Córdoba by a strong earthquake and the wind rose when the prayer of al-Magrib, unleashing a cloud carrying darkness, thunder and lightning. Six people were struck down and thrown on their backs. Two of them died. All the people fell prostrate except the Imam, who remained standing. The two men who died were from the people closest to the imam. The hair of one of them was*

burned and his face and his left side blackened, and the other appeared with his right side black, and the four passed out remained motionless until the imam was filled with unease, and they were asked about what they had felt and said: "We have felt fire like a heavy sea wave." And the people of the mosque were found dying of fire and no trace of lightning was found on the ceiling (or acicafe) or on the wall and the fortresses and mountains were shaken, and the people of the fortresses fled to the fields, humiliating themselves before God, exalted be his name, and the earthquake was general from the Ax-Xemí sea to the extreme Guf and the last of the land of Christendom, that there has been no one who has a different opinion about it.

burned and his face and left side blackened, while the other showed black his right side. The four taken down remained that way until the imam was unoccupied. They were asked about what they felt, and they answered: "We feel a fire like a heavy wave." The people of the mosque smelled the fire, but no trace of the spark was found on roofs or walls. As a result of this earthquake, the fortresses and mountains shook, and the people fled to the open fields, supplicating God, the Almighty. [The intensity of] this earthquake ranged from the Mediterranean Sea to the northernmost and even the farthest polytheistic land, without experiencing any variation.

REFERENCES

Acién Almansa, M, Castaño Aguilar, JM, Navarro Luengo, I et al (2003), Cerámicas tardorromanas y altomedievales en Málaga, Ronda y Morón. Cerámicas tardorromanas y altomedievales en la Península Ibérica. *Anejos del Archivo Español de Arqueología*. XXVIII (*II Simposio de Arqueología. Mérida* 2001). Madrid, 411-454.

Acién Almansa, M & Salado Escaño, JB (2009). Del fundus a la qarya. Bezmiliana: origen y evolución de una alquería. *Xelb*, 9: 141-154.

Alonso Chaves, FM, García Navarro, E, Camacho Cerro, MA, Fernández Rodríguez, C (2011). Propuesta sismotectónica para la terminación oriental de la Zona de Fractura Azores–Gibraltar entre el Banco de Gorringe y el Banco del Guadalquivir. *Geogaceta* 50, 1: 11-14.

Álvarez Gómez, J, Aniel Quiroga, Í, González, M, Otero Díaz, LJ (2011). Tsunami hazard at the Western Mediterranean Spanish coast from seismic sources. *Natural Hazards*, 11: 227-240.

Álvarez Gómez, JA, Martín, R, Pérez López, R, Stich, D, Cantavella, JV, Martínez Díaz, JJ, Carreño, E (2016). La serie sísmica de Alhucemas 2016. Partición de la deformación e interacción de estructuras en un límite de placas difuso. *Geotemas* 16 (2): 491-494.

Argus, DF, Demets, C, Gordon, RG, Stein, S, Woods, D (1986). Plate motions between the North American, African, and Eurasian plates over the past 10 Ma. *EOS*, 67: 1-1199.

Arteaga Cardineau, C, Blánquez Pérez, J, Roldán Gómez, L (2015). Consideraciones paleogeográficas en la bahía de Algeciras. Acerca de un posible tsunami en la Carteia romana (San Roque, Cádiz). *Cuaternario y geomorfología: Revista de la Sociedad Española de Geomorfología y Asociación Española para el Estudio del Cuaternario*, 29 (1-2): 137-156.

Arteaga Cardineau, C & González Martín, JA (2004). Presencia de marinos y dunares sobre un alfar romano en la Bahía de Algeciras (Cádiz, España). *VIII Reunión Nacional de Geomorfología*, Toledo: 393-400.

Baptista, MA, Miranda, PMA, Miranda, JM, Víctor, LM (1998). Constrains on the source of the 1755 Lisbon tsunami inferred from numerical modelling of historical data on the source of the 1755 Lisbon tsunami. *Journal of Geodynamics*, 25 (1-2): 159-174.

Bernal Casasola, D (2018). Continuidad y cesura en las ciudades tardorromanas del Estrecho de Gibraltar. Sabine Panzram y Laurent Callegarin (eds.), *Entre civitas y madīna. El mundo de las ciudades en la Península Ibérica y en el norte de África (siglos iv-ix),* Collection de la Casa de Velázquez (167), Madrid, 2018, 105-118.

Bouyoucos, GJ (1936). Directions for making mechanical analyses of soils by the hydrometer method. *Soli Science* 42 (3): 225-230.

Cailleux, A & Tricart, J (1963). *Initiation à l'étude des sables et des galets*. Vol. 1. Centre de documentation universitaire.

Calvo Capilla, S (2016). La religiosidad nazarí en época de Yūsuf I (1332-54), según un texto traducido por José Antonio Conde, después llamado 'Código de Yūsuf. *AlHadra* 2 (3-4): 201-232

Calvo Pérez, J (2003). José Antonio Conde (1766-1820), traductor. *Quaderns de Filologia. Estudis lingüistics*, 8: 181-203.

Carandini, A (2007). *Historias en la tierra. Manual de excavación arqueológica*. Barcelona: Crítica Arqueología.

Carreño, E (2005). Peligrosidad de Tsunamis en las costas españolas. Simulaciones, *La Enseñanza de las Ciencias de la Tierra*, 13(1): 60-64.

Conde, JA (1820) *Historia de la dominación de los árabes en España*, sacada de varios manuscritos y memorias arábigas. Imprenta que fue de García, Madrid.

Courty, MA, Goldberg, P, MacPhail, R (1989). *Soils and micromorphology in archaeology*. Ed. Cambridge.

Day, PR (1965). Particle fractionation and particle-size analysis. In *Methods of soils analysis*. Part 1: 545-567.

DeMets, C, Gordon, RG, Argus, DF (2010). Geologically current plate motions. *Geophysical Journal International*, 181(1): 1-80.

Derr, JS, St-Laurent, F, Freund, FT, Thériault, R (2011). Earthquake lights. In *Encyclopedia of Earth Sciences Series. Encyclopedia of Solid Earth Geophysics*. Springer. Part 5: 165-167.

Domínguez Prats, AB (2006). José Antonio Conde (1766-1820). Autor de Historia de la dominación de los árabes en España (Madrid 1820/21), descubridor de la literatura aljamiada, y primer historiador español moderno que usó las fuentes árabes en lengua original. In *Antigüedad y cristianismo: Monografías históricas sobre la Antigüedad tardía* 23: 883-898.

El Mrabet, T (1991). *La sismicité historique du Maroc*. Tesis de Licenciatura, Faculté des Lettres et des Sciences Humaines, Université Mohammed V, Rabat.
Fernández Fonfría, L (2010). Dos Crónicas Magrebíes Medievales: Al-Ḏajira Al-Saniyya y Rawd al-Qirtas. *El Futuro del Pasado: revista electrónica de historia* 1: 465-474.
Fernández González, F (traductor)(1860). *Historias de Al-Ándalus, por Aben-Adhari de Marruecos*, traducidas directamente del arábico y publicadas con notas y un estudio histórico-crítico por Doctor Don Francisco Fernández González. Original of Ahmad Ibn-Muḥammad Ibn Idari Al-Marrakusi. Imprenta de Don Francisco Ventura y Sabatel, Granada.
Florido del Corral, D, Menanteau, L, (2006). Geohistoria de las almadrabas del golfo íbero-marroquí (siglos XVI XXI). In *Historia de la Pesca en el ámbito del Estrecho*, II. Sevilla: Consejería de Innovación, Ciencia y Empresa y Consejería de Agricultura y Pesca: 855-926 .
Folk, RL, Ward, WC (1957). Brazos River bar [Texas]; a study in the significance of grain size parameters. *Journal of Sedimentary Research*, 27(1): 3-26.
French, CA (2003). *Geoarchaeology in action: studies in soli micromorphology and landscapes evolution*. Psychology Press.
French, CA (2015). *A handbook of geoarchaeological approaches to settlement sites and landscapes*. Vol.1. Oxbow Books.
Galbis Rodríguez, J (1932). *Catálogo sísmico de la zona comprendida entre los meridianos 5º E y 20º W de Greenwich y los paralelos 45º y 25º N*. Dirección General del Instituto Geográfico, Catastral y de Estadística, Madrid. Tomo I.
Galbis Rodríguez, J (1940). *Catálogo sísmico de la zona comprendida entre los meridianos 5º E y 20º W de Greenwich y los paralelos 45º y 25º N*. Dirección General del Instituto Geográfico, Catastral y de Estadística, Madrid. Tomo II.
Goodman-Tchernov, Beverly, N (2009). Tsunami waves generated by the Santorini eruption reached Eastern Mediterranean shores. *Geology*, 37, 10: 943-946.
Goldberg, P, MacPhail, R (2006). *Practical and theoretical geoarchaeology*. Malden.
Gonzalez, M, Medina, R, Olabarrieta, M, Otero, L (2010). Tsunami hazard assessment on the Southern Coast of Spain. *Turkish Journal of Earth Sciences*, 19(3): 351-366.
Goto, K, Kawana, T, Imamura, F (2010). Historical and geological evidence of boulders deposited by tsunamis, southern Ryukyu Islands, Japan. *Earth-Science Reviews*, 102(1-2): 77-99.
Govorushko, SM (2012). *Natural processes and human impacts: interactions between humanity and the environment*. Springer Science & Business Media, Dordrecht.
Gracia, E, Vizcaino, A, Escutia, C, Asioli, A, Rodes, A, Pallas, R, Goldfinger, C (2010). Holocene earthquake record offshore Portugal (SW Iberia): testing turbidite paleoseismology in a slow-convergence margin. *Quaternary Science Reviews*, 29 (9-10): 1156-1172.
Guerra-Merchán, Antonio (1996). Análisis sedimentológico y paleoecológico del yacimiento plioceno de Parque Antena (Estepona, Málaga). *Revista Española de Paleontología*, 11: 226-234.
Gutiérrez Lloret, S (2011). El reconocimiento arqueológico de la islamización. Una mirada desde al-Andalus. *Zona arqueológica*, 15 (1): 189-210.

Hamdache, M, Peláez, JA, Talbi, A, Casado, CL (2010). A unified catalog of main earthquakes for Northern Algeria from AD 856 to 2008. *Seismological Research Letters*, 81 (5): 732-739.

Haro Cortés, M (2012). La traducción castellana inédita de Calila e Dimna árabe (José Antonio Conde, 1797). *Boletín de la Real Academia Española,* XCII: 85-116.

Harris, EC (1991). *Principios de Estratigrafía Arqueológica*. Barcelona: Crítica Arqueología.

Hitchcock, R (1986). Hispano-Arabic historiography: the legacy of J. A. Conde. In *Arabia and the Gulf: From Traditional Society to Modern States. Essays in Honour of M. A. Shaban's 60th Birthday* (16th November 1986). London.

Huici Miranda, A (traductor)(1964). *Rawd al-Qirtas. Original of 'Ali ibn 'Abd Allah Ibn Abi Zar' al-Fasi*. Anúbar Ediciones, Valencia. Volumen 1.

Ictio. Term (2007). *Base de datos terminológicos y de identificación de especies pesqueras de las costas de Andalucía*. Ministerio de Economía y competividad. CSIC.

IGME (1978). *Memoria del Mapa Geológico de España, Hoja 1072, Estepona*. Servicio de Publicaciones del Ministerio de Industria. Instituto Geológico y Minero de España. Madrid.

IGN- Instituto Geográfico Nacional (2020). *Leyenda del Catálogo de Tsunamis de las Costas de España*.

Javaloy, A, Galindo-Zaldivar, J, González-Lodeiro, F (2002). Palaeostress evolution of the Iberian Peninsula. *Testonophysics* 357 (1-4): 159-186.

Kench, PS, Nichol, SL, Smithers, SG, Mclean, RF, Brander, RW (2008). Tsunami as agents of geomorphic change in mid-ocean reef islands. *Geomorphology*, 95(3-4): 361-383.

Komatsubara, J, Fujiwara, O, Takada, K, Sawai, Y, Aung, TT, Kamataki, T (2008). Historical tsunamis and storms recorded in a coastal lowland, shizuoka prefecture, along the pacific coast of japan. *Sedimentology*, 55(6): 1703-1716.

Lapida Gutiérrez, E (1997). *Cómo los musulmanes llamaban a los cristianos hispánicos*. Generalitat Valenciana, Conselleria de Cultura, Educació i Ciència: Instituto de Cultura "Juan Gil-Albert". Diputación Provincial de Alicante.

Lario, J, Luque, L, Zazo, C, Goy, JL, Spencer, C, Cabero, A, González-Delgado, JÁ (2010b). Tsunami vs. storm surge deposits: a review of the sedimentological and geomorphological records of extreme wave events (EWE) during the Holocene in the Gulf of Cadiz, Spain. *Zeitschrift für Geomorphologie, Supplementary Issues*, 54(3): 301-316.

Lario, J, Zazo, C, Goy, JL, Silva, PG, Bardají, T, Cabero, A, Dabrio, CJ (2010a). Registro geológico de tsunamis en el SW peninsular durante el Holoceno. *Primera Reunión Ibérica sobre Fallas Activas y Paleosismología, resúmenes*: 167-170.

Lario, J, Zazo, C, Goy, JL, Silva, PG, Bardají, T, Cabero, A, Dabrio CJ (2011). Holocene palaeotsunami catalogue of SW Iberia. *Quaternary International*, 242 (1): 196-200.

Lindner, G (2008). *Guide des coquillages marins. Plus de 1000 espèces des mers du munde*. Dlachaux et Niestlé. Paris.

Lorito, S, Tiberti, MM, Basili, R, Piatanesi, A, Valensise, G (2008). Earthquake‐generated tsunamis in the Mediterranean Sea: Scenarios of potential threats to southern Italy. *Journal of Geophysical Research: Solid Earth*, 113.

Macías, J, Fernández-Salas, LM, González-Vida, JM, Vázquez, JT, Castro, MJ, Bárcenas, P, Parés, CM (2013). *Deslizamientos submarinos y tsunamis en el Mar de Alborán. Un ejemplo de modelización numérica*. Instituto Español de Oceanografía Ministerio de Economía y Competitividad.

Manzanares de Cirre, M (1968). Gloria y descrédito de D. José Antonio Conde. *Anuario de Estudios Medievales*, 6: 553-563.
Manzano Moreno, E (2006). *Conquistadores, emires y califas. Los omeyas y la formación de al-Andalus*. Barcelona: Crítica, Serie Mayor.
Maramai, A, Brizuela, B, Graziani, L (2014). The Euro-Mediterranean Tsunami Catalogue. *Annals of Geophysics*, 57 (4): 435.
Martínez Enamorado, V (2003). *Al-Andalus desde la periferia. La formación de una sociedad musulmana en tierras malagueñas (siglos VIII-X)*. Málaga: Diputación Provincial.
Martínez Enamorado, V (2009). *Cuando Marbella era una tierra de alquerías*. Marbella: Ayuntamiento de Marbella.
Martínez Solares, JM (2017). El Terremoto de Lisboa de 1 de noviembre de 1755. *Física de la Tierra*, 29: 47.
Martínez Solares, JM & Mezcua Rodríguez, J (2002). *Catálogo sísmico de La Península Ibérica (880 a.C. – 1900)*. Dirección General del Instituto Geográfico Nacional. Ministerio de Fomento, Madrid.
Melero García, F, Oliver León, A & Loriguillo Millán, ME (2015). La alquería altomedieval de Valsequillo (Antequera, Málaga): génesis, reocupación y abandono. *Mainake*, XXXV (2014-2015), pp. 241-276.
Miall, AD (2016). Stratigraphy: the modern synthesis. In *Stratigraphy*: A Modern Synthesis: 311-370. Springer, Cham.
Molina, L (2005). La historia de los omeyas de al-Andalus en los Masālik al-Absār. Al-Qantara. *Revista de estudios árabes*, 26 (1): 123-139.
Morton, RA, Gelfenbaum, G, Jaffe, BE (2007). Physical criteria for distinguishing sandy tsunami and storm deposits using modern examples. *Sedimentary Geology*, 200 (3-4): 184-207.
Mottershead, DN, Bray, MJ, Soar, PJ, Farres, PJ (2015). Characterisation of erosional features associated with tsunami terrains on rocky coasts of the Maltese islands. *Earth Surface Processes and Landforms*, 40 (15): 2093-2111.
Murphy, MW (1986). *Relationships between micromorphology and impact properties of injection moulded isotactic polypropylene*. Doctoral dissertation. Brunel University.
Navarro Luengo, I, Bravo Jiménez, S, Suárez Padilla, J & Fernández Rodríguez, LE (1998). Turrus Jusayn y Munt Nis: una propuesta de identificación para dos fortificaciones hafsuníes en la Costa Occidental malagueña. *Actas del I Congreso de Fortificaciones en al-Andalus*. Algeciras, pp. 433-439.
Nott, J (2004). The tsunami hypothesis—comparisons of the field evidence against the effects, on the Western Australian coast, of some of the most powerful storms on Earth. *Marine geology*, 208(1): 1-12.
Papadopoulos, GA, Gerassimos, A, Fokaefs, Anna (2005). Strong tsunamis in the Mediterranean Sea: a re-evaluation. *ISET Journal of Earthquake Technology*, 42 (4): 159-170.
Papadopoulos, GA, Gràcia, E, Urgeles, R, Sallares, V, De Martini, PM, Pantosti, D, Salamon, A (2014). Historical and pre-historical tsunamis in the Mediterranean and its connected seas: Geological signatures, generation mechanisms and coastal impacts. *Marine Geology*, 354: 81-109.

Pararas-Carayannis, G., 1992. The tsunami generated from the eruption of the volcano of Santorin in the Bronze Age. *Nat. Hazards* **5,** 115–123 (1992). https://doi.org/10.1007/BF00127000

Pararas-Carayannis, G. and Mader L.C., 2010. THE EARTHQUAKE AND TSUNAMI OF 365 A.D. IN THE EASTERN MEDITERRANEAN SEA. Proceedings of the 9th U.S. National and 10th Canadian Conference on Earthquake Engineering. Compte Rendu de la 9ième Conférence Nationale Américaine et 10ième Conférence Canadienne de Génie Parasismique July 25-29, 2010, Toronto, Ontario, Canada • Paper No 1846 https://www.caee.ca/10CCEEpdf/2010EQConf-001846.pdf

Pararas-Carayannis, G. 2011. THE EARTHQUAKE AND TSUNAMI OF JULY 21, 365 AD IN THE EASTERN MEDITERRANEAN SEA - Review of Impact on the Ancient World - Assessment of Recurrence and Future Impact. January 2011 Science of Tsunami Hazards 30(4):253-292 (last paper in the journal Vol. 40 N. 1, 2021 below) http://tsunamisociety.org/304GPC.pdf

Pararas-Carayannis George, 2021.THE GREAT LISBON EARTHQUAKE AND TSUNAMI OF 1 NOVEMBER 1755 Evaluation of the Compression Convergence Mechanism, http://www.tsunamisociety.org/STHVol40N1Y2021c.pdf

Penelas, M & Molina, L (2011). Dos fragmentos inéditos del volumen II del "Muqtabis" de Ibn Hayyan. *Al-qantara: Revista de estudios árabes*, 32 (1): 229-241.

Reicherter, K, Becker-Heidmann, P (2009). Tsunami deposits in the western Mediterranean: remains of the 1522 Almería earthquake? *Geological Society, London, Special Publications*, 316(1): 217-235.

Reicherter, K, Vonberg, D, Koster, B, Fernández-Steeger, T, Grützner, C, Mathes-Schmidt, M (2010). The sedimentary inventory of tsunamis along the southern Gulf of Cádiz (southwestern Spain). *Zeitschrift für Geomorphologie, Supplementary Issues*, 54(3): 147-173.

Roskam, S (2002). *Teoría y práctica de la excavación*. Barcelona: Crítica Arqueología.

Roux, G (1934). Notes sur les tremblements de terre ressentis au Maroc avant 1933. *Extrait Mem. Soc. Scien. Nat. Du Maroc*, núm. XXXIX: 30.

Ruiz, F, Rodríguez-Vidal, J, Cáceres, LM, Carretero, MI, Pozo, M, Gómez-Toscano, F, Abad, M (2013). Morpho-sedimentary evidence of Holocene tsunamis in Southwestern Spain estuaries: a summary. *VIII Reunión de Cuaternario Ibérico.*

Ruiz Zapatero, G (2013). La excavación arqueológica. En García-Díez M y Zapata L (ed). *Métodos y Técnicas de análisis y estudio en arqueología prehistórica. De lo técnico a la reconstrucción de los grupos humanos*. Universidad del País Vasco: 39-72.

Salado Escaño, JB & Navarro Luengo, I (2001). El Nicio (Málaga): un yacimiento de transición entre los últimos elementos feudales y la sociedad islámica. *Mil anos de Fortificaçoes na Península Ibérica e no Magreb (500-1500): Actas do Simposio Internacional sobre Castelos*. Lisboa, Ediçoes Colibri/ Câmara Municipal de Palmela: 161-169.

Sánchez, FV (2011). El terremoto de Alhama de Granada de 1884 y su impacto. *Anuari Verdaguer*: 11-45.

Santonja, G (1998). *Incierta memoria de las tempestades y el terremoto de 1680*. Ed. Universidad de Salamanca. Salamanca.

Shinozaki, T, Fujino, S, Ikehara, M, Sawai, Y, Tamura, T, Goto, K, Abe, T (2015). Marine biomarkers deposited on coastal land by the 2011 tohoku-oki tsunami. *Natural Hazards*, 77(1): 445-460.

Smol, J, Stoermer, E (Eds) (2010). *The diatoms: applications for the environmental and earth sciences*. Cambridge University Press, Cambridge.

Soil Survey Division Staff (1993). *Soil survey manual.* Soil Conservation Service. U.S. Department of Agriculture Handbook 18.

Soloviev, SL, Solovieva, ON, Go, CN, Kim, KS, Shchetnikov, NA (2013). *Tsunamis in the Mediterranean Sea 2000 BC-2000 AD*, Vol. 13, Springer Science & Business Media.

Souto, JA (1992). Fuentes magrebíes relativas a la Marca Superior de al-Andalus: el volúmen II de *al-Bayan al-Mugrib* de Ibn Idari. In *Historia, ciencia y sociedad: actas del II Coloquio Hispano-Marroquí de Ciencias Históricas*, Granada: 299-322.

Souto, JA (1995). El emirato de Muhammad I en el Bayān al-Mugrib de IBN ‘Idārī. *Anaquel de Estudios Árabes*, VI: 209-245

Srivastava, SP, Roest, WR, Kovacs, LC, Oakey, G, Levesque, S, Verhoef, J, Macnab, R (1990). Motion of Iberia since the Late Jurassic: results from detailed aeromagnetic measurements in the Newfoundland Basin. *Tectonophysics*, 184 (3-4): 229-230.

St-Laurent, F (2000). The Saguenay, Québec, earthquake lights os November 1988-January 1989. *Seismol. Res. Lett.* 71: 160-174.

Suárez Padilla, J, Tomassetti Guerra, JM, León Martín, CA, Martín Escarcena, AM, Torres Abril, F (2017). Excavación arqueológica preventiva en calle Real nº 98 de Estepona (Málaga). Secuencia urbana entre los siglos IV y XXI d. C. *Anuario Arqueológico de Andalucía*, 2017 (In press).

Thériault, R, St-Laurent, F, Freund, FT, Derr, JS (2014). Prevalence of earthquake lights associated with rift environments. *Seismological Research Letters*, 85 (1): 159-178.

Trask, PD & Wu, Z (1932). *Origin and environment of source sediments of petroleum*. Gulf Publishing Company.

Udías, A (2015). Historical earthquakes (before 1755) of the Iberian Peninsula in early catalogs. *Seismological Research Letters*, 86(3): 999-1005.

Udías, A (2017). Terremotos de la Península Ibérica antes de 1900 en los catálogos sísmicos. *Física de la Tierra*, 29: 11-27.

Usami, K, Ikehara, K, Jenkins, RG, Ashi, J (2017). Benthic foraminiferal evidence of deep-sea sediment transport by the 2011 Tohoku-oki earthquake and tsunami. *Marine Geology*, 384: 214-224.

ISSN 8755-6839

SCIENCE OF **TSUNAMI HAZARDS**

Journal of Tsunami Society International

Volume 40 **Number 4** **2021**

EVALUATION OF SEISMIC AND TSUNAMI RESISTANCE OF POTENTIAL SHELTERS FOR VERTICAL EVACUATION IN CASE OF A TSUNAMI IMPACT IN MANTA AND SALINAS, CENTRAL COAST OF ECUADOR

Theofilos Toulkeridis[1]*, Irma Narciza Barahona-Quelal[1], Edisson Oscar Pilco-Paguay[1], Diana Maribel Cacuango-Casco[1], Brayan Steven Guilcaso-Tipán[1] and Wilson Paúl Sailema-Hurtado[1]

[1]Universidad de las Fuerzas Armadas ESPE, Sangolquí, Ecuador

*Corresponding author: ttoulkeridis@espe.edu.ec

ABSTRACT

The current study is a pioneer work of an improved technical risk assessment, where alternative solutions are proposed of how lives may be better saved during a potential tsunami impact in the coastal cities of Manta and Salinas in the central coast of Ecuador. As Ecuador has been already the target of several tsunamis during recorded history, further tsunami impacts are rather the rule than the exception. Due to short times between generation and impact of tsunamis and due to long distances to natural elevated safe sites, alternative solutions may be more required such as close-by buildings with certain heights. Those potential shelters as result of vertical evacuation needed to be evaluated for their seismic resistance as well as their resistance towards a tsunami. Both qualifications have been examined by the application of the Modified Italian Methodology in order to calculate the seismic vulnerability index (SVI) and subsequently also in order to determine the tsunami vulnerability index (TVI). In this respect we evaluated 18 buildings of such characteristics in Manta and further 99 in Salinas. Unfortunately, although many buildings stand the applied evaluations, due to the fact that almost all edifices are of private property, both entrance and stairs remain limited for the general public. Therefore, we propose that given regulations need to improve in order to allow the access to the general public during a tsunami emergency within an evacuation plan besides the implementation of an efficient early alert system.

Keywords: *Vertical evacuation, physical structural vulnerability, tsunami resistance, early alert system, Ecuador.*

Vol 40. No. 4, page 286 (2021)

1. INTRODUCTION

The search of live-saving solutions is the first task of any responsible and efficient risk assessment analysis including all types of natural hazards (Feng & Wang, 2003; Aitsi-Selmi et al., 2015; Kalkman & de Waard, 2017; Solinska-Nowak et al., 2018;). As the impact of tsunamis are mostly time-sensitive, proposals of reduction of loss of lives need to be sometimes creative and certainly on hand if other matters fail such as relocation or missing financial alternatives (Russell, 2005; Olson & Wu 2015; Sellnow & Seeger, 2021). In this respect, when it comes to evacuation routes and safe zones, any meter and or second counts (Gregg et al., 2006; Taubenböck et al., 2009; Wood & Schmidtlein, 2012; 2013). A tsunami is often a destructive and lethal force of nature, especially where human settlements have been constructed in their course of seashore impact (Pararas-Carayannis, 1977; Pararas-Carayannis, 2002; Pararas-Carayannis, 2003; Pararas-Carayannis, 2006; Pheng et al., 2006; Pararas-Carayannis, 2010; Mikami et al., 2012; Rodriguez et al., 2016; Toulkeridis et al., 2017a; Rodriguez et al., 2017; Suárez-Acosta et al., 2021).

Tsunamis occur worldwide, but mostly in the coastal areas of the Pacific Ring of Fire, which includes the coasts of Ecuador in northwestern South America (Pararas-Carayannis, 2012; Chunga and Toulkeridis, 2014; Pararas-Carayannis, 2017; Toulkeridis et al., 2017b). Along an 800 km long coast, the continental part of Ecuador has been impacted by a variety of tsunamis within the recorded history and paleo-tsunami deposits (Chunga and Toulkeridis, 2014; Ioualalen et al., 2014; Chunga et al., 2017; 2018; Toulkeridis et al., 2018; Toulkeridis et al., 2019). There is a high vulnerability of the infrastructure as well as the corresponding settled population, which goes along with a low degree of preparation of both, authorities and the public (Celorio-Saltos et al., 2018; Matheus-Medina et al., 2018; Edler et al., 2020; Martinez and Toulkeridis, 2020).

Inevitably, and due little to no knowledge of previous impacts of tsunamis, the construction along coastal areas prone to tsunamis has let to the establishment of human settlements and associated infrastructure in areas of a high degree of vulnerability towards the impact zones of future tsunamis (Alcántara-Ayala, 2002; Papathoma & Dominey-Howes, 2003; Frankenberg et al., 2013). Massive residences, factories and other industrial or strategic constructions, as well as commercial and touristic activities are among the most inopportune situated places within these zones of high vulnerability in Ecuador and elsewhere (Papathoma et al., 2003; Calgaro & Lloyd, 2008; Calgaro et al., 2014; Barros et al., 2015; Matheus-Medina et al., 2018; Suárez-Acosta et al., 2021).

Additionaly, in many developing countries like in Ecuador, risk assessment and reduction, hazard evaluation, land use, territorial zoning and the need of relocation distant to vulnerable sites is almost never practiced, especially when political and economic crisis are more common than times of prosperity and tranquility. Therefore, living with the natural hazards has been the common policy of Ecuador, when applying risk assessment measures towards recurrent processes of hydro-meteorological or geologic origin, such as floods, droughts, hydric deficit, climate change, mass movements and landslides, volcanic activities, earthquakes and especially tsunamis (Toulkeridis et al., 2007; Padrón et al., 2008; Ridolfi et al., 2008; Padrón et al., 2012; Toulkeridis et al., 2015a; b; Toulkeridis et al. 2016; Vaca et al., 2016; Rodriguez et al., 2017; Toulkeridis and Zach, 2017; Mato and Toulkeridis, 2017; Jaramillo Castelo et al., 2018; Zafrir Vallejo et al., 2018; Aguilera et al.,

2018; Palacios Orejuela, and Toulkeridis, 2020; Toulkeridis et al., 2020a; b; Poma et al., 2021). Still, based on recent catastrophic seismic and volcanic events, Ecuador's policy started to develop from a more passive turn towards a more proactive risk assessment, at least from the side of the academy, which proposed a variety of solutions such as improved and more controlled land use management, signage of evacuation routes, drilling of the population and preventive education as well as even mitigation structures where affordable prior potential impacts (Toulkeridis, 2016; Toulkeridis et al., 2020c; Yépez et al., 2020; Herrera-Enríquez et al., 2020).

In case of the coastal part of Ecuador, a high amount of tsunami evacuation signs have been installed, although many more are needed, while several are inadequately placed, indicating a longer than needed path towards safety among other issues (Celorio-Saltos et al., 2018; Matheus-Medina et al., 2018). Hereby, evacuation routes may be often too long in order to arrive safe in case of a short-time warning if any, of a potential tsunami impact (Matheus Medina et al., 2016; Rodriguez et al., 2016; Toulkeridis et al., 2017a). Therefore, as an alternative solution, specific buildings may be used, which should have a sufficient amount of floors for an eventual vertical evacuation within a temporary shelter (Yeh et al., 2005; Park et al., 2012; Matheus Medina et al., 2016; Mostafizi et al., 2019). In order to comply with such requirements, these buildings need to be resistant to strong seismic movements as well as towards the impact of tsunami waves (Lukkunaprasit & Ruangrassamee, 2008; Meyyappan et al., 2013; Navas et al., 2018; Belash & Yakovlev, 2018; Aviles-Campoverde et al., 2021; Del-Pino-de-la-Cruz et al., 2021; Suárez-Acosta et al., 2021).

We have chosen Manta and Salinas, two of the most developed, frequented and touristic coastal cities of Ecuador in order to apply an enhanced risk assessment and management, by evaluating the possibility of using high buildings as potential shelters in case of a tsunami emergency. Such potential may be reached by the determination of the seismic and tsunamic resistance of these edifices when applying the Modified Italian Methodology in order to calculate the seismic vulnerability index (SVI) and subsequently also in order to determine the tsunami vulnerability index (TVI). This pioneering investigation applied on 117 buildings will allow an improved relationship between existing hazard zones and a corresponding land use policy in the coastal area of Ecuador.

2. GEODYNAMIC SETTING AND STUDY AREAS

Ecuador is situated within the interaction of a variety of continental and oceanic tectonic plates, along the Pacific Rim and therefore generated strong seismic activity and subsequently several tsunamis within recorded history (Pararas-Carayannis, 1980; Herd et al., 1981; Kanamori & McNally, 1982; Mendoza & Dewey, 1984; Pararas-Carayannis, 2012; Chunga & Toulkeridis, 2014). Such tsunamis have produced devastating results within coastal areas and its relatively unprepared population as well as their settlements (Gusiakov, 2005; Ioualalen et al., 2011; 2014; Pararas-Carayannis, 2012; Rodriguez et al., 2016; Heidarzadeh et al., 2017). This active continental margin is given due to the geodynamic constellation, which results from the subduction of the oceanic Nazca Plate together with its above-situated Carnegie Ridge below the continental South American and Caribbean Plates, both being separated by the Guayaquil-Caracas Mega Shear (Fig. 1; Kellogg et al., 1995; Gutscher et al., 1999; Egbue and Kellog, 2010).

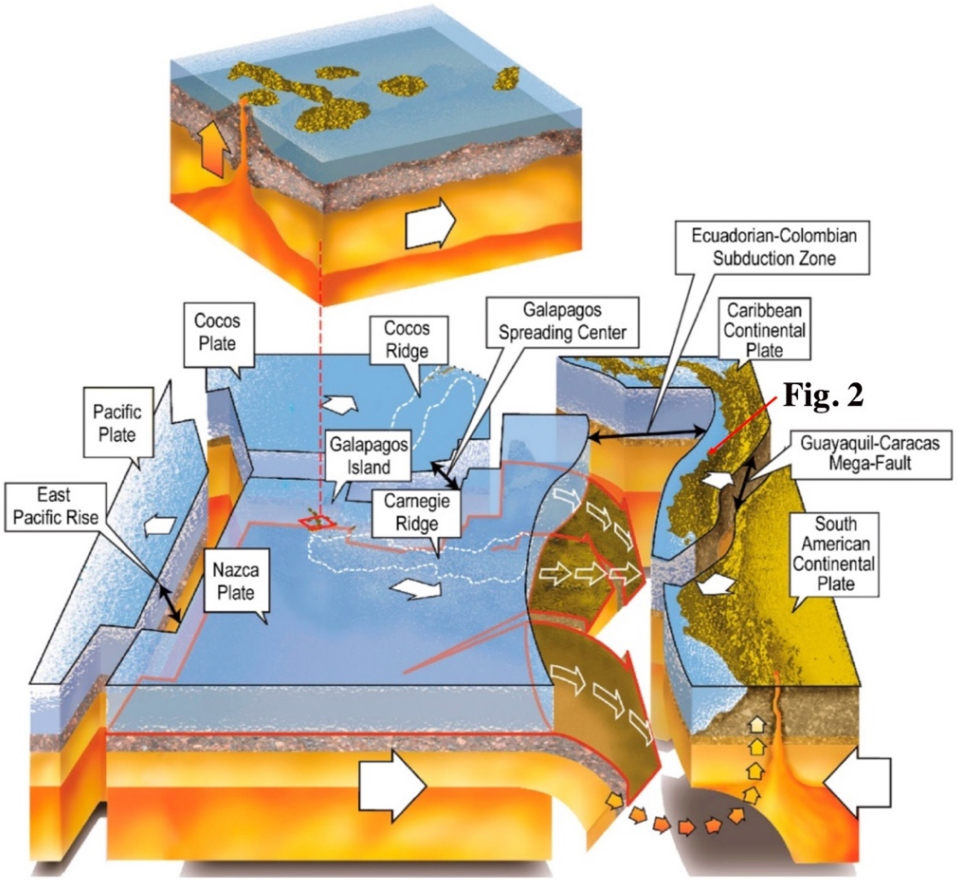

Fig. 1. Geodynamic setting of Ecuador with associated oceanic and continental plates and a variety of plate boundaries, such as the divergent plate boundaries named East Pacific Rise and Galapagos Spreading Center, the convergent plate boundary represented by the Ecuadorian-Colombian Subduction zone, as well as the transcurrent plate boundary represented by the Guayaquil-Caracas Mega-Fault. Also shown the Galapagos Islands and the Carnegie Ridge. Adapted from Toulkeridis, 2013, modified of Toulkeridis et al., 2017a.

This rises to a variety of tsunamis of tectonic as well submarine landslide origin (Moberly et al., 1982; Pontoise and Monfret, 2004; Ratzov et al, 2007; 2010; Ioualalen et al., 2011; Pararas-Carayannis, 2012). Besides the regular tsunamis, also even iminamis may be generated by massive sector collapses of volcanoes in the Galapagos archipelago (Kates, 1976; Cannon, 1994; Keating & McGuire, 2000; Pararas-Carayannis, 2002; Whelan & Kelletat, 2003; McGuire, 2006; Glass et al., 2007; Pinter & Ishman, 2008; Toulkeridis, 2011).

Therefore, Ecuador has been impacted by several seismic and tsunami hazards, based on the occurrence of local earthquakes, such as on January 31, 1906 (8.8 Mw), October 2, 1933 (6.9 Mw), May 14, 1942 (7.8 Mw), December 12, 1953 (7.3 Mw), January 16, 1956

(7.0), January 19, 1958 (7.6 Mw), December 12, 1979 (8.2 Mw), August 4, 1998 (7.2 Mw) and April 16, 2016 (7.8 Mw), besides other less intense occurrences (Berninghausen, 1962; Kanamori and McNally, 1982; Pararas-Carayannis, 2012; Chunga and Toulkeridis, 2014; Toulkeridis et al., 2017a; 2017b; 2018). Furthermore, a variety of distantly-generated tsunamis have impacted Ecuador, such as the tsunami of Japan in March 11, 2011 (8.9 Mw), which resulted to a considerable run-up in the Galápagos islands and the Ecuadorian mainland (Simons et al., 2011; Norio et al., 2011; Rentería et al., 2012; Lynett et al., 2013). A similar event based on a tsunami of Chile in February 27, 2010 (8.8 Mw) had only minor effects in the Galapagos Islands, as the main waves impacted during times of low tide (Rentería et al., 2012; Lynett et al., 2013)

The study area comprises the cities of Manta and Salinas, which are situated on the central coastal area of the Province of Manabí and Santa Elena respectively. Both are considered to hold the touristically most active and frequented beaches of the entire country. The economic development of both cities due to the fishing industry, import and export activities and strong tourism, has led to a considerable prosperity and hereby a dense human settlement along the oceanic shore close to the nice beaches (Fig. 2 and 3).

The peninsula of Salinas in the province of Santa Elena in western Ecuador, is without doubt the most touristic developed city of the entire country, receiving annually hundreds of thousands of visitors, making it to a perfect target within an upcoming tsunami, as most of the tourists are unaware of such hazards (Matheus-Medina et al., 2018; San Martin et al., 2018). The mostly flat areas of Salinas are made of Quaternary deposits of sandstones, conglomerates and calcareous banks of the Tablazo formation (Bosworth, 1922; Sheppard, 1930; Marchant, 1961; DeVries, 1988). Between this formation and specially in the western side of Salinas, appear several Cretaceous outcrops with more resistant rocks of mostly volcano-clastic origin mixed with some intercalated lavas and sedimentary rocks belonging to the Cayo Formation (Bristow, 1976; Wallrabe-Adams, 1990). To the eastern side of Salinas towards higher morphological elevations appear Eocene clastic sedimentary rocks of the Ancón Group (Stainforth, R. M. (1948; Jaillard et al., 1995).

Manta, which is the most important oceanic port of Ecuador (Carvache-Franco et al., 2018; González Santa Cruz et al., 2019; Carvache-Franco et al., 2020). It is mostly upon sediments of the Tablazo formation with some minor parts of sediments of the early middle Miocene Tosagua Formation within the western side of the city (Stainforth, 1948; Whittaker, 1988). The Manta peninsula and therefore most of the city is elevated right next to the beaches during a recent Plio-Queternary uplift based mainly on the subducted Carnegie Ridge (Pedoja et al., 2006; Freisleben et al., 2021).

Fig. 2. Geographic setting of the study areas with the cities of Manta and Salinas. Width of image is of about 17 km. Both images were taken from Google Earth in 2021.

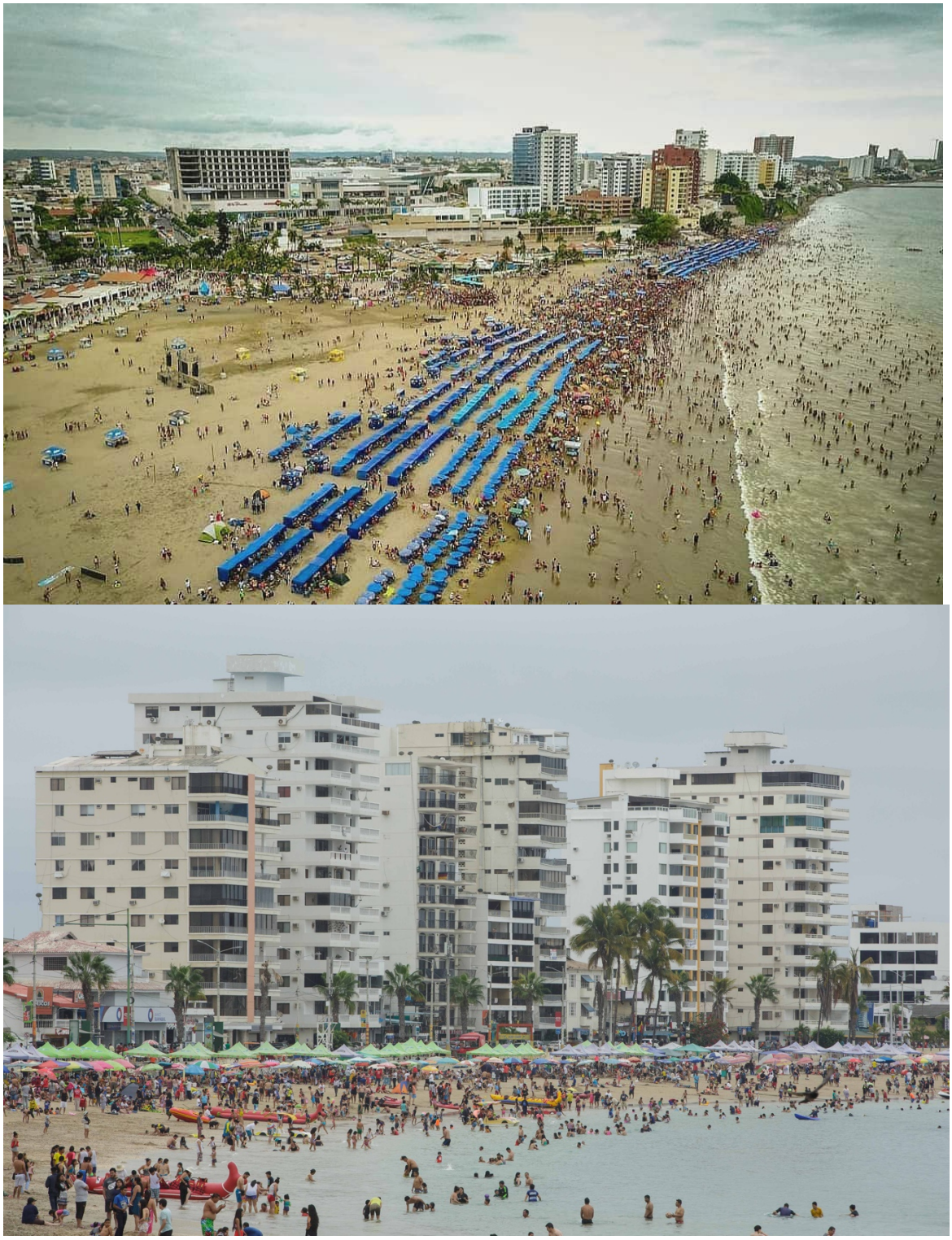

Fig. 3. Typical tourist activity on the beaches of Manta (upper image) and Salinas (lower image). Credit: GAD de Manta and Alexander Moya.

The problems and inadequate signage of tsunami warnings and indication of safe areas are omnipresent. One example may serve o explain such issue. In figure 4, we may demonstrate a case where in the northern side of the Salinas peninsula (Fig. 4a), just 260 meters of the beach (Fig. 4b), there is a correct signage of the safe areas with contradictory indication of the safest spot. Those citizens or tourists who would look to the signage towards east and may direct themselves towards this direction would have to evacuate for a distance of 1930 meters, while standing on the same spot, but watching the signage towards west, people would have to cross some 4700 meters to reach a safe, elevated site (Figure 4c).

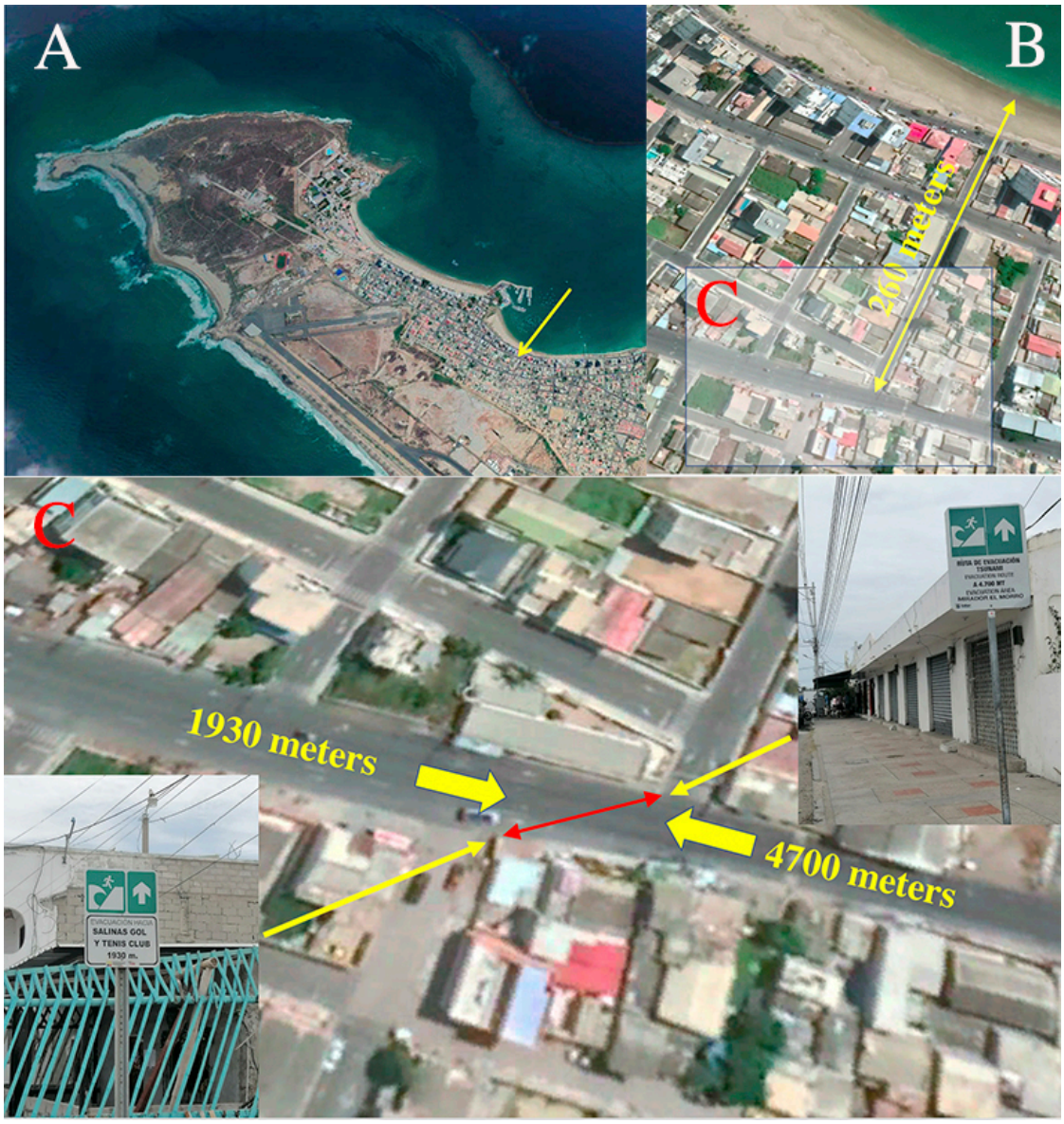

Fig. 4. Inadequate signage of tsunami warnings and safe areas in Salinas. Explained in the text.

3. METHODOLOGY

A total of 117 buildings have been encountered along the coastline of Manta (18) and Salinas (99), which were subsequently evaluated for their seismic as well as tsunami resistance (Fig. 3) in order to assess their feasibility as provisional shelters for vertical evacuation in case of an impact by a tsunami. The elevation of the tsunami impact has been considered to be of 24 meters based on a given picked simulation as chosen from many. The pre-selection of buildings was performed according to their height, considering those with more than four floors. The evaluation of each building was performed by couples of trained personnel with civil engineering expertise in order to minimize any subjectivity.

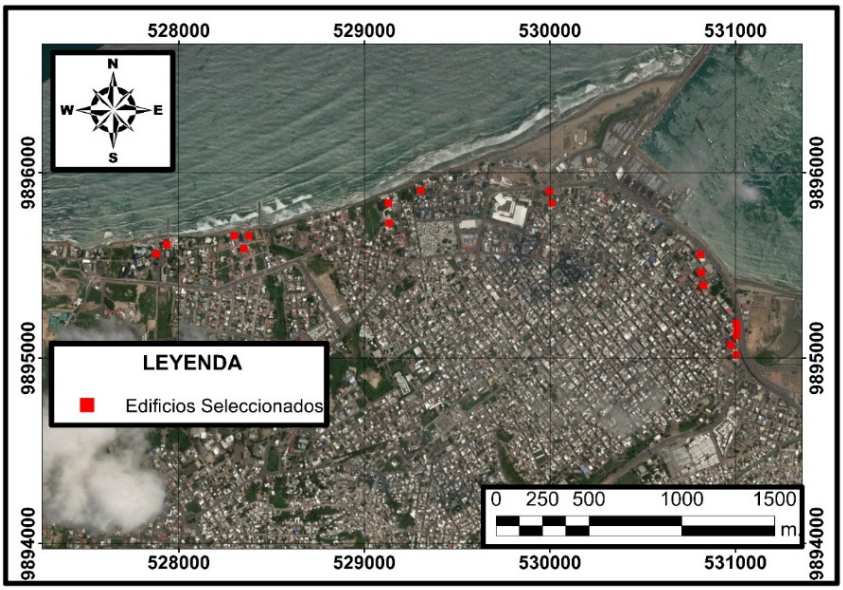

Fig 5. Map with the location of the 18 evaluated buildings in the city of Manta.

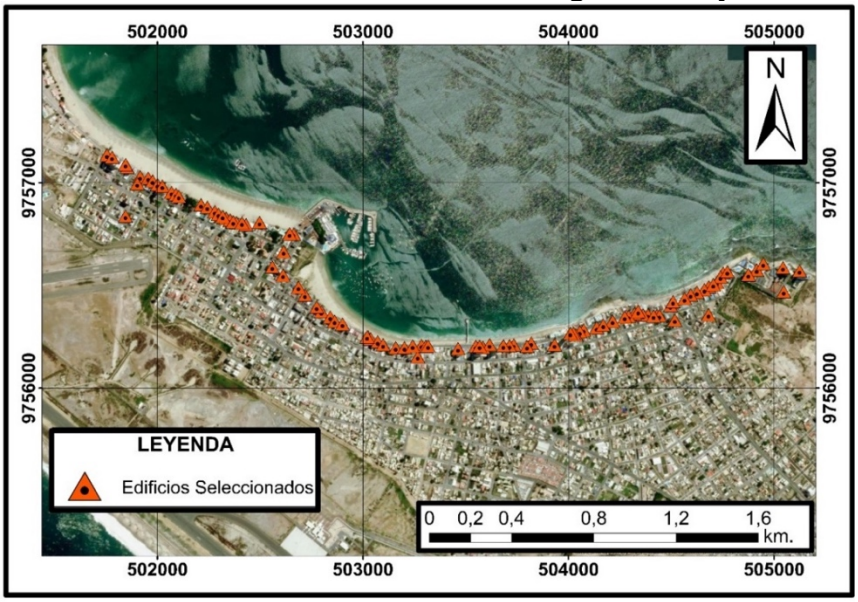

Fig 6. Map with the location of the 99 evaluated buildings in the city of Salinas.

Within this field approach, basic data were collected such as name of the building, geographical location, address, total number of floors, number of floors below and above surface, average altitude of each floor, area and year of construction, current use as well as capacity. After this initial data collection, an evaluation was conducted in order to reveal the seismic resistance of each building, by using a dozen of criteria based on the Modified Italian Methodology. This has served in order to calculate the seismic vulnerability index (SVI) prior to the tsunami impact evaluation (Table 1; Calvi et al., 2006; Amellal et al., 2012; Kassem et al., 2019). Furthermore, we added an additional evaluation, for the corresponding tsunami resistance of each building (Table 2). Hereby, the tsunami evaluation contained ten criteria which were defined by following the Guidelines for Design of Structures for Vertical Evacuation from Tsunamis of the Federal Emergency Management Agency of the United States of America (FEMA, 2019).

Table 1: Modified Italian Methodology to calculate the SVI (Aguiar&Rivas, 2018)

Criteria	**Classes / Ki**			Weighting
	A	**B**	**C**	**Wi**
1. Organization of the resistant system	0	6	12	1,00
2. Quality of the resistant system	0	6	12	0,50
3. Conventional Resistance	0	11	22	1,00
4. Position of the building and foundations	0	2	4	0,50
5. (Floor)Slab	0	3	6	1,00
6. Floor configuration	0	6	12	1,00
7. Configuration in Elevation	0	11	22	1,00
8. Connection in critical elements	0	3	6	0,75
9. Low ductility elements	0	6	12	1,00
10. Non-structural elements	0	4	10	0,25
11. State of Conservation	0	10	20	1,00
12. Structure reinforced after earthquake	0	11	22	1,00

Table 2. Methodology to calculate the tsunami vulnerability index

Criteria	**Classes / Ki**			Weighting
	A	**B**	**C**	**Wi**
1. Building orientation	0	6	12	1,2
2. Access. Entrance	0	6	12	1,2
3. Access. Stairs	0	6	12	1,2
4. Building location. Potential hazards	0	6	12	0,5
5. Building location. Parking, traffic, streets	0	6	12	0,5
6. Structural system	0	6	12	1,0
7. Foundation system	0	6	12	0,5
8. Year of construction	0	6	12	1,0
9. Building Height	0	11	22	1,5
10. Floor system	0	6	12	1,0

In both the seismic and the tsunami evaluation of vulnerability, each criterion was classified in three vulnerability classes, being “A”, “B” and “C”. In this case “A” shall represent the most resistant building, while “C” shall reflect the most vulnerable structure,

where each class corresponds to a value (Ki). Furthermore, each criterion was assigned to a fixed weighting coefficient (Wi) according to the importance of the criteria. The total seismic and tsunami vulnerability index for each building was calculated according to the equation:

$$IV = i = 112\ Sor\ 10(T)\ \ Ki\ Wi$$

According to table 1, the maximum value for the seismic vulnerability index is 143 while the maximum value for the tsunami vulnerability index is 130.2 (Table 2). Considering the aforementioned, the following general categorization for vulnerability is proposed:

Resistant structure
if $Iv \leq 30$
Highly vulnerable structure
If $Iv \geq 80$
Further evaluation is needed:
If $30 < Iv < 80$

This occurs especially with the calculation of the ratio between the building height and the vibration period of the structure (Duque Eslava et al., 2017; Aguiar and Zambrano 2018; Rodriguez, 2019).

4. RESULTS AND DISCUSSION

In order to evaluate the seismic vulnerability of the structures located in Salinas and Manta, the modified Italian methodology was used; in addition, to evaluate the resistance to tsunamis, parameters extracted from the FEMA were used. Through the results obtained, it was possible to categorize each of the buildings and identify those that can be considered as safe shelters in the event of a needed vertical emergency evacuation. These evaluation methods are fast, so it is advisable to accompany them with other analyzes or studies that allow to complement them and, in this way, obtain more effective results.

4.1 Salinas

A high rate of seismic activity brings with it great possibilities that after the occurrence of any of them, a tsunami may occur that impacts the buildings located a few meters from the coastline of the city of Salinas, which is why the city needs to have available relevant evacuation plans for the population in order to safeguard as many lives as possible. From the tip of San Lorenzo to the La Ensenada sector along a coastline of approximately 4.00 km, 99 buildings were identified subject to evaluation. Of these 90 were evaluated thanks to the collection of data in the field and making use of other additional information means, which represents 91% of the evaluated structures. The remaining 9% represents a total of nine structures that were not possible to be analyzed mainly due to the lack of information and collaboration on the part of the managers of the respective residences (Table 3; Fig. 7 and 8).

Table 3: Summary of seismic and tsunami vulnerability index (SVI & TVI) of ninety buildings in Salinas, while on nine additional recognized buildings we were denied access (see text).

N°	Building	SVI	TVI	N°	Building	SVI	TVI
1	VISTAMAR	24,50	29,4	**46**	EL DORAL	38,50	50,4
2	ALDILÁ	55,50	60,2	**47**	COSTA AZUL	54,75	36,6
3	VIRREINA DEL MAR	58,75	48,2	**48**	BAHÍA CHIPIPE	40,00	34,8
4	PRINCESA DEL MAR	60,25	40,4	**49**	EL NAVEGANTE	32,50	53,4
5	REY DEL MAR	68,25	46,7	**50**	AQUARIUM	29,50	43,2
6	CASAMAGNA	26,25	30,9	**51**	CALIPSO	64,25	31,8
7	EL EXCLUSIVO	43,00	49,2	**52**	RIVIERA DEL MAR	35,00	40,8
8	SOLARIS	51,25	48,4	**53**	ATLANTIC	61,50	34,8
9	GALAXIE	47,50	52,8	**54**	LA PLAYA	85,75	40,8
10	SORRENTO	59,50	42,0	**55**	LA ENSENADA	31,00	48,0
11	ANCONA	31,75	46,2	**56**	EL VELERO AZUL	29,00	42,0
12	CASTELLAMARE	26,00	35,0	**57**	NEPTUNO	39,50	43,2
13	MANSIÓN DEL MAR	44,75	40,8	**58**	EL TIBURÓN	60,00	39,0
14	SAINT TROPEZ	49,75	40,4	**59**	CASA BLANCA	41,50	50,4
15	EL CAPITÁN	67,25	53,4	**60**	EL PLAZA	50,50	55,2
16	MEDITERRANE	43,50	36,0	**61**	PLAYASOL	29,50	48,0
17	CASTENUOVO	70,25	34,2	**62**	GIRALDA	46,50	43,2
18	TESORO DEL MAR	34,50	39,6	**63**	PLAYAMAR	64,50	47,4
19	REMOLINO	46,75	41,0	**64**	SOLANA	73,00	50,4
20	VISTA MARINA	70,50	36,8	**65**	COSTA BRAVA	59,50	45,0
21	AQUA SOL	26,50	34,8	**66**	CABO AZUL	29,50	45,0
22	EL PICUDO	62,50	49,2	**67**	CORAL DE CHIPIPE	40,50	40,2
23	ANACAPRI TORRE A	26,25	39,8	**68**	MARENOSTRUM	25,00	34,2
24	HOTEL COLÓN SALINAS	49,25	30,2	**69**	HOTEL SUITES SALINA	40,00	37,8
25	EL EMPERADOR	42,50	42,0	**70**	DUQUESA DEL MAR	27,00	42,6
26	MONTECARLO	29,50	40,8	**71**	ALBACORA	76,50	49,2
27	REMANSO	31,25	39,0	**72**	HOTEL BLUE BAY	39,00	44,9
28	CONDESA DEL MAR	71,50	47,4	**73**	ALAMAR	26,50	35,4
29	EL REFUGIO	36,50	48,6	**74**	GIRASOL	48,00	53,6
30	ACROPOLIS	36,50	40,2	**75**	HOTEL MALECÓN	33,50	41,8
31	SANTORINI	65,50	35,4	**76**	CORBETA	71,50	43,2
32	CORINTO	28,00	47,4	**77**	LAS PALMERAS	56,50	50,8
33	BAY POINT	22,75	32,4	**78**	LA GOLETA	69,50	46,2
34	PETROPOLIS	34,50	49,2	**79**	LAS CANARIAS	56,50	45,6
35	TERRAMAR	87,25	31,8	**80**	EL CONQUISTADOR	41,50	40,8
36	TORREMAR	56,50	49,2	**81**	BALBOA	67,00	43,2
37	PERLA DE MAR	57,00	50,4	**82**	MAR DE PLATA	86,50	43,2
38	PORTOFINO	27,75	40,8	**83**	KONA BAY	29,50	24,2
39	PERLAZUL	22,75	27,0	**84**	VENTURA	29,00	47,4
40	AQUAMIRA	29,50	36,6	**85**	PUNTA DE PACÍFICO	27,00	29,4
41	MÁLAGA	21,00	19,8	**86**	EL MIRADOR	70,50	43,2
42	IBIZA	27,00	38,4	**87**	EL ALMIRANTE	49,00	40,4
43	LA SIESTA	74,50	36,0	**88**	BARLOVENTO	80,25	48,6
44	TORRE BLANCA	43,50	43,2	**89**	COSTA BELLA	74,25	48,6
45	TORREMOLINOS	42,50	50,4	**90**	COMODORO	47,00	43,2

Some 64% and 85% of structures have a seismic and tsunami vulnerability index between 30 and 80 respectively. For this reason, these intermediate values do not allow the structures to be categorized as safe or vulnerable. Therefore, additional studies should be considered to help improve their classification and define their vulnerability range.

Of the 90 buildings evaluated, only 23 of them obtained a seismic vulnerability index of less than 30, which categorizes them as seismically resistant and safe structures. However, only 5 of the 23 have a vulnerability index to tsunami less than 30 (Vistamar, Perlazul, Málaga, Kona Bay and Punta Pacífico), which represents 5% of structures that can be considered as safe in the event of the two natural events and that can be used as temporary shelters for emergent vertical evacuation. Those buildings whose seismic vulnerability index is less than 30 but their vulnerability index against tsunami is higher, it was mainly due to the limitations found in the accesses and internal stairways that did not have an adequate capacity of users in case of vertical evacuations that require access to high places at optimal times.

In order to improve the category of those buildings whose vulnerability index to tsunami exceeded 30 points and after analyzing different alternatives with which, through its adaptation, a building improves its vertical evacuation capacity in the event of a tsunami, it must be defined that the most efficient proposal is the implementation of external emergency stairs. For this, an exterior staircase model needs to be designed for a nine-story building (Marenostrum). This proposal, being calculated, would result to a referential budget of some 27,884.33 USD, not including VAT. This budget is not fixed because, depending on the number of floors and dimensions calculated according to the building where it is going to be built, the costs will vary. Considering the relative magnitude of structural costs versus total construction costs in the design of buildings suitable for vertical evacuation in the event of tsunamis, a structure resistant to tsunamis, earthquakes and progressive collapse is expected to experience an increase in the order of 10% to 20% in total construction costs over those required for traditional buildings.

It is fundamental that the structures defined as safe places for vertical emergency evacuation are far from potential dangerous or hazardous places (gas tanks, gas stations, ports, among others) in order to avoid possible additional accidents that put the population at risk. In addition, structures suitable for vertical evacuation need to consider, for a reaction time of 30 minutes, to be located a maximum of 1.60 km from any given starting point, or 3.21 km between structures, so that an average healthy person traveling 1.8 m / s can arrive and be safe.

When designing and building a structure, both seismic and tsunami resistance parameters should be considered in order to serve as safe shelters for vertical evacuation in the future. Mainly improving the accesses and internal stairs by making them wider, thus avoiding crowds, accidents and optimizing the time and fluidity of movement of the personnel. It is recommended to use the buildings categorized as earthquake resistant tsunami for vertical evacuations because in Salinas there is little presence of high points to perform appropriate horizontal evacuations in case the arrival time of the tsunami does not allow the population to reach a safe site. In addition, it is recommended to accompany other studies, both the modified Italian methodology and the FEMA to complement them, such as an equivalent system of one degree of freedom as proposed national regulations in order to obtain more efficient categorizations. Since 96% of the buildings in Salinas are residential, whose entry is strictly allowed only for apartment owners, it is necessary to make agreements between the municipality and the building owners in order to allow the use of

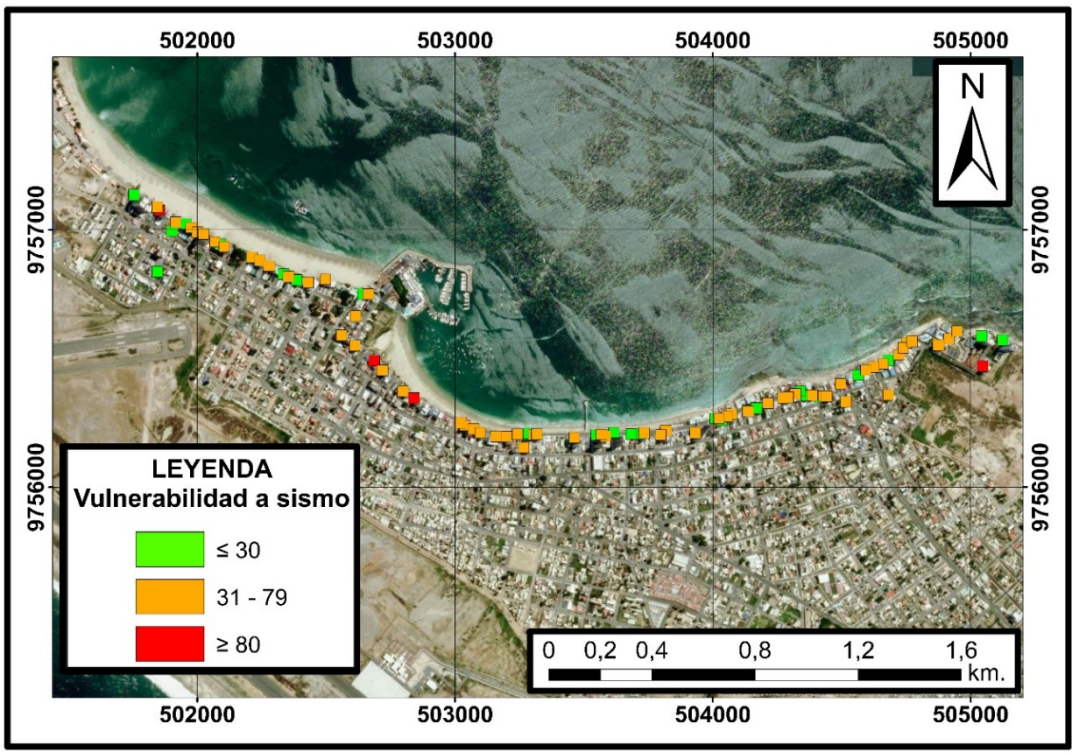

Fig 7. Map of the three categories assigned to seismic vulnerability of the 99 (90) evaluated buildings in the city of Salinas.

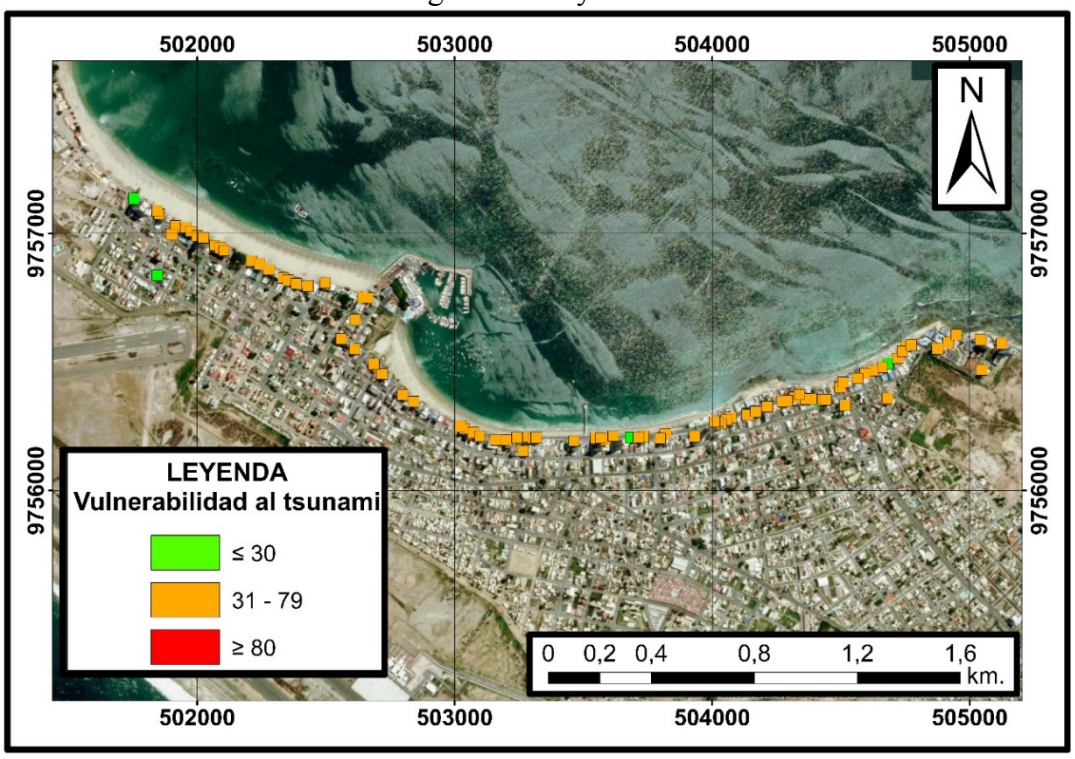

Fig 8. Map of the three categories assigned to tsunami vulnerability of the 99 (90) evaluated buildings in the city of Salinas.

promoting the sense of collaboration and empathy between human beings. For buildings that are already built and do not have these attributes, it is recommended to expand the entrances to the building and also the vertical circulation by adapting external stairs, as suggested before. In addition to the implementation of external emergency staircases, the possibility of defining a strategic space in the city to implement ad-hoc buildings, as has already been done in other countries, can be considered as a vertical evacuation alternative that, in addition to providing room for more people to protect themselves, they can provide other uses during non-emergency times such as, for example religious, sports, community, among others and thus, take full advantage of the benefits that this type of construction has. The design of emergency stairs for vertical evacuation is advisable to carry out with X-shaped diagonals on each floor, which with this implementation will help the structure to be more solid throughout its height and the displacement in the head of the same will not be so considerable.

4.2 Manta

In order to realize the current evaluation in Manta, 18 buildings were pre-selected, among which there are three that are for public use, three banks, four hotels, seven for residential use and one whose construction is suspended (Table 4). It is worth mentioning that one building was not worked on because there was not enough information for its evaluation. Before the 1998 earthquake whose epicenter was in the city of Bahia and which slightly affected some cities of Manabí, eight (44.44%) buildings were built. Another eight (44.44%) were built after this event and after the earthquake of April 16, 2016 (Mw 7.8) two buildings were built, which means that they are less than five years old. The total construction area of the 18 pre-selected buildings gives a total of 18757.18 m^2, and an average area of 1042.07 m^2. The El Dorado II building is the one with the largest construction area (3150 m^2), followed by the Poseidón Hotel (2252 m^2) and the Vigía (1800 m^2). It should be noted that a larger construction area presents a greater capacity in case of an evacuation (Fig. 9 and 10).

Table 4: Summary of seismic and tsunami vulnerability index (SVI & TVI) of 18 buildings in Salinas, while one additional recognized building was denied access (see text).

N°	Building	SVI	TVI	N°	Building	SVI	TVI
1	Corporación Nac, Electr.	28,00	35,0	**10**	Hotel el Navegante	56,25	38,4
2	Empresa Públ. Aguas Manta	84,25	88,5	**11**	Edif. el Dorado II	45,50	64,8
3	Edif. Sin Nombre 1	117,75	85,8	**12**	Edif. Ibiza	24,00	27,4
4	Edif. Sin Nombre 2	117,75	81,3	**13**	Edif. las Olas	36,25	52,5
5	Edif. Banco Pichincha	47,25	66,0	**14**	Edif. Oasis Marino (Abandon.)	113,00	66,0
6	Banco de Bank	29,00	29,8	**15**	Edif. Buzios	26,75	31,4
7	Edif. el Vigía	110,25	80,2	**16**	Edif. Manta Host	29,75	35,2
8	Museo Centro Cult. Manta	46,00	40,8	**17**	Hotel Poseidón	51,00	35,4
9	Balandra Hotel	41,25	43,6	**18**	N.D.		

Most of the buildings, a total of ten, have more than ten floors. While six have less than ten floors and only two have more than twenty floors. Six of the eighteen buildings do not have floors below the surface, the rest have a maximum value of seven basements, this being the case of the Hotel Manta Host. The maximum floor height is 4 m and the minimum 2.5 m, of the total of buildings only six have a floor height greater than or equal

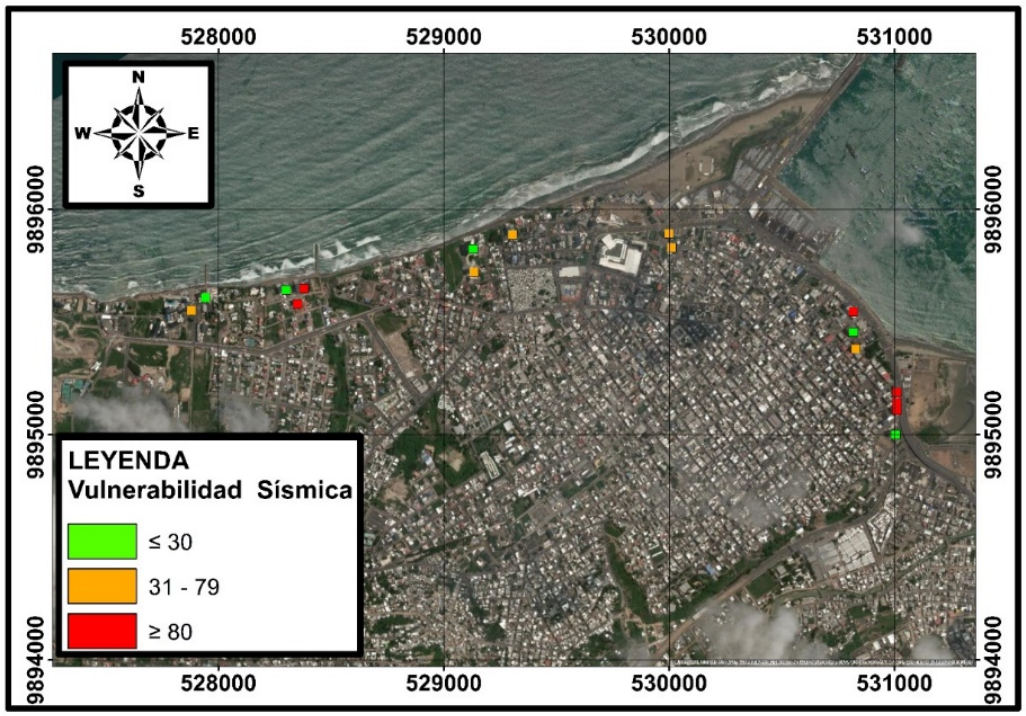

Fig 9. Map of the three categories assigned to seismic vulnerability of the 18 (17) evaluated buildings in the city of Manta.

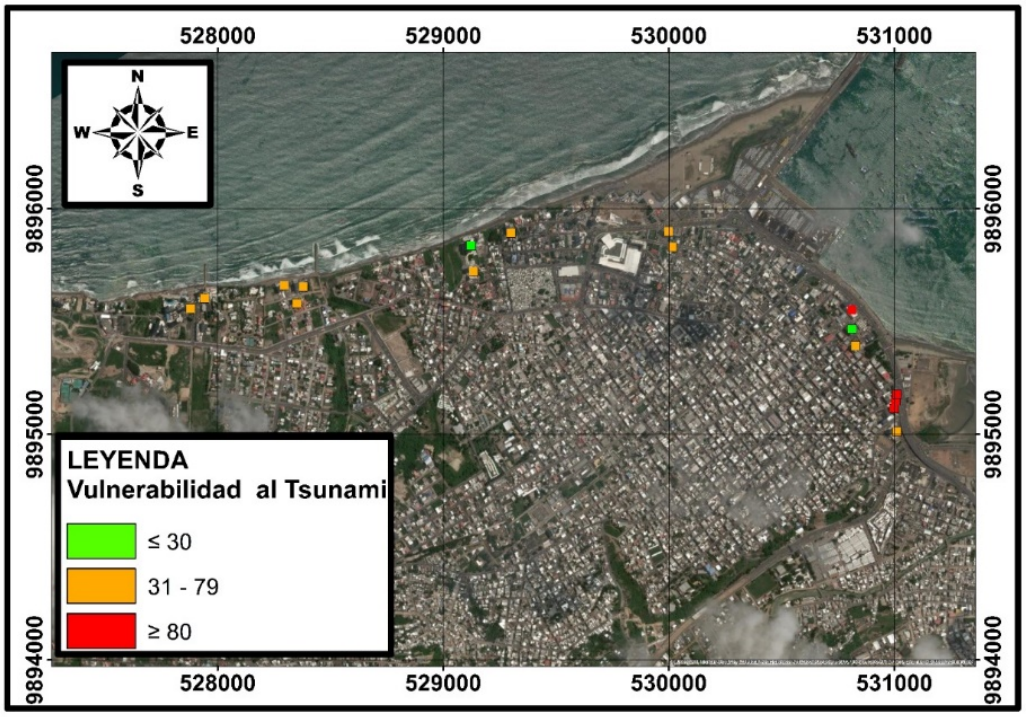

Fig 10. Map of the three categories assigned to tsunami vulnerability of the 18 (17) evaluated buildings in the city of Manta.

to 3 m, while the most frequent floor heights found during the inspection was 2.8 m. Seven of the eighteen buildings are on the beachfront, of the 17 buildings evaluated, one only is uninhabited and abandoned, one is in the process of being reinforced and two show obvious damage. Among the buildings analyzed, it was obtained as a result that five structures, which represent approximately 27.78%, have a seismic vulnerability index ≤30. While buildings with a vulnerability index ≥ 80 add five of them (27.78%), which means that they are highly vulnerable. In the same way, those structures that exhibit a seismic vulnerability index between 30 and 80 are a total of seven (38.88%), for this reason they may require an additional evaluation. The remaining 5.55% or one of eighteen buildings, corresponds to that building in which the required information was not obtained, either due to the lack of collaboration of the administrators or for their safety.

The minimum value of the seismic vulnerability index is 24 belonging to the Ibiza building. The highest values of the vulnerability index are obtained, as expected, by the two buildings that presented obvious damage due to the damage suffered previously and the abandoned building, as can be seen listed in Table 4. Due to the danger that these represent in future seismic events, both for adjacent buildings and for the population, a controlled demolition should be taken considered. Of the buildings evaluated, five (11.11%) have a vulnerability index lower than 30, six (61.11%) yield a vulnerability index to tsunamis between 30 and 80, therefore, they require additional studies in order to know what category could be assigned to them. Four (22.22%) have an index higher than eighty, which means that they are very vulnerable to a tsunami and there are three (5.56%), which did not access the necessary information for their respective evaluation.

Therefore, once the evaluation of the 18 pre-selected buildings is completed, only two (11.11%) buildings are classified as resistant to both hazards (earthquake and tsunami). The aforementioned buildings are Banco del Bank and Edificio Ibiza, among the attributes that helped these structures present a vulnerability index lower than 30, the following may be mentioned, they are rigid structures, they have a good state of conservation, they were repaired at the masonry or structural level and are taller than the maximum height the wave would reach. Of the safe buildings, its orientation is parallel to the most potential direction of the incoming tsunami wave from the Pacific coast, which makes it experience smaller hydrodynamic forces. One of these buildings is located on the first line of the beach; it is in a critical zone of the tsunami and has entrances wide enough to allow the access of several persons and thanks to the breadth of their construction area and number of floors they allow to shelter a large number of people.

On the other hand, there are three buildings that were categorized as earthquake resistant but have a tsunami vulnerability index between 30 and 36, this value was obtained mainly because there is an important limitation for vertical evacuation with regard to access to stairs and due to because it is located in front of a very busy road. An alternative to improve this problem is the implementation of improvements in the accesses of the stairs, in this way the vulnerability index to tsunamis would be reduced, turning it into a potential refuge for efficient vertical evacuation, considering the evolution of capacities and smart building technologies. It is vital to unequivocally define the responsibility for opening the vertical shelter and assign additional emergency support personnel (FEMA, 2019).

Physical adaptations are proposed to improve vertical circulation at the adequate shelter level of the structure, such as the installation of supplementary entrances, ramps or stairs, which should preferably be exterior, since they are easy to build and do not present obstructions that affect its visibility (FEMA, 2019). As an additional option, the municipality of the city of Manta should consider the design and construction of a public and accessible multipurpose tsunami-resistant building that is located in a central part of the critical zone and that is not located near the buildings that are considered safe, so that in this way people who cannot reach these buildings evacuate to this building. All proposed activities in the event of a potential incoming tsunami disaster are pending the implementation of an early warning system as proposed in a variety of studies (Toulkeridis et al., 2017; 2018; 2019).

5. CONCLUSIONS

Populations and the corresponding tourists of the cities of Manta and Salinas have only a limited time to reach an elevated, safe area in case of an impact of an incoming tsunami and those distances are too long or too far for the available. Therefore, for both sites we evaluated the possibility of vertical evacuations within existing buildings of more than four floors close to the shoreline

Based on the vulnerability evaluation of seismic and tsunami resistance of the 117 pre-selected buildings along the Pacific Ocean in Manta and Salinas, we may ascertain that several of the buildings could withstand a seismic event and most potentially an impact by a tsunami.

Most of the evaluated buildings have a limited if any capacity of receiving the escaping public in case of an incoming tsunami, as being almost all in private property, lack to allow other than residents to enter the buildings and perform a vertical evacuation. Many buildings could improve their tsunami performance if access is improved, ideally through external adaptations.

It is necessary to implement an early alert system for tsunamis and have an agreement between municipality and owners of the buildings, which will allow the escaping public and tourists to enter the buildings and stay safe in elevated floors during a tsunami crisis.

6. REFERENCES

Aguiar, R. & Rivas, A. (2018). Microzonificación sísmica de Ambato. Gobierno Autónomo Descentralizado de Ambato, Ambato, Ecuador.

Aguiar, R. & Zambrano, V. (2018). Relation h/t in structures of Bahía de Caraquez and the 2016 Earthquake. Revista Internacional de Ingeniería de Estructuras, 23, 2, 227-241

Aguilera, C., Viteri, M., Seqqat, R., Ayala, L., Toulkeridis, T., Ruano, A., & Torres, M. (2018). Biological impact of exposure to extremely fine-grained volcanic ash. Journal of Nanotechnology, Article number 7543859

Aitsi-Selmi, A., Egawa, S., Sasaki, H., Wannous, C., & Murray, V. (2015). The Sendai framework for disaster risk reduction: Renewing the global commitment to people's resilience, health, and well-being. International journal of disaster risk science, 6(2), 164-176.

Alcántara-Ayala, I. (2002). Geomorphology, natural hazards, vulnerability and prevention of natural disasters in developing countries. Geomorphology, 47(2-4), 107-124.

Amellal, O., Bensaibi, M., & Grine, K. (2012). Seismic vulnerability index method for steel structures. In Proceedings of the 15th World Conference on Earthquake Engineering (WCEE).

Aroca, J., Gómez, M., Morales, E., & Romo, M. (2018). Study of the performance of seismic isolators of Pier no. 12 of the Bridge "Los Caras", during the earthquake of April 16. Revista Internacional de Vol, 23(3), 305-339.

Aviles-Campoverde, D., Chunga, K., Ortiz-Hernández, E., Vivas-Espinoza, E., Toulkeridis, T., Morales-Delgado, A., & Delgado-Toala, D. (2021). Seismically induced soil liquefaction and geological conditions in the city of Jama due to the Mw7.8 Pedernales earthquake in 2016, NW Ecuador. Geosciences, 11, 20

Barreto-Álvarez, D.E., Heredia-Rengifo, M.G., Padilla-Almeida, O. & Toulkeridis, T. (2020). Multitemporal evaluation of the recent land use change in Santa Cruz Island, Galapagos, Ecuador. In Conference on Information and Communication Technologies of Ecuador (pp. 519-534). Springer, Cham.

Barros, J. L., Tavares, A. O., Santos, A., & Fonte, A. (2015). Territorial vulnerability assessment supporting risk managing coastal areas due to tsunami impact. Water, 7(9), 4971-4998.

Belash, T. A. & Yakovlev, A. D. (2018). Seismic stability of a tsunami-resistant residential buildings. Magazine of Civil Engineering, 80(4).

Berninghausen, W.H. (1962). Tsunamis reported from the west coast of South America 1562-1960. Bull. of the Seismological Soc. of America, 52 (4): 915-921.

Bosworth, T.O., 1922. Geology of the Tertiary and Quaternary periods in the northwest part of Peru. MacMillan an Company, London.

Bristow, C. R. (1976). The age of the Cayo Formation, Ecuador. Newsletters on Stratigraphy, 169-173.

Calgaro, E. and Lloyd, K. (2008). Sun, sea, sand and tsunami: examining disaster vulnerability in the tourism community of Khao Lak, Thailand. Singapore Journal of Tropical Geography, 29(3), 288-306.

Calgaro, E., Dominey-Howes, D., & Lloyd, K. (2014). Application of the Destination Sustainability Framework to explore the drivers of vulnerability and resilience in Thailand following the 2004 Indian Ocean Tsunami. Journal of Sustainable Tourism, 22(3), 361-383.

Calvi, G. M., Pinho, R., Magenes, G., Bommer, J. J., Restrepo-Vélez, L. F., & Crowley, H. (2006). Development of seismic vulnerability assessment methodologies over the past 30 years. ISET journal of Earthquake Technology, 43(3), 75-104.

Cannon, T. (1994). Vulnerability analysis and the explanation of 'natural' disasters. Disasters, development and environment, 1, 13-30.

Carvache-Franco, M., Carvache-Franco, O., Carvache-Franco, W., Villagómez Buele, C., & Arteaga Peñafiel, M. (2018). The tourist demand from the perspective of the motivation, assessment and satisfaction in a sun and beach destination: the Manta case, Ecuador. GeoJournal of Tourism and Geosites. 22 (2), 561–572.

Carvache-Franco, M., Carvache-Franco, W., Carvache-Franco, O., Hernández-Lara, A. B., & Buele, C. V. (2020). Segmentation, motivation, and sociodemographic aspects of tourist demand in a coastal marine destination: A case study in Manta (Ecuador). Current Issues in Tourism, 23(10), 1234-1247.

Carver, S. J. (1991). Integrating multi-criteria evaluation with geographical information systems. International Journal of Geographical Information System, 5(3), 321-339.

Celorio-Saltos, J.C., García-Arias, J.M., Guerra-Luque, A.B., Barragan-Aroca, G., & Toulkeridis, T. (2018). Vulnerability analysis based on tsunami hazards in Crucita, central coastal of Ecuador. Science of Tsunami Hazards, 38(3): 225-263.

Cheng, C., Qian, X., Zhang, Y., Wang, Q., & Sheng, J. (2011). Estimation of the evacuation clearance time based on dam-break simulation of the Huaxi dam in Southwestern China. Natural Hazards, 57(2), 227-243.

Chunga K., Livio F., Mulas M., Ochoa-Cornejo, Besenzon D., Ferrario M., & Michetti AM. (2018). Earthquake ground effects and intensity of the 16 April 2016, Mw 7.8 Pedernales Earthquake (Ecuador): implications for the source characterization of large subduction earthquakes. Bulletin of the Seismological Society of America 108 (6): 3384-3397.

Chunga, K. & Toulkeridis, T. (2014). First evidence of paleo-tsunami deposits of a major historic event in Ecuador. Science of tsunami hazards, 33: 55-69.

Chunga, K., Livio, F.A., Martillo, C., Lara-Saavedra, H., Ferrario, M.F., Zevallos, I., & Michetti, A.M. (2019b). Landslides Triggered by the 2016 Mw 7.8 Pedernales, Ecuador Earthquake: Correlations with ESI-07 Intensity, Lithology, Slope and PGA-h. Geosciences, 9, 371.

Chunga, K., Mulas, M., Alvarez, A., Galarza, J., & Toulkeridis, T. (2019a): Characterization of seismogenetic crustal faults in the Gulf of Guayaquil, Ecuador. Andean Geology, 46(1): 66-81.

Chunga, K., Toulkeridis, T., Vera-Grunauer, X., Gutierrez, M., Cahuana, N., & Alvarez, A. (2017). A review of earthquakes and tsunami records and characterization of capable faults on the northwestern coast of Ecuador. Science of tsunami hazards, 36: 100-127.

Del-Pino-de-la-Cruz, C.E., Martinez-Molina, B.D., Haro-Baez, A.G., Toulkeridis, T. and Rentería, W., 2021: The proposed design of a smart parking area as a multiple use building for the eventual vertical evacuation in case of tsunami impacts in Salinas, Ecuador. Science of Tsunami Hazards, 40(3), 146-165

DeVries, T.J., 1988. The geology of late Cenozoic marine terraces (tablazos) in northwestern Peru. Journal of South American Earth Sciences 1 (2), 121–136.

Duque Eslava, A.C.,Rojas Mendoza, F. A., Rodríguez Gómez, H., & Vielma Pérez, J.C. (2017). Analysis of outer RC beam-column joint strengthened with CFRP. Revista Internacional de Ingeniería de Estructuras, 22, 2, 113-134.

Echegaray-Aveiga, R.C., Rodríguez, F., Toulkeridis, T., & Echegaray-Aveiga, R.D. (2019). Effects of potential lahars of the Cotopaxi volcano on housing market prices. J. of Applied Volcanology, 9, 1-11.

Edler, D., Otto, K.H., & Toulkeridis, T. (2020). Tsunami hazards in Ecuador – Regional differences in the knowledge of Ecuadorian high-school students. Science of Tsunami Hazards, 39(2), 86-112.

Egbue, O., & Kellogg, J. (2010). Pleistocene to present North Andean "escape". Tectonophysics, 489(1-4), 248-257.

FEMA (2019). Guidelines for design of structures for vertical evacuation from tsunamis. FEMA P646. Washington, DC: FEMA. 202pp

Feng, C. M., & Wang, T. C. (2003). Highway emergency rehabilitation scheduling in post-earthquake 72 hours. Journal of the 5th Eastern Asia Society for Transportation Studies, 5(3281), 3276-3285.

Frankenberg, E., Sikoki, B., Sumantri, C., Suriastini, W., & Thomas, D. (2013). Education, vulnerability, and resilience after a natural disaster. Ecology and society: a journal of integrative science for resilience and sustainability, 18(2), 16.

Freisleben, R., Jara-Muñoz, J., Melnick, D., Martínez, J. M., & Strecker, M. R. (2021). Marine terraces of the last interglacial period along the Pacific coast of South America (1° N–40° S). Earth System Science Data, 13(6), 2487-2513.

Glass, J. B., Fornari, D. J., Hall, H. F., Cougan, A. A., Berkenbosch, H. A., Holmes, M. L.,... & De La Torre, G. (2007). Submarine volcanic morphology of the western Galápagos based on EM300 bathymetry and MR1 side-scan sonar. Geochemistry, Geophysics, Geosystems, 8(3).

González Santa Cruz, F., Torres-Matovelle, P., Molina-Molina, G., & Pérez Gálvez, J. C. (2019). Tourist Clusters in a Developing Country in South America: The Case of Manabì Province, Ecuador. Sustainability, 11(16), 4329.

Gregg, C. E., Houghton, B. F., Paton, D., Lachman, R., Lachman, J., Johnston, D. M., & Wongbusarakum, S. (2006). Natural warning signs of tsunamis: human sensory experience and response to the 2004 great Sumatra earthquake and tsunami in Thailand. Earthquake Spectra, 22(3_suppl), 671-691.

Griffin, J., Latief, H., Kongko, W., Harig, S., Horspool, N., Hanung, R., ... & Cummins, P. (2015). An evaluation of onshore digital elevation models for modeling tsunami inundation zones. Frontiers in Earth Science, 3, 32.

Gusiakov, V. K. (2005). Tsunami generation potential of different tsunamigenic regions in the Pacific. Marine Geology, 215(1-2), 3-9.

Gutscher, M.A., Malavieille, J.S.L., & Collot, J.-Y. (1999). Tectonic segmentation of the North Andean margin: impact of the Carnegie Ridge collision. Earth and Planetary Science Letters 168, 255–270.

Heidarzadeh, M., Murotani, S., Satake, K., Takagawa, T., & Saito, T. (2017). Fault size and depth extent of the Ecuador earthquake (Mw 7.8) of 16 April 2016 from teleseismic and tsunami data. Geophysical Research Letters, 44(5), 2211-2219.

Herd, D. G., Youd, T. L., Meyer, H., Arango, J. L., Person, W. J., & Mendoza, C. (1981). The great tumaco, colombia earthquake of 12 december 1979. Science, 211(4481), 441-445.

Herrera-Enríquez, G., Toulkeridis, T., Rodríguez-Rodríguez, G., & Albuja-Salazar (2020). Critical Factors of Business Adaptability during Resilience in Baños de Agua Santa, Ecuador, due to Volcanic Hazards . CIT, in press

Intergovernmental Oceanographic Commission. Fourth Edition. Tsunami Glossary (2019). Paris, UNESCO, IOC Technical Series, 85. (English, French, Spanish, Arabic, Chinese) (IOC/2008/TS/85 rev.4).

Ioualalen, M., Monfret, T., Béthoux, N., Chlieh, M., Adams, G. P., Collot, J. Y., ... & Gordillo, G. S. (2014). Tsunami mapping in the Gulf of Guayaquil, Ecuador, due to local seismicity. Marine Geophysical Research, 35(4), 361-378.

Ioualalen, M., Ratzov, G., Collot, J. Y., & Sanclemente, E. (2011). The tsunami signature on a submerged promontory: the case study of the Atacames Promontory, Ecuador. Geophysical Journal International, 184(2), 680-688.

Jaillard, E., Ordonez, M., Suárez, J., Toro, J., Iza, D., & Lugo, W. (2004). Stratigraphy of the late Cretaceous–Paleogene deposits of the Cordillera Occidental of central Ecuador: geodynamic implications. Journal of South American Earth Sciences, 17(1), 49-58.

Jaramillo Castelo, C.A., Padilla Almeida, O., Cruz D´Howitt, M., & Toulkeridis, T. (2018). Comparative determination of the probability of landslide occurrences and susceptibility in central Quito, Ecuador. 2018 5th International Conference on eDemocracy and eGovernment, ICEDEG 2018 8372318: 136-143.

Kalkman, J. P., & de Waard, E. J. (2017). Inter-organizational disaster management projects: Finding the middle way between trust and control. International Journal of Project Management, 35(5), 889-899.

Kanamori, H. & McNally, K.C. (1982). Variable rupture mode of the subduction zone along the Ecuador-Colombia coast. Bulletin of the Seismological Society of America, 72(4): 1241-1253.

Kassem, M. M., Nazri, F. M., & Farsangi, E. N. (2019). Development of seismic vulnerability index methodology for reinforced concrete buildings based on nonlinear parametric analyses. MethodsX, 6, 199-211.

Kates, R. W. (1976). Experiencing the environment as hazard. In Experiencing the environment (pp. 133-156). Springer, Boston, MA.

Keating, B. H., & McGuire, W. J. (2000). Island edifice failures and associated tsunami hazards. Pure and Applied Geophysics, 157(6-8), 899-955.

Kellogg, J. N., Vega, V., Stallings, T. C., & Aiken, C. L. (1995). Tectonic development of Panama, Costa Rica, and the Colombian Andes: constraints from global positioning system geodetic studies and gravity. Special Papers-Geological Society of America, 75-75.

Lukkunaprasit, P., & Ruangrassamee, A. (2008). Building damage in Thailand in the 2004 Indian Ocean tsunami and clues for tsunami-resistant design. The IES Journal Part A: Civil & Structural Engineering, 1(1), 17-30.

Lynett, P., Weiss, R., Renteria, W., Morales, G. D. L. T., Son, S., Arcos, M. E. M., & MacInnes, B. T. (2013). Coastal impacts of the March 11th Tohoku, Japan tsunami in the Galapagos Islands. Pure and Applied Geophysics, 170(6-8), 1189-1206.

Marchant, S. (1961). A photogeological analysis of the structure of the western Guayas province, Ecuador: with discussion of the stratigraphy and Tablazo Formation, derived from surface mapping. Quarterly Journal of the Geological Society, 117(1-4), 215-231.

Martinez, N. & Toulkeridis, T. (2020). Tsunamis in Panama – History, preparation and future consequences. Science of Tsunami Hazards, 39(2), 53-68.

Matheus Medina, A.S., Cruz D´Howitt, M., Padilla Almeida, O., Toulkeridis, T., & Haro, A.G. (2016). Enhanced vertical evacuation applications with geomatic tools for tsunamis in Salinas, Ecuador. Science of Tsunami Hazards, 35, (3): 189-213

Matheus-Medina, A.S., Toulkeridis, T., Padilla-Almeida, O., Cruz-D´ Howitt, M., & Chunga, K. (2018). Evaluation of the tsunami vulnerability in the coastal Ecuadorian tourist centers of the peninsulas of Bahia de Caráquez and Salinas. Science of Tsunami Hazards, 38(3): 175-209.

Mato, F. & Toulkeridis, T. (2017). The missing Link in El Niño's phenomenon generation. Science of tsunami hazards, 36: 128-144.

McGuire, W. J. (2006). Lateral collapse and tsunamigenic potential of marine volcanoes. Geological Society, London, Special Publications, 269(1), 121-140.

Mendoza, C., & Dewey, J. W. (1984). Seismicity associated with the great Colombia-Ecuador earthquakes of 1942, 1958, and 1979: Implications for barrier models of earthquake rupture. Bulletin of the seismological society of America, 74(2), 577-593.

Meyyappan, P., Sekar, T., & Sivapragasam, C. (2013). Investigation on Behaviour Aspects of Tsunami Resistant Structures-An Experimental Study. Disaster advances, 6(2), 39-47.

Mikami, T., Shibayama, T., Esteban, M., & Matsumaru, R. (2012). Field survey of the 2011 Tohoku earthquake and tsunami in Miyagi and Fukushima prefectures. Coastal Engineering Journal, 54(1), 1250011-1.

Moberly, R., Shepherd, G. L., & Coulbourn, W. T. (1982). Forearc and other basins, continental margin of northern and southern Peru and adjacent Ecuador and Chile. Geological Society, London, Special Publications, 10(1), 171-189.

Morales, E., Filiatrault, A., & Aref, A. (2018). Seismic floor isolation using recycled tires for essential buildings in developing countries. Bulletin of Earthquake Engineering, 16(12), 6299-6333.

Mostafizi, A., Wang, H., Cox, D., & Dong, S. (2019). An agent-based vertical evacuation model for a near-field tsunami: Choice behavior, logical shelter locations, and life safety. International journal of disaster risk reduction, 34, 467-479.

Navas, L., Caiza, P., & Toulkeridis, T. (2018). An evaluated comparison between the molecule and steel framing construction systems – Implications for the seismic vulnerable Ecuador. Malaysian Construct. Res. J. 26 (3), 87–109.

NEC (Norma Ecuatoriana de la Construcción) (2015). Estructura de Acero, Cargas No Sísmicas.

Norio, O., Ye, T., Kajitani, Y., Shi, P., & Tatano, H. (2011). The 2011 eastern Japan great earthquake disaster: Overview and comments. International Journal of Disaster Risk Science, 2(1), 34-42.

Olson, D. L., & Wu, D. D. (2015). Enterprise risk management (Vol. 3). World Scientific Publishing Company.

Padrón, E., Hernández, P.A., Marrero, R., Melián, G, Toulkeridis, T., Pérez., N.M., Virgili, G., & Notsu, K. (2008). Diffuse CO_2 emission rate from the lake-filled Cuicocha and Pululagua calderas, Ecuador. Journal of Volcanology and Geothermal Research (Special Volume on Continental Ecuador volcanoes), 176: 163-169.

Padrón, E., Hernández, P.A., Pérez, N.M., Toulkeridis, T., Melián, G., Barrancos, J., Virgili, G., Sumino H., & Notsu, K. (2012). Fumarole/plume and diffuse CO_2 emission from Sierra Negra volcano, Galapagos archipelago. Bull. Of Volcanol., 74: 1509-1519.

Palacios Orejuela, I. & Toulkeridis, T. (2020). Evaluation of the susceptibility to landslides through diffuse logic and analytical hierarchy process (AHP) between Macas and Riobamba in Central Ecuador. 2020 7th International Conference on eDemocracy and eGovernment, ICEDEG 2020, 200-206

Papathoma, M., & Dominey-Howes, D. (2003). Tsunami vulnerability assessment and its implications for coastal hazard analysis and disaster management planning, Gulf of Corinth, Greece. Natural Hazards and Earth System Sciences, 3(6), 733-747.

Pararas-Carayannis, G. (1977). Catalog of tsunamis in Hawaii (Vol. 4). World Data Center A for Solid Earth Geophysics.

Pararas-Carayannis, G. (1980). Earthquake and tsunami of 12 December 1979 in Colombia. Tsunami Newsletter, 13(1), 1-9.

Pararas-Carayannis, G. (2002). Evaluation of the threat of mega tsunami generation from postulated massive slope failures of island stratovolcanoes on La Palma, Canary Islands, and on the island of Hawaii. Science of Tsunami Hazards, 20(5), 251-277.

Pararas-Carayannis, G. (2003). Near and far-field effects of tsunamis generated by the paroxysmal eruptions, explosions, caldera collapses and massive slope failures of the Krakatau volcano in Indonesia on august 26-27, 1883. Science of Tsunami Hazards.

Pararas-Carayannis, G. (2006). The potential of tsunami generation along the Makran Subduction Zone in the northern Arabian Sea: Case study: The earthquake and tsunami of November 28, 1945. Science of Tsunami Hazards, 24(5), 358-384.

Pararas-Carayannis, G. (2010). The earthquake and tsunami of 27 February 2010 in Chile–Evaluation of source mechanism and of near and far-field tsunami effects. Science of Tsunami Hazards, 29, 2: 96-126.

Pararas-Carayannis, G. (2011). Tsunamigenic source mechanism and efficiency of the march 11, 2011 Sanriku earthquake in Japan. Science of Tsunami Hazards, 30(2): 126-152

Pararas-Carayannis, G. (2012). Potential of tsunami generation along the Colombia/Ecuador subduction margin and the Dolores-Guayaquil Mega-Thrust. Science of Tsunami Hazards, 31, 3: 209-230.

Pararas-Carayannis, G., & Zoll, P. (2017). Incipient evaluation of temporal El Nino and other climatic anomalies in triggering earthquakes and tsunamis-Case Study: The Earthquake and Tsunami of 16 th April 2016 in Ecuador. Science of Tsunami Hazards, 36(4), 262-291.

Park, S., Van de Lindt, J. W., Gupta, R., & Cox, D. (2012). Method to determine the locations of tsunami vertical evacuation shelters. Natural hazards, 63(2), 891-908.

Pedoja, K., Dumont, J. F., Lamothe, M., Ortlieb, L., Collot, J. Y., Ghaleb, B., ... & Labrousse, B. (2006). Plio-Quaternary uplift of the Manta Peninsula and La Plata Island and the subduction of the Carnegie Ridge, central coast of Ecuador. Journal of South American Earth Sciences, 22(1-2), 1-21.

Pheng, L. S., Raphael, B., & Kit, W. K. (2006). Tsunamis: some pre-emptive disaster planning and management issues for consideration by the construction industry. Structural survey, 24(5), 378-396.

Pinter, N., & Ishman, S. E. (2008). Impacts, mega-tsunami, and other extraordinary claims. GSA today, 18(1), 37-38.

Poma, P., Usca, M., Fdz-Polanco, M, Garcia-Villacres, A., & Toulkeridis, T. (2021). Landslide and environmental risk from oil spill due to the rupture of SOTE and OCP pipelines, San Rafael Falls, Amazon Basin, Ecuador. International Journal on Advanced Science, Engineering and Information Technology, 11(4): 1558-1566.

Pontoise, B., & Monfret, T. (2004). Shallow seismogenic zone detected from an offshore-onshore temporary seismic network in the Esmeraldas area (northern Ecuador). Geochemistry, Geophysics, Geosystems, 5(2).

Ratzov, G., Collot, J. Y., Sosson, M., & Migeon, S. (2010). Mass-transport deposits in the northern Ecuador subduction trench: Result of frontal erosion over multiple seismic cycles. Earth and Planetary Science Letters, 296(1-2), 89-102.

Ratzov, G., Sosson, M., Collot, J. Y., Migeon, S., Michaud, F., Lopez, E., & Le Gonidec, Y. (2007). Submarine landslides along the North Ecuador–South Colombia convergent margin: possible tectonic control. In Submarine mass movements and their consequences (pp. 47-55). Springer, Dordrecht.

Rentería, W., Lynett, P., Weiss, R. & De La Torre, G. (2012). Informe de la investigación de campo de los efectos del tsunami de Japón Marzo 2011, en las islas Galápagos. Acta Oceanográ ca del Pací co. Vol. 17(1): 177 - 203.

Ridolfi, F., Puerini, M., Renzulli, A., Menna, M., & Toulkeridis, T. (2008). The magmatic feeding system of El Reventador volcano (Sub-Andean zone, Ecuador) constrained by mineralogy, textures and geothermobarometry of the 2002 erupted products. Journal of Volcanology and Geothermal Research (Special Volume on Continental Ecuador volcanoes), 176: 94-106.

Robayo N, A., Llorca, J., & Toulkeridis, T. (2020). Population, territorial and economic analysis of a potential volcanic disaster in the city of Latacunga, Central Ecuador based on GIS techniques – Implications and potential solutions. In Conference on Information and Communication Technologies of Ecuador (pp. 549-563). Springer, Cham.

Rodríguez Espinosa, F., Toulkeridis, T., Salazar Martinez, R., Cueva Girón, J., Taipe Quispe, A., Bernaza Quiñonez, L., Padilla Almeida, O., Mato, F., Cruz D´Howitt, M., Parra, H., Sandoval, W., & Rentería, W. (2017). Economic evaluation of recovering a natural protection with concurrent relocation of the threatened public of tsunami hazards in central coastal Ecuador. Science of tsunami hazards, 36: 293-306.

Rodriguez, F., Cruz D´Howitt, M., Toulkeridis, T., Salazar, R., Ramos Romero, G.E., Recalde Moya, V.A., & Padilla, O. (2016). The economic evaluation and significance of an early relocation versus complete destruction by a potential tsunami of a coastal city in Ecuador. Science of tsunami hazards, 35, 1: 18-35.

Rodriguez, F., Toulkeridis, T., Padilla, O., & Mato, F. (2017). Economic risk assessment of Cotopaxi volcano Ecuador in case of a future lahar emplacement. Natural Hazards, 85, (1): 605-618.

Rodríguez, M.E. (2019). Interpretación de los daños y colapsos en edificaciones observados en la ciudad de México en el terremoto del 19 de septiembre 2017. Revista de Ingeniería Sísmica, 101, 1-18

Russell, T. E. (2005). The humanitarian relief supply chain: analysis of the 2004 South East Asia earthquake and tsunami (Doctoral dissertation, Massachusetts Institute of Technology).

Saji, G. (2014). Safety goals for seismic and tsunami risks: Lessons learned from the Fukushima Daiichi disaster. Nuclear Engineering and Design, 280, 449-463.

San Martín, T. V., Rosado, G. R., Vargas, P. A., & Gutierrez, L. (2018). Population and building vulnerability assessment by possible worst-case tsunami scenarios in Salinas, Ecuador. Natural hazards, 93(1), 275-297.

Sellnow, T. L., & Seeger, M. W. (2021). Theorizing crisis communication. John Wiley & Sons.

Sheppard, G., 1930. The geology of southwestern Ecuador. American Association of Petroleum Geologists Bulletin 14, 263–309.

Simons, M., Minson, S.E., Sladen, A., Ortega, F., Jiang, J., Owen, S.E., Meng, L., Ampuero, J.P., Wei, S., Chu, R., & Helmberger, D.V. (2011). The 2011 magnitude 9.0 Tohoku-Oki earthquake: Mosaicking the megathrust from seconds to centuries. science, 332(6036), pp.1421-1425.

Solinska-Nowak, A., Magnuszewski, P., Curl, M., French, A., Keating, A., Mochizuki, J., ... & Jarzabek, L. (2018). An overview of serious games for disaster risk management–Prospects and limitations for informing actions to arrest increasing risk. International journal of disaster risk reduction, 31, 1013-1029.

Stainforth, R. M. (1948). Applied micropaleontology in Coastal Ecuador, Jour. Paleontology, 22: 142- 146.

Suango Sánchez, V. d. R., Acosta Tafur, J.R., Rodríguez De la Vera, K., Andrade Sánchez, M.S., López Alulema, A.C., Avilés Ponce, L.R., Proaño Morales, J.L., Zambrano Benavides, M.J., Reyes Pozo, M.D., Yépez Campoverde, J.A., & Toulkeridis, T. (2019). Use of geotechnologies and multicriteria evaluation in land use policy – the case of the urban area expansion of the city of Babahoyo, Ecuador. 2019 6th International Conference on eDemocracy and eGovernment, ICEDEG 2019, 194-202.

Suárez-Acosta, P.E., Cañamar-Tipan, C.D., Ñato-Criollo, D.A., Vera-Zambrano, J.D., Galarza-Vega, K.L., Guevara-Álvarez, P.M., Fajardo-Cartuche, C.N., Herrera-Garcés, K. K., Ochoa-Campoverde, C.V., Torres-Orellana, J.S., Rentería, W., Chunga, K., Padilla, O., Sinde-González, I., Simón-Baile, D. and Toulkeridis, T., 2021: Evaluation of seismic and tsunami resistance of potential shelters for vertical evacuation in case of a tsunami impact in Bahia de Caráquez, central coast of Ecuador. Science of Tsunami Hazards, 40(1), 1-37.

Sun, C., Xu, J., Jia, L., Qin, Y., Zhan, K., & Zhang, J. (2017, October). Passenger Flow Assignment of Evacuation Path in the Station Based on Time Reliability. In International Conference on Electrical and Information Technologies for Rail Transportation (pp. 301-310). Springer, Singapore.

Taubenböck, H., Goseberg, N., Setiadi, N., Lämmel, G., Moder, F., Oczipka, M., ... & Klein, R. (2009). " Last-Mile" preparation for a potential disaster–Interdisciplinary approach towards tsunami early warning and an evacuation information system for the coastal city of Padang, Indonesia. Natural Hazards and Earth System Sciences, 9(4), 1509-1528.

Thompson, P. A., & Marchant, E. W. (1995). A computer model for the evacuation of large building populations. Fire safety journal, 24(2), 131-148.

Titov, V. V., Moore, C. W., Greenslade, D. J. M., Pattiaratchi, C., Badal, R., Synolakis, C. E., & Kânoğlu, U. T. (2011). A new tool for inundation modeling: Community Modeling Interface for Tsunamis (ComMIT). Pure and Applied Geophysics, 168(11), 2121-2131.

Titov, V., Kânoğlu, U. and Synolakis, C. (2016). "Development of MOST for Real-Time Tsunami Forecasting." Journal of Waterway, Port, Coastal, and Ocean Engineering 142, no. 6: 03116004.

Toulkeridis, T. (2011). Volcanic Galápagos Volcánico. Ediecuatorial, Quito, Ecuador: 364 pp

Toulkeridis, T. (2013). Volcanes activos Ecuador. Santa Rita, Quito, Ecuador: 152pp

Toulkeridis, T. (2016). Unexpected results of a seismic hazard evaluation applied to a modern hydroelectric plant in central Ecuador. Journal of Structural Engineering, 43, (4): 373-380.

Toulkeridis, T. & Zach, I. (2017). Wind directions of volcanic ash-charged clouds in Ecuador – Implications for the public and flight safety. Geomatics, Natural Hazards and Risks, 8(2): 242-256.

Toulkeridis, T., Arroyo, C.R., Cruz D'Howitt, M., Debut, A., Vaca, A.V., Cumbal, L., Mato, F., & Aguilera, E. (2015a). Evaluation of the initial stage of the reactivated Cotopaxi volcano - Analysis of the first ejected fine-grained material. Natural Hazards and Earth System Sciences, 3, (11): 6947-6976.

Toulkeridis, T., Buchwaldt, R., & Addison, A. (2007). When Volcanoes Threaten, Scientists Warn. Geotimes, 52: 36-39.

Toulkeridis, T., Chunga, K., Rentería, W., Rodriguez, F., Mato, F., Nikolaou, S., Cruz D´Howitt, M., Besenzon, D., Ruiz, H., Parra, H., & Vera-Grunauer, X. (2017b). The 7.8 M_w Earthquake and Tsunami of the 16th April 2016 in Ecuador - Seismic evaluation, geological field survey and economic implications. Science of tsunami hazards, 36: 197-242.

Toulkeridis, T., Mato, F., Toulkeridis-Estrella, K., Perez Salinas, J.C., Tapia, S., & Fuertes, W. (2018). Real-Time Radioactive Precursor of the April 16, 2016 Mw 7.8 Earthquake and Tsunami in Ecuador. Science of tsunami hazards, 37: 34-48.

Toulkeridis, T., Parra, H., Mato, F., Cruz D´Howitt, M., Sandoval, W., Padilla Almeida, O., Rentería, W., Rodríguez Espinosa, F., Salazar martinez, R., Cueva Girón, J., Taipe Quispe, A., & Bernaza Quiñonez, L. (2017a). Contrasting results of potential tsunami hazards in Muisne, central coast of Ecuador. Science of tsunami hazards, 36: 13-40

Toulkeridis, T., Porras, L., Tierra, A., Toulkeridis-Estrella, K., Cisneros, D., Luna, M.,Carrión, J.L., Herrera, M., Murillo, A., Perez-Salinas, J.C., Tapia, S., Fuertes, W., & Salazar, R. (2019). Two independent real-time precursors of the 7.8 Mw earthquake in Ecuador based on radioactive and geodetic processes—Powerful tools for an early warning system. Journal of Geodynamics, 126: 12-22

Toulkeridis, T., Porras, L., Tierra, A., Toulkeridis-Estrella, K., Cisneros, D., Luna, M., Carrión, J.L., Herrera, M., Murillo, A., Perez-Salinas, J.C., Tapia, S., Fuertes, W. and Salazar, R., 2019. A potential early warning system for earthquakes based on two independent real-time precursors – the case of Ecuador´s 7.8 Mw in 2016. Proceedings of the International Conference on Natural Hazards and Infrastructure 2019, 2nd International Conference on Natural Hazards and Infrastructure, ICONHIC 2019; Chania; Greece; 23 June 2019 through 26 June 2019; Code 257429

Toulkeridis, T., Rojas-Agramonte, Y., & Noboa, G. P. (2020c). Ocean Policy of the UNCLOS in Ecuador Based on New Geodynamic and Geochronological Evidences. Smart Innovation, Systems and Technologies., 181: 485-495.

Toulkeridis, T., Seqqat, R., Torres, M., Ortiz-Prado, E., & Debut, A. (2020b). COVID-19 Pandemic in Ecuador: a health disparities perspective. Revista de Salud Publica de Colombia, 22 (3), 1-5.

Toulkeridis, T., Rodríguez, F., Arias Jiménez, N., Simón Baile, D., Salazar Martínez, R., Addison, A., Freyre Carryon, D., Mato, F., & Díaz Perez, C. (2016). Causes and consequences of the sinkhole at El Trébol of Quito, Ecuador - Implications for economic damage and risk assessment. Natural Hazards and Earth Science System, 16: 2031–2041.

Toulkeridis, T., Simón Baile, D., Rodríguez, F., Salazar Martínez, R., Arias Jiménez, N., & Carreon Freyre, D. (2015b). Subsidence at the "trébol" of Quito, Ecuador: An indicator for future disasters?. Proceedings of the International Association of Hydrological Sciences, Volume 372, 12 November 2015: 151-155

Toulkeridis, T., Tamayo, E., Simón-Baile, D., Merizalde-Mora, M.J., Reyes –Yunga, D.F., Viera-Torres, M., & Heredia, M. (2020a). Climate change according to Ecuadorian academics–Perceptions versus facts. La Granja, 31(1), 21-49

Tsai, J., Fridman, N., Bowring, E., Brown, M., Epstein, S., Kaminka, G. A., ... & Tambe, M. (2011, May). ESCAPES: evacuation simulation with children, authorities, parents, emotions, and social comparison. In AAMAS (Vol. 11, pp. 457-464).

Vaca, A.V., Arroyo, C.R., Debut, A., Toulkeridis, T., Cumbal. L., Mato, F., Cruz D´Howitt, M., & Aguilera, E. (2016). Characterization of fine-grained material ejected by the cotopaxi volcano employing X-ray diffraction and electron diffraction scattering. Biology and Medicine, 8: 3

Wallrabe-Adams, H. J. (1990). Petrology and geotectonic development of the western Ecuadorian Andes: the Basic Igneous Complex. Tectonophysics, 185(1-2), 163-182.

Whelan, F., & Kelletat, D. (2003). Submarine slides on volcanic islands-a source for mega-tsunamis in the Quaternary. Progress in Physical Geography, 27(2), 198-216.

Whittaker, J.E., 1988. Benthic Cenozoic Foraminifera from Ecuador. British Museum London (Natural History), 194 pp.

Wood, N. J., & Schmidtlein, M. C. (2012). Anisotropic path modeling to assess pedestrian-evacuation potential from Cascadia-related tsunamis in the US Pacific Northwest. Natural Hazards, 62(2), 275-300.

Wood, N. J., & Schmidtlein, M. C. (2013). Community variations in population exposure to near-field tsunami hazards as a function of pedestrian travel time to safety. Natural hazards, 65(3), 1603-1628.

Wood, N., Jones, J., Schelling, J., & Schmidtlein, M. (2014). Tsunami vertical-evacuation planning in the US Pacific Northwest as a geospatial, multi-criteria decision problem. International journal of disaster risk reduction, 9, 68-83.

Yeh, H. H. J., Robertson, I., & Preuss, J. (2005). Development of design guidelines for structures that serve as tsunami vertical evacuation sites (Vol. 4). Washington: Washington State Department of Natural Resources, Division of Geology and Earth Resources.

Yépez, V., Toledo, J., & Toulkeridis, T. (2020). The Armed Forces as a State institution in immediate response and its participation as an articulator in the risk management in Ecuador. Smart Innovation, Systems and Technologies 181, 545-554.

Zafrir Vallejo, R., Padilla-Almeida, O., Cruz D´Howitt, M., Toulkeridis, T., Rodriguez Espinosa, F., Mato, F., & Morales Muñoz, B. (2018). Numerical probability modeling of past, present and future landslide occurrences in northern Quito, Ecuador – Economic implications and risk assessments. 2018 5th International Conference on eDemocracy and eGovernment, ICEDEG 2018 8372318: 117-125.

Zapata, A.,, Sandoval, J., Zapata, J., Ordoñez, E., Suango, V., Moreno, J., Mullo, C., Tipán, E., Rodríguez, K.E., & Toulkeridis, T. (2020). Application of quality tools for evaluation of the use of geo-information in various municipalities of Ecuador. In Conference on Information and Communication Technologies of Ecuador (pp. 420-433). Springer, Cham.

Zhang, L., Liu, M., Wu, X., & AbouRizk, S. M. (2016). Simulation-based route planning for pedestrian evacuation in metro stations: A case study. Automation in Construction, 71, 430-442.

Zhong, M., Shi, C., Tu, X., Fu, T., & He, L. (2008). Study of the human evacuation simulation of metro fire safety analysis in China. Journal of Loss Prevention in the Process Industries, 21(3), 287-298.

ISSN 8755-6839

SCIENCE OF **TSUNAMI HAZARDS**

Journal of Tsunami Society International

Volume 40 Number 4 2021

RISK ASSESSMENT OF EARHQUAKES, TSUNAMIS AND OTHER DISASTERS IN CHINA AND TAIWAN

George Pararas-Carayannis

Tsunami Society International

ABSTRACT

The historical record indicates that China's extensive east coast and the rim of the Cross-Straits region bordering Taiwan, are vulnerable to the destructive impact of major weather-related disasters, as well to major catastrophes by earthquakes and tsunamis. The provinces of Shanghai, Guangdong, Fujian, and Zhejiang in China, as well as the neighoring Taiwan, are particularly threatened. Mitigating the impact of future disasters in this region requires an integrated multi-disciplinary planning approach which entails, first identifying the disasters, then assessing their individual impacts, defining geographical limits of vulnerabilities, predicting recurrence frequencies, developing possible scenarios of future socio-economic impacts, resolving Land Use conflicts of vulnerable areas and, finally, preparing a comprehensive plan for preparedness. This present study reviews, assesses and analyzes potential disasters of such multiple types of diasters in China, with particular emphasis on earthquakes and tsunamis along the Cross-Straits region bordering with Taiwan, and further North to the Bohai Bay region, bordering with North Korea. Furthermore, the present study outlines sustainable, adaptive measures and strategies that must be implemented to help minimize potential future losses of lives and damage to property in these regions from such disasters. Finally, the study proposes guidelines for the preparation of a comprehensive disaster plan for China, the Cross-Straits region and further North – a plan which should be implemented or expanded in order to mitigate future adverse impacts on human lives and significant economic resources.

1. INTRODUCTION

China and Taiwan are vulnerable to multiple types of natural disasters, including weather-related and of major earthquakes and tsunamis. The regional vulnerability to earthquakes and tsunamis is particularly high because of the long coastlines and proximity to many inland and coastal faults. China's coastline extends for 1800 km from its border with Korea in the north to its border with Vietnam in the south, and includes about 6,500 coastal islands. China's eight provinces, which includes two mega cities, several medium and small-sized cities, and one autonomous region, border this extensive coastline. More than 40 percent of the population, or about 500 million people live in coastal areas - a trend which continues to rise at a high rate. Critical infrastructure facilities have been built in potentially vulnerable regions with inadequate risk assessment of the need for more stringent engineering guidelines for both static and dynamic stabilities from the impact of future extreme disaster events such as storms, landslides, earthquakes or tsunamis.

The present analysis provides a background of the tectonic evolution of both China and Taiwan, a brief overview of historical data, discusses some of the major past earthquakes, tsunamis, typhoons, storm surges and landslides, and outlines regional and local vulnerabilities, particularly in the higher populated Cross-Straits region (Fig. 1).

Fig. 1. China / Cross-Straits Region

In order to illustrate future challenges in mitigating the potential impact that disasters can have, the study summarizes the geological and geophysical characteristics of the two prominent seismic zones that can produce destructive earthquakes and tsunamis - the Fuzian Province's seismic zone along the western side of the Cross-Straits, and Taiwan's seismic zone of active subduction and collision. Additionally, the present analysis provides

a brief overview of recent typhoon disasters, scenarios of potential future events, and dynamic mechanisms that can produce flooding of low-lying areas from storm surges and tsunamis. Finally, the overview explains some of the maximum probable events which engineers and planners may face in the future, and summarizes the approach that must be taken to develop the necessary criteria for proper land use, adequate building codes, engineering guidelines, and finally recommends strategies that can be adopted to mitigate the future impact of different disasters in order to achieve the sustainable development of coastal cities along the Cross-Straits region and further North to China's Bohai Bay.

2. SEISMOTECTONICS OF CHINA AND OF THE CROSS-STRAITS REGION

The following overview of the seismotectonics of China's Central and Coastal regions provides background information on the complex, long term, geodynamic development of the Cross-Straits region and the potential for destructive earthquakes, tsunamis and other collateral hazards along China's extensive coastalines.

2.1 China's Seismotectonic Evolution

Before the Paleozoic Era, the Eurasian tectonic plate mainly controlled China's geological activity. However, in the middle of the Cenozoic Era, the activity was affected mainly by the interactions of the Pacific and Indian plates (Hellinger et al, 1985). The high seismicity of central and eastern Asia resulted from the northward collisional convergence (at 50 mm/y) of the India tectonic plate against the Eurasian plate (See Fig. 2).

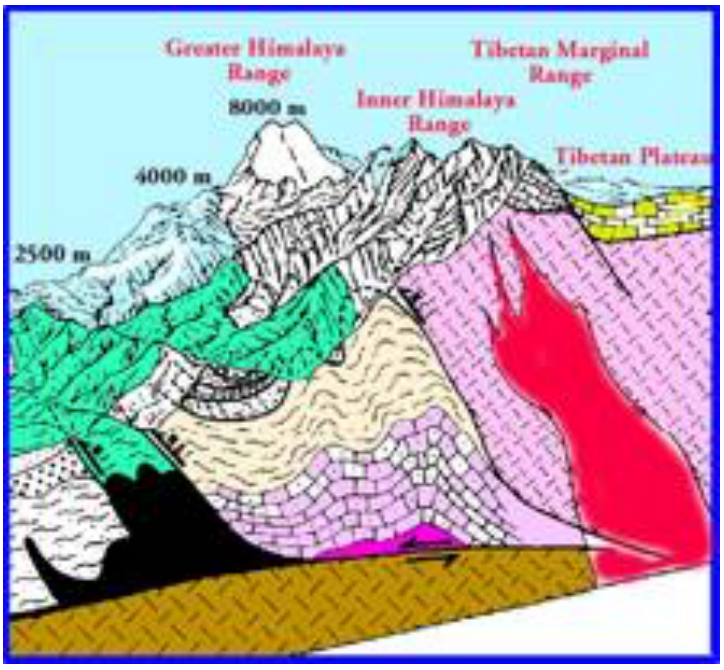

Fig 2. Uplift of the Himalayas, and of the Qinghai - Tibet Plateau

This tectonic convergence - which begun about 55 million years ago - uplifted the Asian highlands and resulted in the growth of the world's largest orogenic belt, the Himalayas, and the associated Qinghai - Tibet Plateau, which has an average elevation of over 16,000 feet - the highest and largest plateau on Earth (See Fig. 2).

The active collision is the continuing cause of frequent large earthquakes between India and Tibet and throughout the surrounding areas. As the India plate kept on moving northward and intruding into Asia by as much as 1,200 kms, regions north of the Himalayas moved laterally to the east and southeast along large strike slip faults such as the Altyn Tagh, pushing into central China and furthermore resulting in extrusion and crustal movement. As the collision continued, there were hundreds of kilometers of crustal block displacement to the east and to the southeast in the direction of China. China's overall seismicity is the result of such collision during the earliest Eocene (~50 Ma) (Ye et al. 1985).

Figure 3 illustrates the source mechanisms of earthquakes in the Qinghai - Tibet plateau region and the extension that takes place to the southeast and to the east in the direction of China. Also, the early seismotectonic evolution is characterized by the merger of several micro-continents throughout the entire Phanerozoic (Zhang et al., 1984; Hendrix and Davis, 2001).

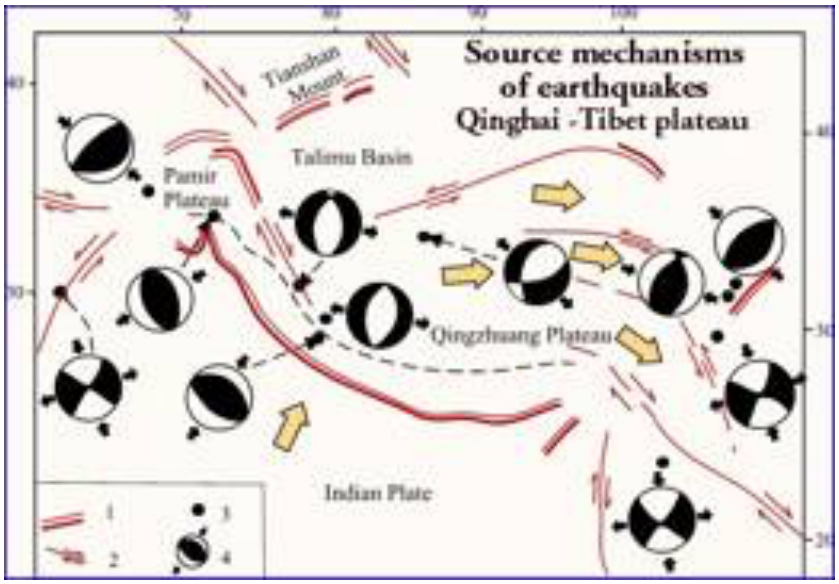

Fig. 3. Interpretation of source mechanism of earthquakes occurring in the Qinghai-Tibet plateau (modified after Zheng Sihua, 1992)

The collision and associated convergence and extension have created 64 major tectonic zones in China, and these can be subdivided into a smaller number of tectonic "regions" (Zhang et al., 1984; Yin and Nie, 1996). Most of the present-day earthquakes in China are generated in the area of plate-connecting belts within the continent where severe geological changes continue to take place. Figure 4 below illustrates the formation of the Longmen Shan Fault.

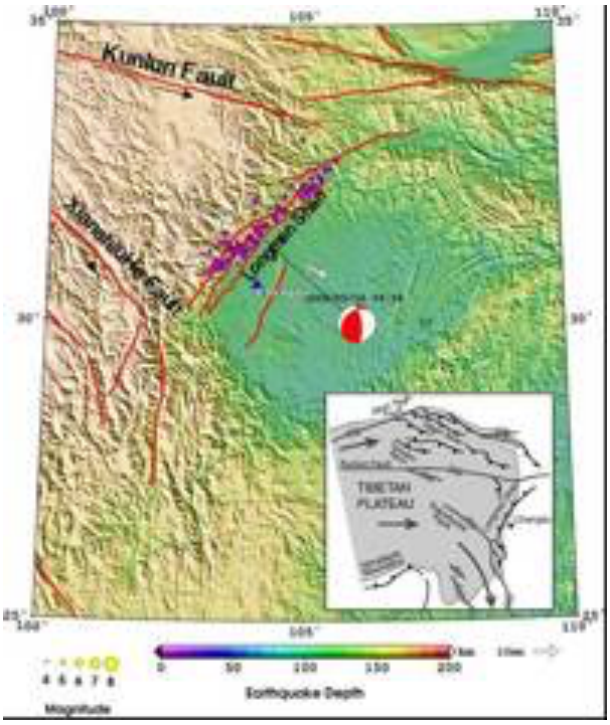

Figure 4. Formation of the Longmen Shan Fault

Figure 5 shows the multiple faults that transverse Central China, the epicenter of many past earthquakes, including that of the destructive Sichuan earthquake of May 12, 1998, which was a recent example of such continuing changes in this region.(Pararas-Carayannis, 2008d).

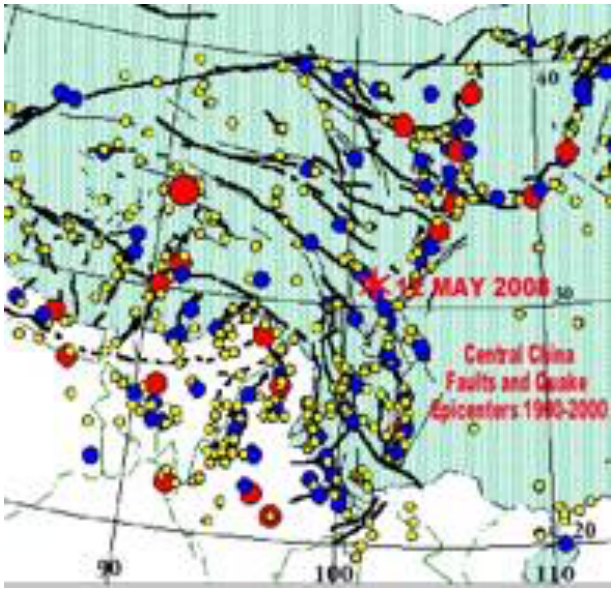

Fig. 5. Central China Faults and Earthquake Epicenters 1900 - 2000.

2.2 Seismotectonic Evolution of China's Coastal, Cross-Straits Region.

China's coastal region underwent complex changes that can account for the present seismotectonic setting of the Cross-Straits region. Both India-Eurasian tectonic collision and Pacific plate subduction may be responsible for structural changes and the formation of several dense seismic zones along the Yellow and the South China Seas. As a result of earlier Tethyan tension, China's coastal regions are now traversed by numerous faults where major earthquakes have occurred and can be expected to occur again in the future (Fig. 6).

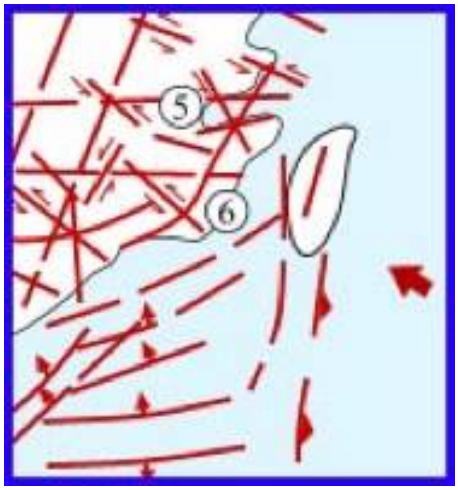

Fig. 6. Schematic map showing the conjugate fault systems in the continental margin of northern South China Sea and surrounding areas (after Ma et al., 1998)

Specifically, since the late Cretaceous period, multi-episode and multi-stage tectonic events resulted in the formation of variable conjugate shear systems in the northern continental margin of the South China Sea (Qiu & Zhou, ?; jgchina.zsu.edu.cn/v32001/html/4qyx.htm).

Adjacent to the Cross-Straits coastal region, the present day coastal Guanzhou-Fujian Seismic Belt was formed less than 5Ma by a conjugate shear system with NWW-SEE compression. The west side of this seismic belt runs from the Zhejiang province to the Guangdong province. Also, as Fig. 6 illustrates, this belt is crisscrossed by a conjugate system that has EW compression and numerous transcurrent faults where major earthquakes could be generated in the future. For example, the Guanzhou-Fujian seismic belt is responsible for past large earthquakes in the region. However, large earthquakes do not only occur along this zone. Large earthquakes along the eastern coast of China and in the Taiwan region are believed to have generated tsunamis in the past, which may have also impacted the Cross-Straits coastal region. Unfortunately however, the available historical information is limited. A first step in fully assessing the impact of historical earthquakes and tsunamis and the potential future risk, should be based on a thorough examination of the historical records. The following is only a brief review of past historical earthquakes and tsunamis along China' coasts and the Cross-Straits region.

2.3 Taiwan's Seismotectonic Evolution

On the eastern Cross-Straits the regional seismotectonics become even more complex in that they involve both subduction and plate convergence. Taiwan is located on the convergent boundary between the Eurasian and the Philippine Sea tectonic plates. Earlier tectonic plate convergence was marked by an apparent eastward subduction of the Eurasian plate underneath the Luzon arc on the Philippine Sea plate. However, this shear motion moved westward with time, forming a broader zone of deformation involving subduction, collision, and plate consumption, rather than a discrete well-defined plate boundary (Pararas-Carayannis, 1999).

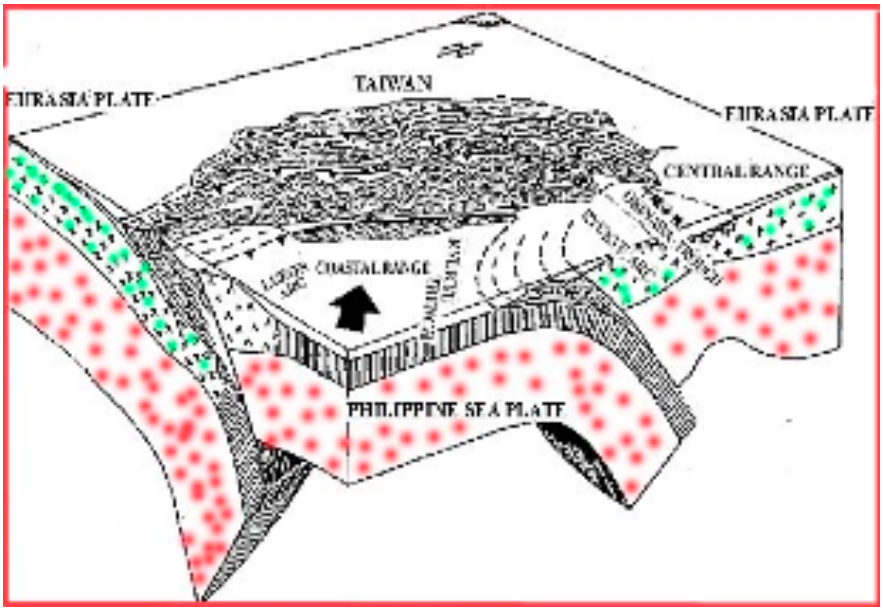

Fig. 7. Northward subduction of the Philippine Sea plate beneath the Ryukyu arc on the Eurasian plate along the Ryukyu Trench.

Thus, tectonic processes do not take place along a simple plate boundary or a subduction zone as commonly conceived, due to the difficulty of subducting a portion of the continental crust, which is significantly buoyant (Fig. 7). Apparently, the wider distributed shear system developed during different stages of arc-continent collision (Fig. 8).

The present day northward movement of the Philippine Sea plate beneath the Eurasian plate is closely related to the Ryukyu and Luzon arc-trench systems, characterized by subduction, convergence and rotation, but marked primarily by the collision of the Luzon volcanic arc with the Asian continental margin (Pararas-Carayannis, 1999). The Ryukyu arc is to the east and northeast, while the Luzon Arc System is southeast of Hong Kong and south of Taiwan. Both volcanic arcs continue onto Taiwan and this wide belt of deformation extends for about 100 km from the western to the eastern offshore region of the island. On the eastern side of the Cross-Straits Region, the seismotectonic belt has an almost N-S orientation.

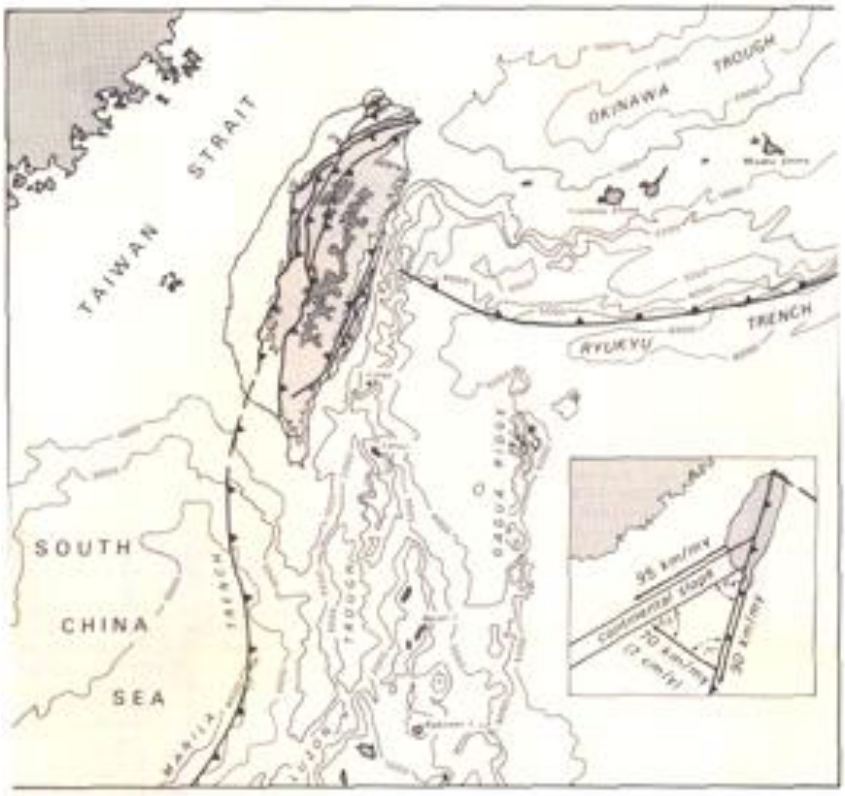

Fig. 8. Arc-continent collision. Triple-point collisional junction in the Taiwan area, east of the Cross-Straits Region.

The present day northward movement of the Philippine Sea plate beneath the Eurasian plate is closely related to the Ryukyu and Luzon arc-trench systems, characterized by subduction, convergence and rotation, but marked primarily by the collision of the Luzon volcanic arc with the Asian continental margin (Pararas-Carayannis, 1999). The Ryukyu arc is to the east and northeast, while the Luzon Arc System is southeast of Hong Kong and south of Taiwan. Both volcanic arcs continue onto Taiwan and this wide belt of deformation extends for about 100 km from the western to the eastern offshore region of the island. On the eastern side of the Cross-Straits Region, the seismotectonic belt has an almost N-S orientation.

3. EARTHQUAKE AND TSUNAMI RISK ASSESSEMENT OF THE CHINA/TAIWAN CROSS-STRAITS REGION

Earthquake and tsunami risk analysis of the China/Taiwan, Cross-Straits region requires examination of the regional seismicity and a review of all available data of past disasters. The following is only a brief overview of a few, major tsunamigenic earthquakes along China's east coast and along the Cross-Straits earthquakes with mostly land impact (See Fig. 9 below). A more detailed review will be required for a comprehensive risk analysis.

3.1 Historical Earthquakes and Tsunamis Along China's Eastern Coasts and the Cross-Straits Region.

According to historical records four thousand one hundred seventeen (4,117) earthquakes of magnitude greater than 4.75 on the Richter scale occurred in China from 1831 B.C. to 1980 A.D. From about 47 B.C. to 1921, it has been estimated that about fifteen of these earthquakes, generated tsunamis on China's east coast (Pararas-Carayannis, 2007, 2008a, b, c). What is also characteristic of earthquakes in the Cross-Straits region is that most are shallow events and thus, some of those occurring along thrust faults, have the potential to generate tsunamis.

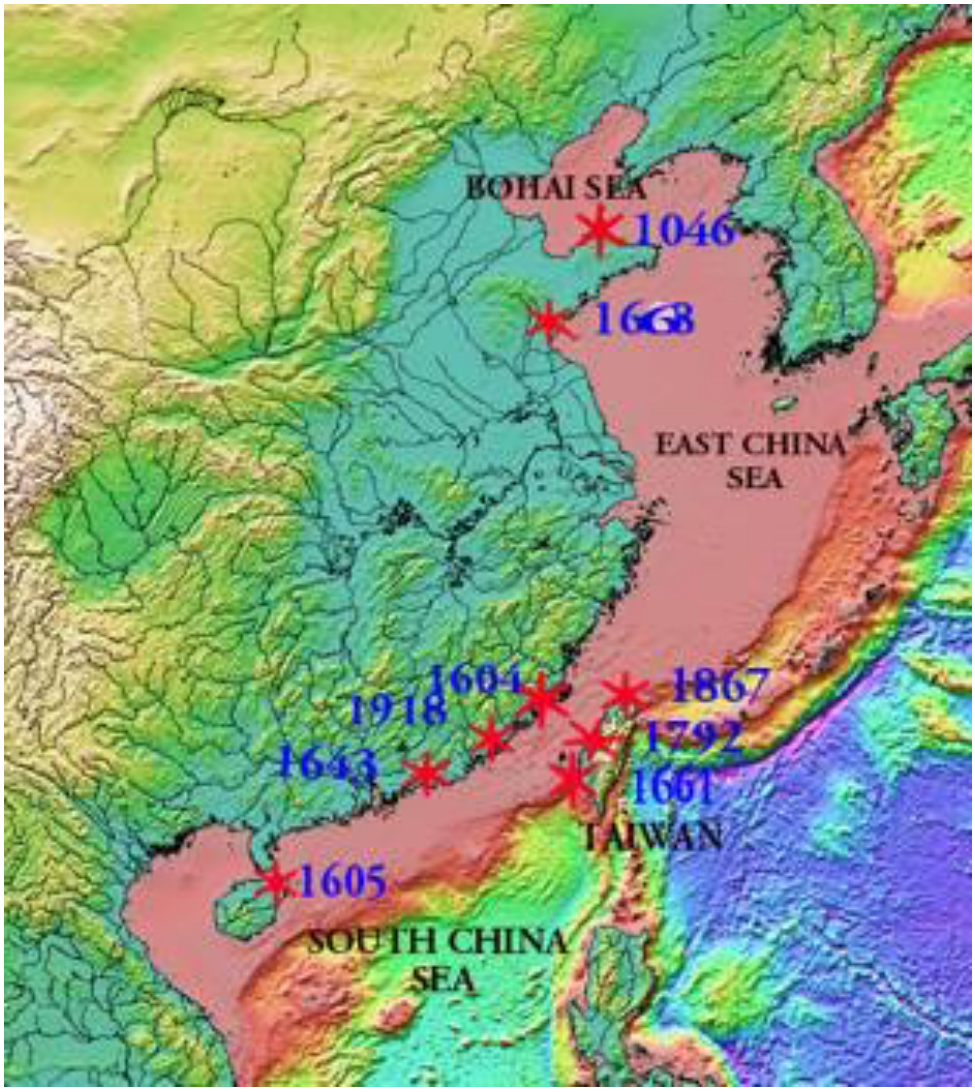

Fig. 9. Epicenters of Historic Tsunamigenic Earthquakes along the East Coast of China and the Cross-Strait Region.

Three of the events characterized as tsunamis in the literature, may have been storm surges. However, even this data given in Figure 9 may be incomplete and in conflict with historical events reported elsewhere in the literature. Major tsunamis that caused 10,000 or more fatalities occurred in 1045, 1329, 1458, 1536, 1776 and 1782 but no specific information could be found. However, there may be mistakes in the historical data as to the dates of these events. For example, the tsunami reported as having occurred in the year 1046 in the Bohai Sea, may be the same event as that reported for 1045.

Similarly, there is no information as to where the tsunamis of 1329, 1458, 1536, 1776, or 1782 may have occurred. There may be errors in dates that need to be further investigated and Chinese calendars need to be properly reconciled with the present astronomical calendar. The data for more recent tsunami events is much more reliable. There have been at least three fairly well documented tsunamis along the eastern coast of China. The first was generated on July 18, 1969 by a 7.4 magnitude earthquake in the Bohai Sea and reportedly caused certain losses in the coastal area near Tangshan, in Hebei Province (Pararas-Carayannis, 2008a, 2009).

The second occurred on January 1-2, 1992 at the southern tip of the Hainan Island and caused some damage (Zhou & Adams, 1986). This event was adequately observed and instrumentally recorded. For example, at the Yulin tide gauge the recorded height of the tsunami was 0.78 meters while at the Sanya port the reported height ranged from 0.5-0.8 meters. The third tsunami occurred in 1994 in the Taiwan Straits but no losses were reported. The following is information on some older tsunamigenic events.

3.1.1 The Earthquake and Tsunami of December 29, 1604

The most significant tsunamigenic earthquake in the Cross-Straits region occurred on December 29, 1604 (Fig. 10).

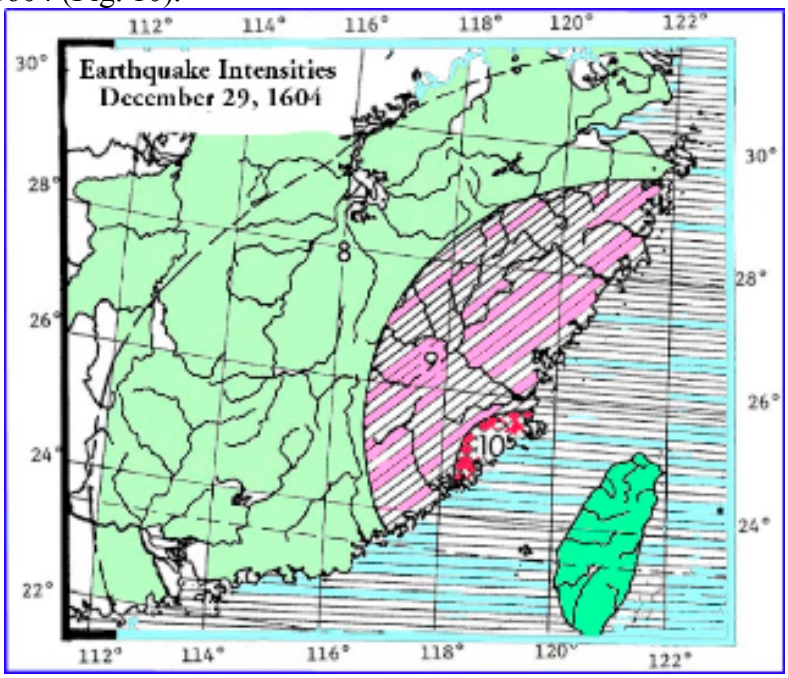

Fig. 10. Intensities of the Earthquake of December 29, 1604. A tsunami was probably generated in the region of intensity 10 and probably intensity 9 (Modified graphic - Nat. Bur. Seismology, 1981).

Given the high intensities of this earthquake as described in the literature (Zhou & Adams, 1986; Pararas-Carayannis, 2007), this was a large magnitude, disastrous event that must have affected Fujian Province and the entire Cross-Strait Region. Its epicenter was in the offshore area of Quanzhou, close to the coastal Guanzhou-Fujian Seismic Belt. No details are available for this early event. However, according to historical records there were widespread effects which included "cracking of the ground", "movement of the water" and the sinking of many boats. Obviously the old descriptions indicate that a tsunami was generated strong enough to sink boats. The generating area of the tsunami was probably within the offshore area where the earthquake's intensities of 9 and 10 can be extended.

3.1.2 The Earthquake and Tsunami of July 25, 1668

This was a tsunamigenic earthquake, which affected mainly the Juxian and Shandong Provinces but not Fujian (Zhou & Adams, 1986; Pararas-Carayannis, 2007). It occurred in an area between Juxian and Dancheng of the Shandong Province on a fault zone, which is presently characterized by uplift caused by compressive thrusts of the ongoing crustal extension (Fig 11). Since compressive thrust and coastal uplift occurred, it is believed that this event caused a considerable tsunami, which needs to be better documented by a risk analysis.

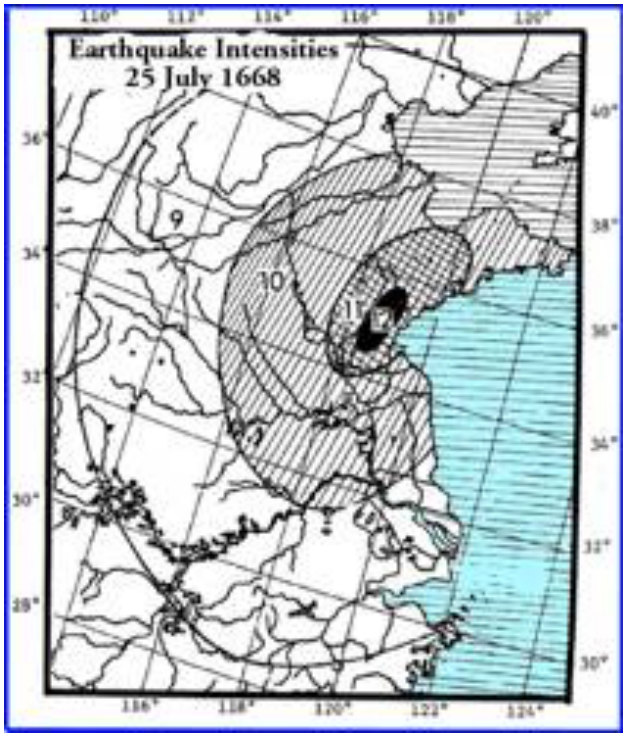

Fig. 11. Intensities of the Earthquake of December 29, 1604. A tsunami was probably generated in the region of intensity 10 and 11 (Mod. graphic, Nat. Bur. Seismology, 1981).

3.1.3 The Earthquake and Tsunami of February 13, 1918

A large earthquake occurred near Nano in the Guangdong Province and caused extensive damage. As with the December 29, 1604 event, the 1918 event was generated on the same seismic belt of the Fujian-Guangdong coast, but further north (Fig. 12). Specifically, the epicenter of this earthquake was near Zhenghe-Haifeng. Crustal movement involved counterclockwise rotation (Nat. Bur. Seismology, 1981a, Zhou & Adams, 1986).

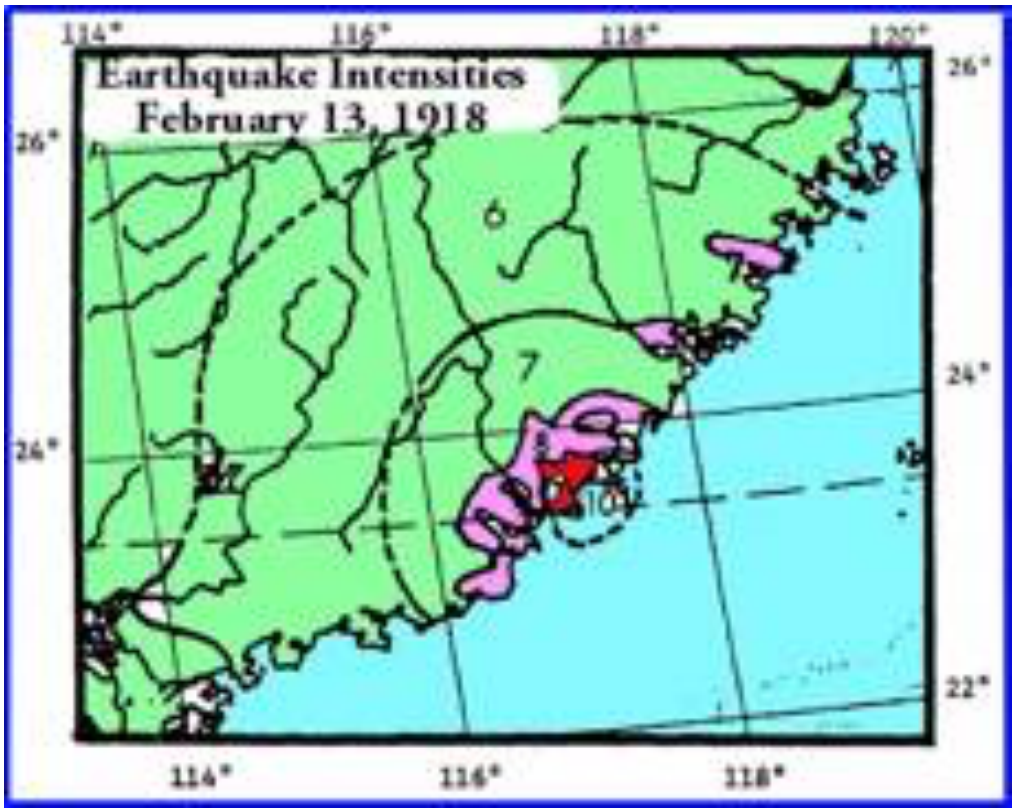

Fig. 12. Intensities of the Earthquake of February 13, 1918. A tsunami was probably generated in the region of intensities 9 and 10 (Mod. graphic - Nat. Bur. Seismology, 1981).

3.1.4 Earthquakes and Tsunamis in the Bohai Sea

The shallow earthquake of July 18, 1969 in the Bohai Sea with an estimated Richter magnitude of M 7.4 generated a small tsunami with a height ranging from 1~2 m. above normal tide level. The tsunami was responsible for losses in the coastal region near Tangshan in the Hebei Province, but no details are available. Also, no details are available as to the height of the tide at the time of the earthquake and whether the 1 to 2 meter reported tsunami occurred at high or low tide (Pararas-Carayannis, 2008a). The earthquake occurred on the Zhangjiakou-Bohai Sea seismotectonic zone, which controls the present-day strong earthquake activities in the northern part of the North China region. Several earthquakes and tsunamis have been generated in this region (Fig. 13, below).

The subsequent 1975 Haicheng and the 1976 Tangshan earthquakes were extremely destructive in the Bohai Bay region (Pararas-Carayannis, 2007, 2009). The two 1976 Tangshan earthquakes in Hebei Province resulted in the greatest death toll in recent history. Their impact on land around Tangshan has been described adequately in the literature but there has been no information on whether a tsunami was generated.

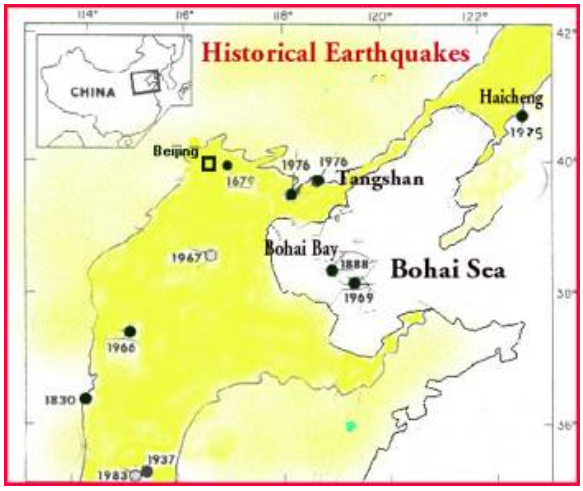

Fig. 13. Earthquakes and Tsunamis in the Bohai Sea (Pararas-Carayannis, 2009)

However, the seismic intensities, the aftershock distribution and the observed crustal movements of the Tangshan quakes indicate that the coastal region of Bohai Bay was impacted, and therefore a local tsunami must have been generated, but not reported. Although not reported, it is believed that the July 26, 1976 Tangshan earthquake also generated a tsunami in Bohai Bay (Fig. 14).

Fig. 14. The Earthquake and Tsunami of July 28, 1976 in the Bohai Bay (Pararas-Carayannis, 2009).

Apparently, the degree of earthquake destruction on land shrouded the damaging effects and impact from a tsunami.

3.1.5 The Earthquake of 20 September 1999 in Taiwan

The complex, 7.7 earthquake, which struck Taiwan on 20 September 1999, is an example of the type of severe events that can occur in the region (Pararas-Carayannis, 1999). Figure 15 illustrates the high seismicity of both Eastern and Western Taiwan, including the Cross-Straits, for a twenty-year period (1977 - 19997) and shows the epicenter of the disastrous earthquake of 20 September 1999.]

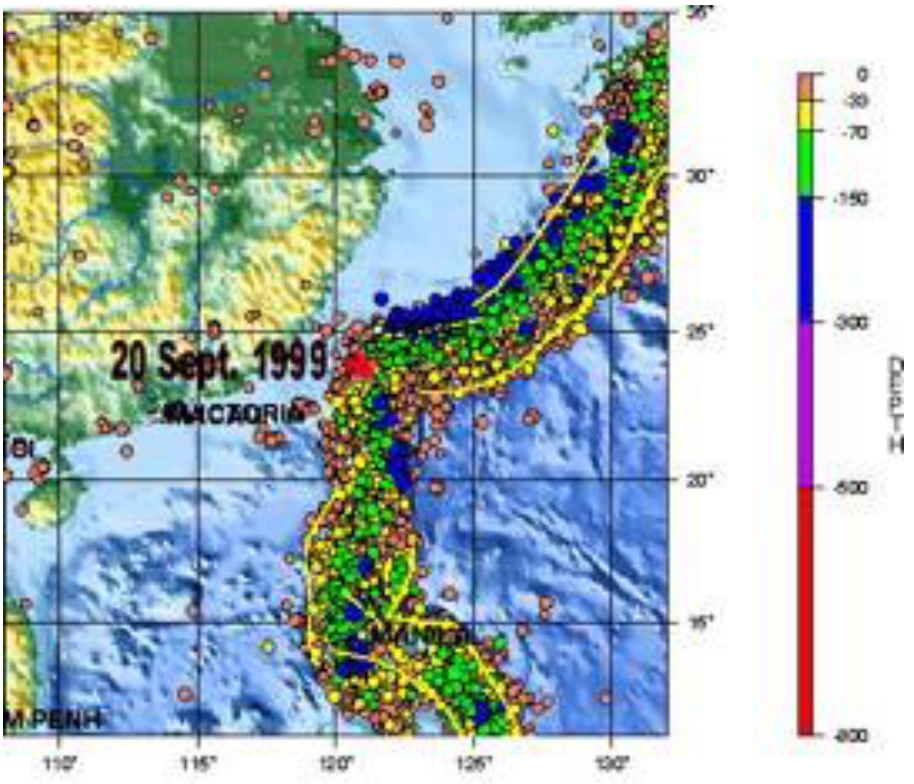

Fig. 15. Seismicity of Taiwan and of the Cross-Straits Region from 1977 to 1997. Epicenter of the September 20, 1999 earthquake (modified graphic of the USGS National Earthquake Data Center).

3.1.6 The Earthquake and Tsunami of August 9, 1792

This earthquake occurred near Jiayi, Taiwan (see Fig. 9). Although it was not a very strong earthquake, it caused a lot of damage. According to the historical record the "water was uplifted several meters", the field "slumped down" and water flooded lower elevations" (Gu et al., 1983, Zhou & Adams, 1986).

4.0 EARTHQUAKE and TSUNAMi HAZARD RISKS AND VULNERABILITIES OF THE CROSS-STRAITS REGION.

The Cross-Straits region is most populous and of highest economic value to China and Taiwan. Earthquakes on land have had great impact in the past. Also, marine disasters, such as tsunamis or typhoon surges, can have a significant impact on coastal populations and the economy of the region. The following is a brief overview of direct and collateral factors that can enhance the generation and impact of tsunami and of other marine and weather-related hazards - such as storm surges. As previously stated, China's overall earthquake and tsunami vulnerabilities are enhanced by the complex and active seismotectonic zones along its coasts, where major destructive earthquakes occur frequently. Earthquakes in the Cross-Straits region are a major risk that needs to be carefully examined to fully evaluate potential future impacts and recurrence frequencies.

Also, there is a need to evaluate the risk of tsunamis generated from larger magnitude earthquakes and from collateral mechanisms, such as stratigraphic folding of the thick sedimentary layers, en-echelon bookshelf failures, or by the triggering of submarine landslides. To assess such potential tsunami mechanisms, the structural and tectonic evolution of the Cross-Straits region must be analytically re-examined and further evaluated. Similarly, typhoons and storm surge flooding are a major threat that needs further study. As the historic record indicates, the Cross Straits region is extremely vulnerable to typhoons and flooding due to storm surges.

4.1 Earthquake and Tsunami Hazards and Vulnerabilities - Potential for Tsunami Generation in the Cross-Straits Region.

Some of the deformational seismic events have the potential to generate destructive local tsunamis. The orientation of the crustal strain beneath the Taiwan Strait appears to be dominated by a North-South extension rather than the East-West compression as along eastern Taiwan (Pararas-Carayannis, 1999). As the historic record indicates, destructive earthquakes occur frequently in the Cross-Straits region. The Straits region is seismically active and capable of generating earthquakes greater than 6.0. For example, the most recent large earthquake in the Taiwan Strait occurred on 16 September 1994. The Peng-Hu Earthquake (mb=6.5), in the western part of the Tainan basin was a very shallow event (depth of 13 km). Its focal mechanism indicated a sea floor movement consistent with normal faulting with its axis along a N-S direction. With earthquake larger than 6, tsunami generation is possible while earthquakes with magnitude greater than 7 and with a large vertical component have the ability to trigger more damaging tsunamis (Pararas-Carayannis, 1999).

4.2 Tsunami Generation from Collateral Mechanisms

With a few exceptions, most of the earthquakes in the region involve primarily crustal movements with lateral strike-slips. Such earthquakes do not generate large tsunamis. However, strong motions from such events could trigger submarine landslides or other

collateral events that could contribute to destructive local tsunamis. Apparently, geological changes have played an important role in the tectonic evolution of the crustal basement and have controlled the scale of palaeochannel development and the changes of ancient river systems and channels which, although now buried by sediments, continue into the Cross-Straits region (Xu et al. 1996). Major rivers deposit large loads of sediments in the Cross-Straits region and this deposition has created unstable slopes on the shelf that could become potential sources of landslide-generated tsunamis.

The tectonic movements associated with the larger earthquakes - and the compressive forces they generate - could interact with the submerged fluvial regimes that contain high sediment loads and thus could generate massive sediment movements - even on relatively gentle bathymetric slopes (Pararas-Carayannis, 2009). Such movements could contribute to local tsunami generation. Folding and en-echelon bookshelf type of failures of the deeper consolidated sediment layers could become collateral mechanisms for greater tsunami generation. Such collateral mechanisms can contribute significantly to the generation of destructive local tsunamis anywhere in the region, but particularly closer to the denser seismic zones of the coastal Guanzhou-Fujian Seismic Belt or along the N-S trending seismotectonic belt on the eastern side of the Cross-Straits Region.

4.3 Tsunamis of Distant Origin

Tsunamis of distant origin do not seem to pose a major threat, mainly because of the sheltering effect of Taiwan and of the island arcs. However, tsunamis originating from earthquakes along the Manila Trench or the Ryukyu Islands could potentially have some impact in the Cross-Straits region. For example, on April 24, 1771, a large earthquake (estimated at M=7.4) occurred near the southernmost Ryukyu Islands (South of the Ishigaki Island area controlled at that time by the Japanese Satsuma Samurais). A tremendous tsunami was generated (records claim maximum run-up of 50m to 85m). The tsunami devastated the islands of this group as well as the more distant islands of the Miyako group (Pararas-Carayannis, 1999). Huge blocks of coral were carried by the waves. A block was found 2.5 km inland. About 11,000 people were killed in the Ryuku islands, however there is no information in the literature about its impact in Taiwan, the Cross-Straits region or anywhere else along the coasts of China.

Tsunamis originating in the Sea of Japan do not appear to pose a major risk for coastal areas along the Yellow or the East China Seas. For example, very little energy entered the Yellow and East China Seas when a destructive tsunami was generated by the earthquake of May 26, 1983 in the Sea of Japan (Fig. 20). Although, the tsunami affected the coastal area of China near Shanghai and possibly other coastal areas along the Yellow and the East China Seas, its height was not significant. A tide station near Shanghai recorded a tsunami of only 42 cm in height.

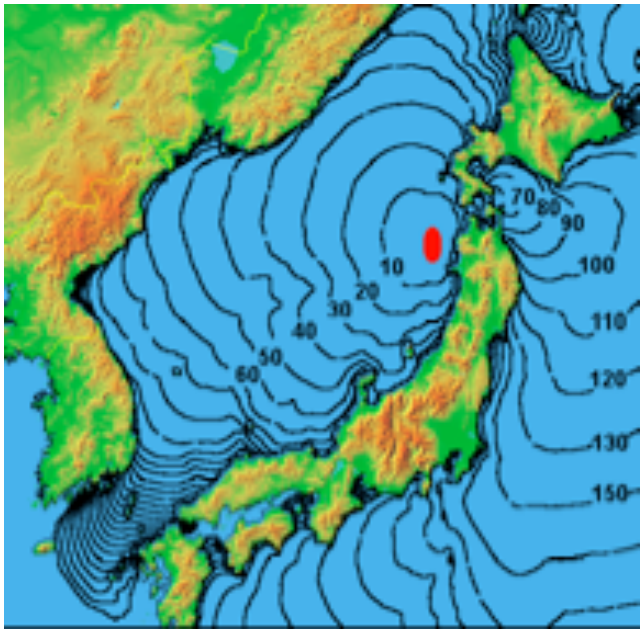

Fig. 20. The Earthquake and Tsunami of May 26, 1983, in the Sea of Japan. Very little tsunami energy entered the East China Sea.

4.4 Effects of Bathymetry

Coastal vulnerability to tsunamis and other marine hazards is greater in the Cross-Straits region and elsewhere along the eastern coasts of China because of the shallow depth of the adjacent seas. The continental shelf adjacent to the provinces of Zhejiang and Fujian is relatively shallow and the water depth averages only a few meters. The greatest depth is about 100 meters. South of the Yangtze River in the East China Sea, the water depth averages about 40 meters but increases to about 300 meters. With such shallow bathymetry and gentle underwater slopes, tsunamis generated from submarine landslides (triggered by earthquakes or other disturbances) would tend to be localized.

4.5 Effects of Astronomical and Atmospheric Tides

Similarly, a significant variability in the astronomical tidal range can contribute to greater coastal vulnerability, particularly if a tsunami or a storm's or typhoon's landfall occur near the time of the higher tidal range. The tides in the region are diurnal. The highest perigean tide in the China Sea is about 3 meters. However, along the shores of Zhejiang and northern Fujian the spring tide reaches a maximum of 5.7 meters. Closer to the coast of Hangzhou, the spring-tide range is 8.0 meters. Shallow bathymetry and local coastal geomorphology may be the reasons for differences in astronomical tidal forcing functions that cause the higher tides. The harmonics of fundamental frequency variations need to be studied to explain such unusual localized deviations along China's eastern coasts and along the Cross-Straits region. Also, further analysis may help understand the unusually high degree of flooding and the high tidal flows that have been observed in Fujian Province and elsewhere in the Cross-Straits region at the onset of typhoon surges.

4.6 Vulnerability of Nuclear Plants and Oil Platforms

Typhoons and associated marine hazard risks and flooding are the more frequent, seasonal disasters that affect the region and need careful re-assessment. Numerous more oil platforms exist in the Yellow as well as the South China Seas. At least 7 nuclear power plants are either operating or under construction along China's east coast (Fig. 21). Two of these plants in operation are located in the Fujian Province, in close proximity to the Guanzhou-Fujian Seismic Belt and to the coastal area subject to flooding by typhoon surges. It may be wise to review again the safety of these sites and of the oil platforms operating in the region for the impact of earthquakes similar to the 1604, as well for the adequacy of elevation of the nuclear plants' cooling systems to possible extreme typhoon surges.

5.0 RECENT TYPHOONS, STORM SURGES AND FLOODS IN THE CROSS-STRAITS REGION

Fig. 21 China's Nuclear Power Plants and Plants Operating in Fujian Province.

5.1 Estimating Wind Forces, Potential Storm Surges/Flooding and Possible Generation of Meteotsunamis

The brief overview in Section 4 of this report illustrates that typhoons, tropical storms and surges constitute great and frequent seasonal hazards for both China and Taiwan. One of the greater challenges in mitigating the impact of such hazards is the prediction of flooding resulting from the combined meteorological, oceanic, and astronomic effects coincident with the arrival of a typhoon at the coast. Such information is important in warning the public and in the planning and the design of important coastal structures.

Increasing requirements for large coastal installations, have required conservative criteria in obtaining estimates of potential storm surges from typhoons or tropical storms. Thus, many numerical models and techniques have been developed to provide forecasts and predictions for engineering projects. Although, modern technology and satellite imagery allow presently the early detection of storms and the tracking of their paths, the impact of storm systems is not always fully predictable. Specific factors which can combine to produce extreme water fluctuations at a coast during the passage of a typhoon include: storm intensity, size, path, duration over water, atmospheric pressure variation, speed of translation, winds and rainfall, bathymetry of the offshore region, astronomical tides, initial water level rise, surface waves and associated wave setup and run up due to wind frictional effects (Pararas-Carayannis, 1975).

The capability to predict storm surges is based primarily on the use of analytic and mathematical models, which estimate the interactions between winds and ocean. The prediction of sea surges resulting with the arrival of a typhoon at the coast is a rather difficult problem to solve. The reason is that a typhoon is a three-dimensional, weather system with ever changing dynamic conditions of wind speeds, directions and atmospheric pressures. Although it is outside the scope of this report to explain exactly how the problem is solved, a brief overview is provided.

Many sophisticated mathematical models have been developed in recent years to provide accurate three-dimensional estimates of energy flux, rise of water on the open coast and of the flooding that can be caused by a passing hurricane/typhoon. Most of the models include an approximation to the complete storm-generation process, of the wind field and make use of the Bathystrophic Storm Tide Theory (Pararas-Carayannis, 1975, 2006.). However all models, regardless of sophistication, are limited by the number of initial conditions and assumptions that must be made by the ever-changing dynamic conditions of the storm system - taking into account the combined effects of direct onshore and along shore wind-stress components on the surface of the water, the effect of the earth's rotation (known as the bathystrophic effect) and the different pressure and frictional effects (Pararas-Carayannis, 1975, 1992, 2004, 2006).

The more recent numerical models use a three dimensional approach, faster and more efficient computers, more accurate weather data from satellites and, thus, have greater potential for more accurate predictions. However, the fundamental principles in the prediction of hurricane/typhoon surges described here, remain essentially the same.

Fig. 22 below illustrates graphically the various components that contribute incrementally to the total hurricane/typhoon surge height on an open coast and to potential flooding (Pararas-Carayannis 1975). However, coastal morphology may also affect the extent of rise of water.

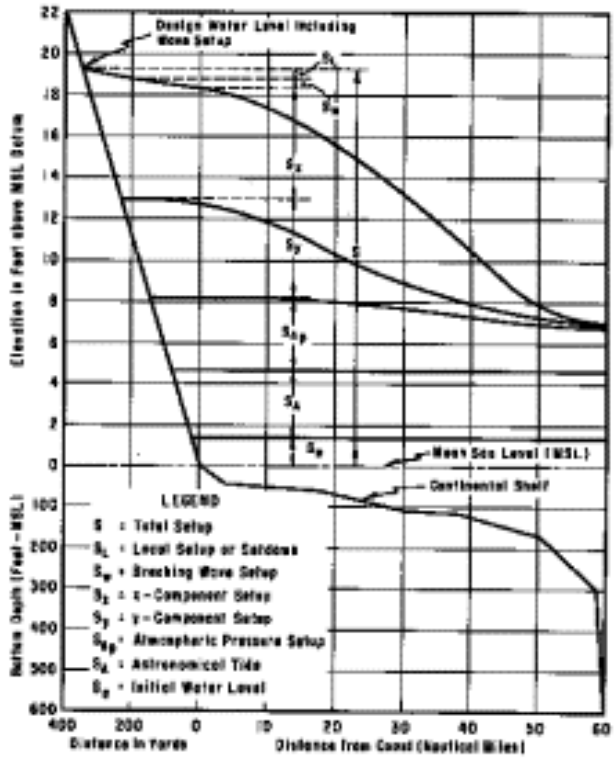

Fig. 22 Diagram showing various components contributing to the hurricane/typhoon surge on the shore (Pararas-Carayannis, 1975).

5.1 Probable Generation of Meteo-tsunamis

Changes in atmospheric pressure caused by rapidly-moving hurricanes/typhoons over the shallow offshore bathymetry of the continental shelf in regions of maximum winds, not only enhance the height of long period sea waves, but have the potential of generating atmospheric meteo-tsunami waves, even along shores distant from the point of their landfall. As a hurricane/typhoon advances on its track, the storm waves convert to sea swells that travel geostrophically at right angles to the storm's direction, often superimposing on other existing waves, thus refracting together and often increasing in height in the shallows of the coastal region.

Although somewhat difficult to quantify, superimposed on breaking swells are often those of meteo-tsunami waves, which contribute to even greater run-up heights on the stricken shores. Such was the case in the Caribbean Sea, when a rapidly-moving Category 2 hurricane passing far south of the Island of Hispaniola on 27–29 August 1916, was responsible for the generation of unusually high swells which superimposed and augmented the breaking waves at Santo Domingo of what was characterized as a meteo-tsunami and caused the total destruction of the USS Memphis on the rocks of the harbor in the shallower water depth near the harbor.

Huge breaking waves near Santo Domingo appeared to undergo both linear and non-linear transformations, apparent chaotic interactions, with increasing kinetic energy and significant wave height augmentation. A wave estimated to be of about 70 feet in height begun breaking, dragging the ship to the rocky shore (Pararas-Carayannis, 2019). In view of such previous impact in Santo Domingo and elsewhere, there must have been similar impacts of typhoon-generated meteo-tsunamis along China's and Taiwan's extensive coastlines.

6.0 PLANNING FOR DISASTER MITIGATION IN CHINA AND TAIWAN

There is nothing that can be done to prevent the occurrence of natural disasters. Disasters will continue to result in losses of lives, destruction to property and the disruption of the social and economic fabric of entire communities in both China and Taiwan. The losses will continue to increase because of population growth in vulnerable areas. But while disasters cannot be prevented, their impact on loss of life and property can be drastically reduced with proper risk assessment and planning (Pararas-Carayannis, 1986, 1988). The need for proper natural disaster risk assessment cannot be overemphasized. There is a need for good understanding, not only of the physical nature of the disaster phenomena in the region, but also of each vulnerable area's combined physical, social, economic and cultural factors. The specific methodology for such planning has been described in detail in the literature (Pararas-Carayannis, 2007).

Disaster-related fatalities, injuries, and property destruction can be avoided or minimized by correct planning, construction, engineering, land utilization, and effective public education and preparedness. Structures can be built that are disaster resistant. Many buildings and homes can be reinforced at a small cost to withstand the effects of a disaster such as an earthquake, a typhoon or a tsunami, and construction codes can be upgraded. Regardless of the frequency of a disaster or the available warning time, an assessment of potential risk and the planning for disaster mitigation must be made well in advance.

A good starting point in assessing the specific vulnerability of each specific region should be the complete identification of potential disasters, the establishment of a historical database of past events, the delineation of the geographical distribution of potential maximum disaster impacts, and the preparation of a plan to mitigate adverse effects and protect life and property. Perhaps disaster risk assessment has been completed for certain disasters and for certain areas in the region. However, these should be reviewed from time to time to ensure their adequacy. The following is only a brief overview of some of the general concepts and basic principles that apply to risk assessment and the mitigation of the most important of the natural disasters that threaten both China and Taiwan.

6.1 Identification of Disaster Risks in China and Taiwan

Advances in science and technology provide the means to reduce significantly losses from disasters. But in order to apply the needed techniques, it is important to first identify the potential disasters that may strike the Cross-Straits region. Any given area may be vulnerable to one or more natural disasters. Some areas in the Straits may be more vulnerable to earthquakes and tsunamis. Other areas may be more vulnerable to typhoons and surge flooding, while still others may be threatened by landslides or other localized hazards. Identifying the most important disasters and associated hazards for each specific area is the first priority in developing a risk assessment study for the Cross-Straits region. For each type of potential disaster the risk assessment study will require a different approach. However, there are some common elements in assessing the impact of all disasters in the region.

6.2 Development of Historical Disaster Databases

After identifying the disasters that may be of threat to China and Taiwan, a good starting point for the disaster risk assessment study is the collection of data of all the historical events that caused destruction in the past (Pararas-Carayannis, 1986). The data collection becomes easier if good records have been kept. A historical disaster database can be developed for the region by researching miscellaneous archives of newspapers and of public records. If such historical data is unavailable, the data may be developed from indirect sources.

Indirect ways in developing a historical data base for past events may be the examination of old correspondence of government officials or of accounts of early settlers. In the absence of historical data, past disaster events can be determined by studying the geologic stratigraphy of a region and using radiocarbon, other isotope dating techniques or dendrochronolgy to establish past disaster occurrences and their severity. For example, by studying past seismic activity, geologists can often speculate on what controls the dynamics of earthquakes and make predictions. Often one earthquake may nucleate an offset along the trace of a fault and such offsets and measurements of strain build-up can be used to forecast, not necessarily the exact time of the next earthquake event further down the fault rupture, but at least its magnitude and location (Pararas-Carayannis, 2007).

The development of a comprehensive and systematic compilation of historical data on disasters is an indispensable tool for disaster risk analysis and can also serve in the operational analysis and real-time evaluation of potential disaster threats by early warning systems. Finally, a historical disaster database can be widely used for coastal zone management, engineering design criteria, educational purposes and disaster preparedness. Internet communications and software can also help make interactive retrieval of historical data on disasters feasible for global sharing, and for international programs of disaster mitigation.

6.3 Assessing Disaster Frequency in China and Taiwan

The most important parameter in assessing risks in China and Taiwan as well as in the Cross-Straits area and for the planning for disaster mitigation, is the determination of the disasters' recurrence frequencies. Assuming that the historic record is long enough for the region and there have been many years of direct observations, it is possible to establish approximately when a disaster may be expected again. However, if the historic record is limited, statistical methods are of little use. The problem is that large catastrophic disasters may take place so infrequently in any one location that there may be no locally available data on which to predict risk and produce a zonation of the hazard.

The lack of historical data should not be misinterpreted to mean that there is no danger. Therefore, the prediction of infrequent disasters such as earthquakes, tsunamis or floods - are often given in statistical terms but with a great deal of ambiguity. For example, when a statistical prediction is made that "there is a 90 percent chance that an earthquake will occur in the next 50 years" in a certain area known for its seismicity, this does not mean that the predicted earthquake cannot happen tomorrow or that it may not be delayed by 50 years (Chinnery and North, 1975). Similarly, floods are estimated in terms of statistical probability of being 50, 100 or 200-year events – which nature may very well prove wrong.

Obviously, statistical predictions of infrequent disasters may not be within a reasonable time frame that can be of usefulness to planners, policy makers, and those in government who deal with public safety. However, the statistical analysis of seasonal disasters such as hurricanes/typhoons or extreme storms can be forecasted more easily and can be fairly accurate. With less frequent disasters such as earhquakes or tsunamis. such forecasting is very difficult. In conclusion, if a good historical database exists, it is possible to develop the statistical probability of a seasonal recurrence of weather disasters recurrence in the Cross-Straits region, but not for other types of disasters such as earthquakes or tsunamis.

6.4 Planning for Appropriate Land Use

In developing a viable disaster preparedness plan for China or Taiwan, all environmental hazards need to be examined individually in order to protect the public and to locate, design, construct and determine the safety and reliability of important infrastructure facilities, particularly in the higher-populated zones. For example, in evaluating the earthquake hazard, the seismic regions should be identified in terms of geographical distribution, the distribution frequency of earthquake/tsunami occurrences should be determined, and the probabilities of recurrences estimated. For earthquakes, the risk assessment should include evaluation of expected peak ground accelerations (horizontal and vertical) and the designation of appropriate building codes. Disaster recurrence frequencies should be estimated with care in differentiating between expected yearly or seasonal occurrences - such as those related to atmospheric disturbances - and for more extreme events such as earthquakes or tsunamis that have much longer cycles (Pararas-Carayannis, 2002).

6. 5 Disaster Risk Mapping

Having completed the preliminary stages, the analysis of the disaster risk must now be translated and reduced from technical and scientific terms to simple forms that can be adopted and used effectively. The analysis must be simplified further into forms that can be understood easily. Thus, the final product of historical, statistical or modeling studies that may be conducted must indicate the spatial variations of the hazard risk in the form of maps. Maps can be prepared for all natural hazards that may impact China and Taiwan as well as the entire higher-populated eastern coastal region of China from Bohai Bay to the South China Sea. The production of maps depicting variations in the degrees of disaster risk is an invaluable tool for the planning process and for proper land management (Pararas-Carayannis, 2002). In this way, high-risk areas can be avoided or used for low intensity development, and safe areas can be designated for public shelters and evacuation of the public. Similarly, the total risk at any point can be easily established, as well as the probability of occurrence for insurance purposes.

6.6 Variation and Acceptability of Risk

Determining the regional variation of risk for China and Taiwan as well as of the entire eastern coastal region of China from Bohai Bay to the South China Sea is a key element in planning and preparing for future disasters. For example, based on historical earthquake or typhoon activity, appropriate maps can be prepared depicting the risks for each region. For example, four zones usually represent seismic risk in accordance to expectancy of earthquake damage. According to this type of zoning, areas may be designated that have no reasonable expectancy of earthquake or tsunami damage; areas where minor damage can be expected; areas where moderate damage can be expected; and finally areas where destructive earthquake or tsunami effects can be expected. Typhoon maps may show their customary tracks, seasonal and chronological occurrences, and areas of past impact and heights of storm surge or frequencies. Analogous maps may be compiled of past recorded or observed tsunami wave inundations, and if suffficient data exists, of statisitical reccurence frequencies (Pararas-Carayannis, 2002).

6.7 Microzonation of China's Disaster Risks

Although mapping of hazards is useful for overall risk assessment, the selective nature of a disaster's destruction in China requires mapping which takes into consideration specific local conditions. This is particularly important for coastal regions where there has been considerable tsunami activity. Public officials and planners can develop better disaster response and recovery plans if they know the possible physical and economic damage and the various disaster scenarios and collateral impacts which may affect structures and businesses.

Also, structural engineers need more accurate analysis and more detailed information in the form of microzonation maps of the hazard so that they can design structures that will withstand the impacts, and additional structural static and dynamic loads of earthquakes or tsunamis or other disasters. Such detailed maps are essential to planning and disaster mitigation. For example, in assessing the specific earthquake risk of a given area, an earthquake source must be postulated of a given magnitude and location. Then all geological materials in the area with similar physical properties can be grouped together. Subsequently, the effects of the postulated earthquake for each geologic unit can be predicted by the type of hazard for failure, specific type of ground shaking, surface rupture, flooding, land sliding, and liquefaction potential. For example, with such maps engineering geologists can estimate potential amplification of ground motions during an earthquake and engineers can design proper new structures or retrofit existing ones (Pararas-Carayannis, 2002).

6.8 Ensuring Safety from Frequent Seasonal Disasters

The Cross-Straits region of China and Taiwan is the worse hit area for natural disasters, particularly typhoons and rainstorms. A meteorological disaster control system is already under construction to serve the Fujian Province of China and Taiwan. Although apparent progress has taken place in improving onshore weather monitoring services, there is also a further need to improve the capabilities in marine climate monitoring, analysis and forecasting by increasing the number of observing stations, data transmission and communication systems, along with a more advanced weather forecast and warning system.

6.9 Ensuring Public Safety

Of paramount importance in land use analysis should be public safety and the means by which it can be assured through proper planning and land utilization. Development policies and decisions on public safety must be based on a comprehensive disaster risk assessment of all environmental hazards impacts that may be unique to each region. Government agencies have the responsibility to formulate land-use regulations that will result in greater public safety. Proper land utilization policies must prohibit urban development in zones that the disaster assessment study identified as potentially vulnerable and may put parts of the population at risk. Furthermore, the government agencies must designate evacuation procedures, post signs and provide proper instructions to the public. Property and business owners could also be educated about steps they can take voluntarily to protect their investments, if these are located in risk areas.

6.10 Disaster Mitigation Through Preparedness

The safety and security of the public in China, Taiwan and elsewhere in this region, will continue to be threatened by numerous disasters. The main reasons for such vulnerabilities may be erroneous perceptions of disasters and the lack of proper planning and preparedness. Therefore, equally important in mitigating loss of life and damage to property is the perception of potential disasters by the people of each threatened region. Disaster

perception by the public is based on a technical understanding of each type of disaster phenomenon - at least at the basic level - and a behavioral response stemming from that understanding and confidence of the public for the authorities to provide safety, timely disaster warnings, and prompt post disaster recovery. Thus, once a disaster risk assessment study has been completed, a program of proper education that promotes disaster awareness and safety rules is an important function of government civil defense authorities.

It is paramount that Emergency Management Planning should become an ongoing activity for all participating agencies in all regions of China and Taiwan, and meetings should be held frequently to review disaster scenarios and how potential hazards could be prevented or their impact be mitigated. Such interagency coordination is extremely important and can be optimized through frequent meetings of managers and by encouraging good interpersonal relationships. Furthermore through hearings, citizen and private involvement should be encouraged to review and evaluate community concerns about potential emergencies. Maintaining comprehensive records during a disaster is another extremely important responsibility in correcting planning deficiencies and mitigating future disaster impacts. Thus a public information function must be clearly defined and established.

The ultimate objective of disaster planning and the mitigation of disaster impact in China and elsewhere in general, is the safety of the public and the protection of property. Therefore, internal alerting procedures must also be established by the responsible agencies, bearing in mind that their ability to alert the public must be maximized through effective warning systems that use all available means of public information, communications and the media.

7.0 SUMMARY AND CONCLUSIONS

Both China and Taiwan are densely populated and have industries of high economic value. Natural disasters such as earthquakes, tsunamis, typhoons and other collateral hazards can have a great impact. Earthquake disasters occur frequently. Tsunamis do not pose as much of a threat, but locally destructive tsunamis could be generated in the future which can be expected to have more significant impact since most of the recent development in the region has taken place along low-lying coastal areas where several mega cities are located and infrastructure facilities exist or are under construction. Local tsunamis may be also generated in the region, particularly in the Cross-Straights region of China and Taiwan, by a combination of collateral mechanisms that could involve folding of thick sedimentary layers, landslides, destabilization/dissociation of gas hydrates deposits and mass sediment flows. Future tectonic movements associated with larger earthquakes in both regions, could interact with the now submerged fluvial regimes that contain high sediment loads and thus could generate massive sediment movements. Folding and en-echelon bookshelf type of failures of the deeper consolidated sediment layers, for example, could become collateral mechanisms for greater tsunami generation, particularly in areas where denser seismic zones are concentrated, the seismicity is stronger, and greater sedimentation has occurred.

Thus the potential for tsunami generation is exacerbated by the thick accumulation of sediments and the multi-layered stereographic distribution of sediments with different shear strengths, densities and rigidities. Dissociation of the abundant gas hydrate deposits by earthquake ground motions, particularly near offshore oil platforms as those near the Bohai Bay region of China, could result in large-scale slip and sediment mass flows. Typhoon and pther associated marine hazards, pose the greatest threat because of their yearly seasonal recurrence. The risks associated with weather related hazards in China and Taiwan Cross-Straits region need to be carefully re-evaluated.

8.0 REFERENCES

Chinnery, M. A., and North, R. G., 1975. "The Frequency of Very Large Earthquakes", Science, Vol. 190, 1975, p. 1197-1198.

Hendrix, M.S., and Davis, G.A., 2001, Paleozoic and Mesozoic tectonic evolution of central Asia: from continental assembly to intracontinental deformation: Boulder, Colo., Geological Society of America, vi, 447 p.

Hellinger, S.J., Shedlock, K.M., Sclater, J.G. and H. Ye, 1985. The Cenozoic evolution of the north China basin, Tectonics 4 (1985) 343–358.

Ma Zongjin, Zhong Jiasheng, and Wang Yipeng. The 3-D deformation and movement episodes and neotectonic domains in the Qinghai-Tibet plateau (In Chinese). Acta Geological Sinica, 1998, 72(3): p.211-227

National Bureau of Seismology, 1981. China Seismic Intensity Report, Published by National Bureau of Seismology (in Chinese).

Pararas-Carayannis, G. 1986. "The Effects of Tsunami on Society". Violent Forces in Nature, Ch. 11, Lamond Publications, 1986, p. 157-169. Impact of Science on Society, Vol. 32, No.1, 1982, p 71-78

Pararas-Carayannis, G., 1988. Risk Assessment of the Tsunami Hazard. Proceedings of the International Symposium on Natural and Man-Made Hazards, Rimouski, Canada, August 3-9, 1986. In Natural and Man-Made Hazards, D. Reidal, Netherlands, pp.171-181, 1988.

Pararas-Carayannis, G. 1999. The Earthquake of 20 September 1999 in Taiwan http://www.drgeorgepc.com/Earthquake1999Taiwan.html

Pararas-Carayannis, G. 2006. Hurricane Surge Prediction - Understanding the Destructive Flooding Associated with Hurricanes. http://www.drgeorgepc.com/HurricaneSurge.html

Pararas-Carayannis, G. 2007. Disaster Risk Assessment - Overview of Basic Principles and Methodology. A report to the Disaster Center, Houston

Pararas-Carayannis, G., 2007. Historical Earthquakes in China. Webpage Article: http://www.drgeorgepc.com/EarthquakesChina.html
Pararas-Carayannis, G., 2008a, The Earthquake and Tsunami of July 18, 1969 in the Bohai Sea, China. Webpage Article: http://drgeorgepc.com/Earthquake1969ChinaBohai.html

Pararas-Carayannis, G., 2008b. The Earthquake of February 4, 1975 in Haicheng, China. Webpage Article:http://drgeorgepc.com/Earthquake1975ChinaHaicheng.html

Pararas-Carayannis, G., 2008c. The Tangshan Earthquake of July 28,1976 in China. Webpage Article: http://drgeorgepc.com/Earthquake1976ChinaTangshan.html

Pararas-Carayannis, G. 2008d. The Earthquake of May 12, 2008 in the Sichuan Province of China. Website: http://www.drgeorgepc.com/Earthquake2008ChinaSichuan.html

Pararas-Carayannis, G. 2009. Keynote Presentation 2009 China Cross-Straits Symposium on the Prevention and Mitigation of Natural Hazards - 19-20 JUNE 2009, FUZHOY, CHINA

Pararas-Carayannis, G. 2009. Assessment of Potential Tsunami Generation in China's Bohai Sea from Direct geotectonic and Collateral Source Mechanisms. Science of Tsunami Hazards, Vol. 28, No. 1, pages 35-66 (2009),

Pararas-Carayannis, G. 2019, Meteotsunami of 29 August 1916 at Santo Domingo, Dominican Republic — analysis of the destruction of the USS Memphis. Вычислительные технологии. Russia, Том 24, No 2, 2019.

Qiu, Yuanxi & Di Zhou, ?. Development of Post-Late Cretaceous Conjugate Shear Systems in the Northern Continental Margin of the South China Sea.
jgchina.zsu.edu.cn/ v32001/html/4qyx.htm

Ye, H., Shedlock, K.M., Hellinger, S.J. and J.G. Sclater, 1985. The north china basin: an example of a Cenozoic rifted intraplate basin, Tectonics 4 (1985) 153– 169.

Yin, A., and Nie, S., 1996. A Phanerozoic palinspastic reconstruction of China and its neighboring regions, in Yin, A., and Harrison, T. M., eds., The Tectonic evolution of Asia: Cambridge [England] ; New York, Cambridge University Press, p. 442-485.

Xu Qinghai, Wu Chen, Yang Xiaolan and Zhang Ningjia, 1996. Palaeochannels on the North China Plain: relationships between their development and tectonics. Studies of the Palaeochannels on the North China Plain, Geomorphology, Volume 18, Issue 1, December 1996, Pages 27-35.

Zhang, Z.M., Liou, J.G., and Coleman, R.G., 1984. An outline of the plate tectonics of China: Geological Society of America Bulletin, v. 95, p. 295-312.

Zheng Sihua, 1992. Depths of earthquake hypocenters in Tibetan plateau and their tectonic implications (in Chinese). China Earthquakes. 1992?11(2): p. 99-106

Zhou, Qinghai, and W. M. Adams, 1986a. Database e of Tsunamigenic Earthquakes in China, presented at the Pacific Congress on Marine Technology, 24-28 March 1986, Honolulu, Hawaii; extended abstract in the Program.

ISSN 8755-6839

SCIENCE OF **TSUNAMI HAZARDS**

Journal of Tsunami Society International

Volume 40 **Number 4** **2021**

IONOSPHERIC TSUNAMI POWER INDEX (ITPI) TESTING FOR TSUNAMI DETECTION

Nurrohmat Widjajanti[1)], Buldan Muslim[2)], Charisma Juni Kumalasari[3)], and Toifatul Ulma[4)]

[1]Department of Geodetic Engineering, Universitas Gajah Mada, Yogyakarta, 55281, Indonesia
[2]Space Research Center, National Research and Innovation Agency, Bandung 40173, Indonesia
[3]Mathematics Department, Master's Programme, Institut Teknologi Sepuluh Nopember, Surabaya 60111, Indonesia
[4]Department of Geomatics Engineering, Institut Teknologi Sepuluh Nopember, Surabaya 60111, Indonesia

Corresponding author: mbuldan@gmail.com

ABSTRACT

Ionospheric Tsunami Power Index (ITPI) has been proposed for tsunami detection. The index is derived from Total Electron Content (TEC) Global Navigation Satellite System (GNSS) data. The ITPI method already used for tsunami detection is limited to two earthquake cases. Therefore, the method needs to be tested before implementing the ITPI method operationally. ITPI testing was conducted for nine tsunami events in Indonesia. The test shows that ITPI can detect tsunami effects on the ionosphere. There are four of nine tsunami events that can be detected with ITPI consistently. The five ITPI tsunami events could not be detected. It is caused by the TEC data being too far from the tsunami epicentre and local tsunamis caused by landslides.

Keywords: *Ionospheric Tsunami Power Index (ITPI), Total Electron Content (TEC), GNSS*

1. INTRODUCTION

A *tsunami* is an earthquake originating from a shallow seabed or coastal subduction zone that causes a tsunami that comes quickly and unexpectedly (Manta et al. 2020). For example, the Sumatra M 7.6 earthquake in 1907, which caused a tsunami on the coast of Simeulue, Nias, and Batu islands, was named the tsunami earthquake by (Kanamori et al. 2020). Likewise, the Mentawai earthquake on October 25, 2010 (Mw7.8) is also known as the tsunami earthquake described by (Lay et al. 2011). (Kanamori et al. 2020) first proposed that the earthquake has the same characteristics. Furthermore, several methods of tsunami detection with TEC GNSS are discussed from the beginning to ITPI. There are several methods before the presence of the ITPI method. The tsunami detection method using the ionosphere has been used by Artru, namely with a high pass filter with a cut-off of 30 minutes (Artru et al. 2005) to eliminate diurnal variations and GNSS receiver bias (Artru et al. 2005). Galvan et al. use another method, namely polynomial and bandpass filtering, whose explanation is as follows:

a. Polynomial Function
   The polynomial functions can eliminate TEC variations with more extended periods, such as diurnal variations and changes in satellite elevation angles.
b. Band Pass Filtering
   Band Pass Filtering applied is 0.5-5 MHz (corresponding to the wave period of 33.3 to 3.3 minutes, with a typical range of tsunami periods). The filter extracts the Mesoscale Traveling Ionospheric Disturbance (MSTID) period caused by the tsunami.

Another way of detecting the effect of a tsunami on the ionosphere is to limit the TEC error to 0.03 TECU. It means that the accuracy of measuring the phase of the GPS carrier wave is less than 1 mm. According to the law of error propagation, the TEC measurement error is about 0.01 TECU. Thus, the TEC measurement error dominates these errors. Under near-quiet conditions, the lowered TEC value will typically fall within three sigmas of around 0.03 TECU. Furthermore, If the TEC value is above 0.03 TECU, can detect the anomaly.

This study focuses on ITPI testing related to the entire spectrum of AGW energy (Manta, et al. 2020). This ITPI indication of the tsunami effect on the ionosphere is not affected by pass-band filtering or polynomial fitting. It means that the ITPI value in the Mentawai case is 14. The disturbance is 14% greater than the average spectrum value of the previous six days in TEC observations (Manta, et al. 2020). The existence of unique characteristics of AGW compared to the mean background level (MBL) was revealed by Manta et al. from TEC data a few days before the earthquake until the time of the earthquake. The ratio between the TEC spectrum on the tsunami day and the average TEC spectrum six days before the tsunami can calculate ITPI. Manta et al. mention that the value can eliminate the influence of ionospheric dynamics. It has been successfully tested in two earthquake cases (Manta, et al. 2020). The paper discusses the results of the ITPI testing for tsunami detection that has occurred in Indonesia. The aim is to know the ITPI used operationally to strengthen the tsunami early warning system in Indonesia.Data and Methodology

1.1 Data

The data are nine earthquakes with the potential for a tsunami, and observed tsunami. The data was downloaded from ngdc.noaa.gov, by filtering 1996-2021 in Indonesia.

Table 1. Data on the 10 largest earthquakes in Indonesia

No.	Year	Month	Day	Hour	Minute	Quake Magn. (SR)	Location Name	Latitude	Long.	Max. Water Height (m)
1	1996	2	17	5	59	8.2	Irian Jaya	-0.891°	136.952°	7.7
2	2000	5	4	4	21	7.6	Sulawesi	-1.105°	123.573°	6
3	2002	10	10	10	50	7.6	Irian Jaya	-1.757°	134.297°	5
4	2004	12	26	0	58	9.1	Offshore West Coastal Sumatra	3.316°	95.854°	50.9
5	2005	3	28	16	9	8.6	Indonesia	2.085°	97.108°	4.2
6	2006	7	17	8	19	7.7	South of Java	-9.254°	107.411°	20.9
7	2007	9	12	11	10	8.4	Sumatra	-4.438°	101.367°	5
8	2010	10	25	14	42	7.8	Sumatra	-3.487°	100.082°	16.9
9	2018	9	28	10	2	7.5	Sulawesi	-0.178°	119.840°	10.73
10	2018	12	22	13	55	n/a	Krakatau	-6.102°	105.423°	85

1.2 Ionospheric Tsunami Power Index (ITPI)

The computation of TEC uses a method similar to (Calais and Minster 1995), namely the carrier wave phase (L1 & L2), not using an inaccurate apparent distance measurement (P1 & P2). TEC of the phase data is computed using Equation (1) (Manta et al. 2020):

$$TEC = \frac{(L1 - L2)}{40.3} \frac{f_1^2 f_2^2}{f_1^2 - f_2^2} \qquad (1)$$

Where f1 and f2 correspond to high and low GPS frequencies and TEC is the Total Electron Content measured in TEC units (1 TECU = 1016 el/m2). A consequence of the integrated nature of TEC is the presence of ionospheric disturbances. The observed ionospheric disturbances are generated in the range from the height of the satellite to the

receiver. However, the combination of TEC variation comes from around the maximum height of ionospheric ionization (F2 layer).
The ITPI index can be made from the TEC data to identify ionospheric disturbances caused by the tsunami using Equation (2) (Manta et al. 2020).

$$ITPI = \left(\frac{PSD_{MAX}}{MBL} - 1 \right) \cdot 100. \qquad (2)$$

The ITPI is proportional to i with the ratio between the TEC spectrum on the day of the tsunami the average spectrum for the previous six days. The intended ratio is the ratio between the Maximum Power Spectral Density (PSDMax) levels of TEC during the event. Mean Background Level (MBL) is defined as the average PSD observed six days before the earthquake. The use of background averaging over several days before an earthquake is intended to remove outliers and smooth out parts of the noise associated with other disturbances in the ionosphere. These parameters are for the automatic identification of tsunamigenic potential (Manta et al. 2020).

Figure 1 below shows the methodology flow. The explanation of each stage in Figure 1 is presented below:

Compute the TEC from observation data of dual-frequency GNSS signal using Equation (1).

1. The TEC calculation is obtained from the observation data of the dual-frequency GNSS signal using Equation (1).
2. Compute the IPP (GNSS signal trajectory in the ionosphere) six days in advance of today's events of earthquake days.
3. Compute the latitude and longitude IPP using Equation (3) to (5) (Pooja et al. 2018).
   latitude_IPP = $\phi + \cos(A)$
   longitude_IPP = $\lambda + z \sin A \cos(latitude\_IPP)$
   With $z = cos - 1rere + h \cos E - E$
   Where, *re:* radius from earth = 6378137.0, *h:* height = 350, ϕ*:* latitude, λ*:* longitude, *E:* elevation angle, *A:* azimuth angle, latitude_IPP: latitude from IPP, longitude_IPP: longitude from IPP.
4. Filter the data using polynomials to eliminate the influence of satellite motion and other biases on TEC data.
5. Analyze the spectrum for each TEC for every one hour of moving observations in 30 seconds.
6. Determine the average PSD for six days before the tsunami computation.
7. Determine the power spectrum distribution on the day with the average power spectrum six days before the tsunami.
8. Compute the ITPI using Equation (2).
9. Analyze the correlation between ITPI and earthquake magnitude.
10. Determine the ITPI correlation with tsunami height.
11. Determine the empirical modelling of the relationship between the ITPI index and tsunami height.
12. Determine the empirical modelling of ITPI's relationship with earthquake magnitude.

The computation of steps 1 to use the GOPI software are as shown in Figure 1.

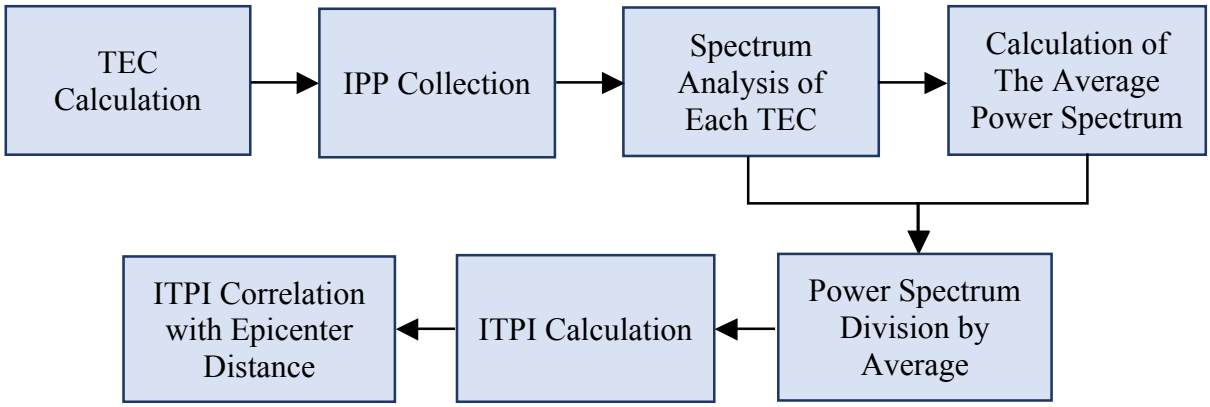

Figure 1. Methodology flow

2. RESULTS AND DISCUSSION

Figure 2 shows the average PSD TEC from satellite number 23 before the Aceh earthquake from December 20 to 25. It means that the maximum spectrum value is around t10 at 5 UT with a frequency of 0.3 MHz Figure 2 shows the PSD on December 26, 2004, in the Aceh tsunami.

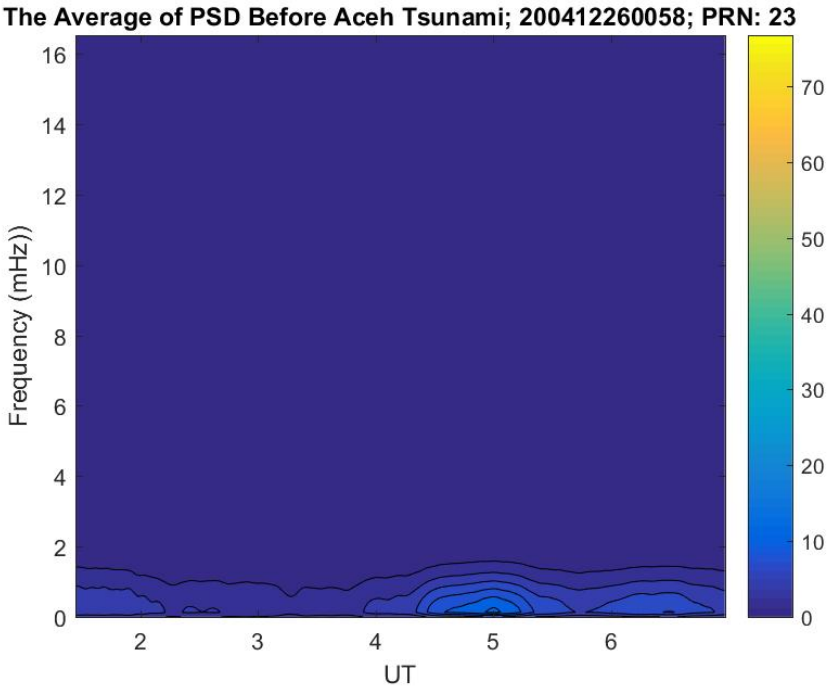

Figure 2. Average PSD before the Aceh earthquake on satellite number 23

The maximum value of the spectrum was above 70 at around 5 UT, with a frequency value of about 0.3 MHz (55.6 minutes period). The increase in spectrum value starts at 3.9 UT. At that time, the ionosphere is at coordinates 13.24° South Latitude, 96.66° East Longitude, and altitude 350 km. Also, from the epicentre of the earthquake at 3.316° South Latitude and 95.854° East Longitude, ionospheric anomalies occurred at a distance of 16.556° latitude and 0.806° longitude. The horizontal distance is 16.575° (1839.89 km).

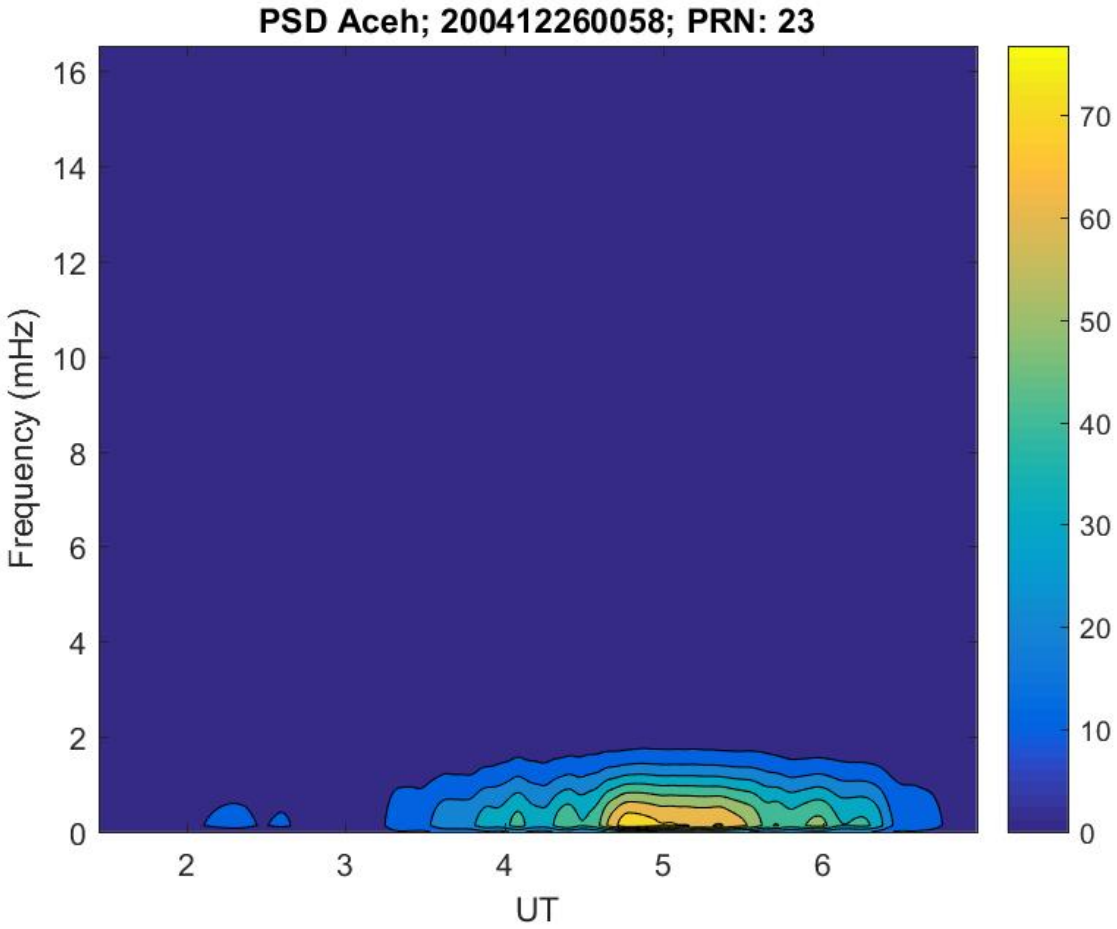

Figure 3. Aceh PSD on satellite number 23

The anomaly propagation time from the tsunami at 0.96 to 3.9 UT is 2.9 hours. Thus, the horizontal velocity is 634.44 km/hour. However, the tsunami events reference shows that the tsunami velocity is around 750 km/hour (Marghany-Maged, 2014). Therefore, the horizontal velocity observed in the ionosphere is lower than that of a typical tsunami.

Figure 3 shows ITPI Aceh during the tsunami. The apparent increase in spectrum values started at 3.5 UT at a frequency of about 1 MHz (period of internal atmospheric gravity waves 16.7 minutes).

An anomaly also appeared at 3 UT, and the frequency was around 5.8 MHz (9.7 minutes). Compared with ITPI, the ITPI method shows more anomaly detection, namely internal gravity waves and acoustic waves whose frequencies are 1MHz and 5.8 MHz, respectively. Therefore, the ITPI is more sensitive in detecting the effects of tsunamis on the ionosphere from TEC data. Based on the horizontal distance of the detected anomaly and its propagation time, the horizontal velocity of the tsunami is obtained. The propagation rates of ionospheric disturbances due to the tsunami are 707.65 km/hour (from internal gravitational waves) and 901.9 km/hour (from acoustic waves). Figure 4 shows the ITPI Aceh on satellite Number 23.

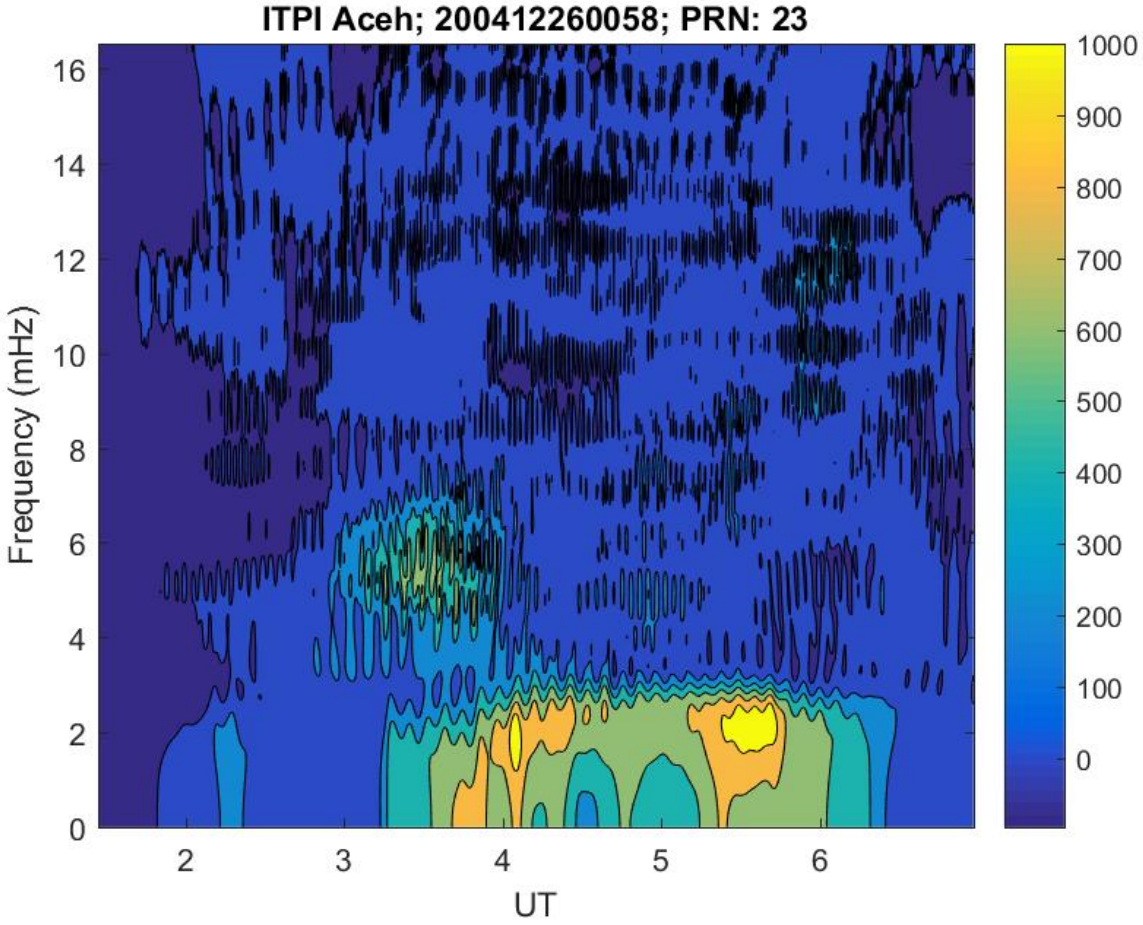

Figure 4. ITPI Aceh on satellite number 23

The other satellite observations and tsunami events in total can be seen in Table 2 below.

Table 2 List of tsunami events relation to distance and ITPI value

Location	Station	Epicenter		Date	Time	Satellite number	ITPI		Frequency (mHz)	Delay (hours)	Distance (km)	ITPI Max	Velocity (km/hr)
		Lat (°)	Long (°)				Lat (°)	Long (°)					
Aceh	COCO	3.32	95.85	26/12/2004	0:58	11	-11.98	98.42	3.0	2.8	1721.581	3500	614.850
		3.32	95.85	26/12/2004	0:58	20	-16.19	97.41	3.2	2.6	2172.044	1600	835.401
		3.32	95.85	26/12/2014	0:58	23	-13.96	96.88	2.5	2.1	1921.015	1000	914.769
		3.32	95.85	26/12/2004	0:58	23	-12.74	96.54	5.0	2.4	1783.842	550	743.267
		3.32	95.85	26/12/2004	0:58	23	-14.14	96.96	0.4	2.2	1941.501	400	882.501
		3.2	95.85	26/12/2004	0:58	31	-13.79	93.07	2.6	2.5	1923.748	3000	769.499
Krakatau	BAKO	-6.10	105.42	22/12/2018	13:55	23	-9.10	106.15	4.2	0.8	342.423	1200	428.028
		-6.10	105.42	22/12/2018	13:55	18	-2.78	109.57	6.0	1.0	589.799	140	589.799
Pangandaran	XMIS	-9.25	107.41	17/07/2006	8:19	19	-13.22	104.91	5.0	0.6	520.449	350	867.414
		-9.25	107.41	17/07/2006	8:19	20	-9.87	101.17	16.0	1.5	696.117	200	464.078
Mentawai	NTUS	-3.49	100.08	25/10/2010	14:42	22	5.18	103.40	3.1	2.8	1030.126	80	367.902
		-3.49	100.08	25/10/2010	14:42	25	1.68	106.50	10.5	3.2	914.579	600	285.806

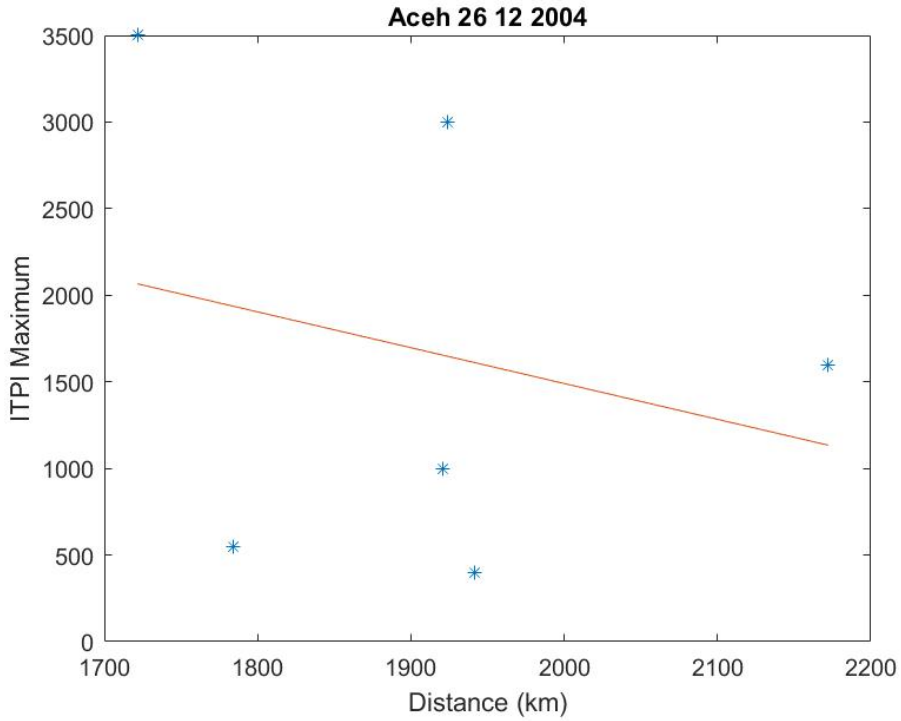

Figure 4. Linear trend of the relationship between the distance of the satellite to the epicentre of the earthquake with the maximum ITPI value

Table 2 shows that the distance and speed of a tsunami are affected by the type of tsunami present. Based on UNESCO's ITIC, there are two types of tsunamis: local and regional tsunamis. A local tsunami is a tsunami originating from a distance of about 100 km or less than 1 hour from the tsunami's travel time from the affected coastline. Meanwhile, regional tsunamis are tsunamis capable of hitting a specific geographic area, generally within 1000 km from the earthquake's epicentre. Regional tsunamis can arrive at the affected coastline within 1-3 hours of movement. Thus, their strength can distinguish the two types of earthquakes.

The Aceh Tsunami is a regional tsunami type with a strength of 9.1 Mw. The ITPI method can show the Aceh tsunami impacting the ionosphere at a distance of more than 1000 km from the epicentre.

If analyzed using a linear trend line, the maximum distance between the ionospheric disturbance and the epicentre is no more than 2200 km. Thus, it proves that the farther the ionospheric satellite observation from the epicentre, the lower the ITPI value.

2. CONCLUSIONS AND RECOMMENDATIONS

The discussion and results show that the closer the earthquake centre is to the satellite, the higher the ITPI value. On the other hand, the farther the distance between the epicentre and the satellite, the lower the ITPI value. In addition, the results are not appropriate in local tsunami events such as (Sulawesi, 28 September 2018). The result is due to several factors, the far distance from the epicentre to satellite observations. Based on ten tsunami events, Aceh uses a model of the tsunami effect on the ionosphere. ITPI results show a tsunami of 4 consistent events, namely (Aceh, Krakatau, Pangandaran, and Mentawai). The four events are global and local tsunamis.

Recommendations for further research are:

a. The study to use local GNSS observation data, which is closer to the tsunami event.
b. The study to use more precise filtering related to the type of wave (acoustic and gravity).
c. To use more GPS station data so that the spatial pattern is clearer.

ACKNOWLEGMENTS

This research was funded through the INSINAS program of the Ministry of Research Technology and Higher Education with a contract No. 14/INS-1/PPK/E4/2020 changed to No. 70/iNS-1/PPK/E4/2020. We express our deepest gratitude to the Indonesian Geospatial Information Agency for its support in preparing GNSS in real-time data. Also, due acknowledgment goes to Joni Efendi for his consultation and suggestion to use RTCM GNSS data for real-time TEC purposes.

REFERENCES

Artru, J., Ducic, V., Kanamori, H., Lognonné, P., and Murakami, M., (2005), "Ionospheric Detection of Gravity Waves Induced by Tsunamis, Geophysics Journal International, 160, 840-48.

Buldan, M., Mokhamad, N.C., Bambang, S., and Charisma, J.K., (2020), "The Simulation Study of GNSS Signal Reflection in Monitoring Sea Levels and Tsunamis", Journal of Tsunami Society International, Vol. 39 No. 4, 192.

Calais, E. and Minster, J.B., (1995), "GPS Detection of Ionospheric Perturbations following January 17, 1994, Northridge Earthquake", Geophysics Research Letter 22, 1045-1048.

Galvan, D., Komjathy, A., Hickey, M., and Mannucci, A., (2011), "The 2009 Samoa and 2010 Chile Tsunamis as Observed in the Ionosphere using GPS Total Electron content", Geophysics Research Letter 116, A06318.

Hertanto, S., "BMKG Map 10 Potentially Earthquake and Tsunami Areas, Megathrust Zones and Active Fault Zones", (2021), WartaKotalive.com, 1-4.

Kanamori, H., Rivera, L., and Lee, W.H.K., (2010), "Historical Seismograms for Unraveling a Mysterious Earthquake: the 1907 Sumatra Earthquake", Geophysics Journal International, 183, 358-374, DOI: 10.1111/j.1365-246X.2010.04731.x.

Lay, T., Ammon, C, J., Kanamori, H., Yamazaki, Y., Cheung, K, F., and Hutko, A,R. (2011), "The 25 October 2010 Mentawai Tsunami Earthquake (Mw 7.8) and the Tsunami Hazard Presented by Shallow Megathrust Ruptures", Geophysics Research Letter 38, L06302.

Manta, F., Occhipinti, G., Feng, L., and Hill, E.M., (2020), "Rapid Identification of Tsunamigenic Earthquakes using GNSS Ionospheric Sounding", Scientific Reports Vol. 10, Article No. 11054.

Marghany, M., (2014), "Simulation of Tsunami Impact on Sea Surface Salinity along with Banda Aceh Coastal Waters, Indonesia", Advanced Geoscience Remote Sensing, DOI: 10.5772/58570.

Pooja, S.K., Pooja, A.K., Hithaishi, M.T., Yashoda, A.B., Santhosh, S., and Jimanshu, S., (2018), "Coordinate Transformation of Satellite Orbits for Ionospheric and Tropospheric Pierce Points: Visualization and Computation", International Journal of Research and Scientific Innovation (IJRSI), Vol. V, Issue IV.

ISSN 8755-6839

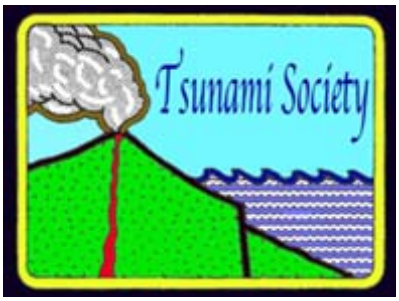

SCIENCE OF **TSUNAMI HAZARDS**

Journal of Tsunami Society International

Volume 40 **Number 4** **2021**

WWW.TSUNAMISOCIETY.ORG

TSUNAMI SOCIETY INTERNATIONAL, 1741 Ala Moana Blvd. #70, Honolulu, HI 96815, USA.

WWW.TSUNAMISOCIETY.ORG